THE
PHYSICAL REVIEW
A Journal of Experimental and Theoretical Physics
VOL. 45, NO. 6 MARCH 15, 1934 SECOND SERIES

The Path of a Secondary Cosmic-Ray Charged Particle in the Earth's Magnetic Field

I. S. BOWEN, *California Institute of Technology*
(Received January 31, 1934)

An analysis is made of the paths of secondary high energy charged particles ejected from the earth's atmosphere by primary cosmic-ray photons. This leads to the following conclusions. (1) As has generally been assumed the decrease in ionization in equatorial regions is much larger than can be explained by the deflection by the earth's magnetic field of the secondaries formed in the earth's atmosphere. (2) The observed east-west dissymmetry of Geiger tube counts can be explained by the deflection of secondaries formed in the earth's atmosphere provided an appropriate value of Q, the excess of positives over negatives, may be assumed. The small amount of the observed dissymmetry at high latitudes however sets so low an upper limit on Q that this mechanism appears to be inadequate to explain all of the observed dissymmetry at low latitudes.

RECENT cosmic-ray measurements by many observers have brought to light two latitude effects.[1] These are the decrease in ionization in an electroscope near the magnetic equator and the appearance of an east-west dissymmetry in Geiger tube counts in the same region. It is generally recognized that these effects are produced by the action of the earth's magnetic field in deflecting the high energy charged particles which are the immediate cause of the cosmic-ray ionization.

The present paper is a theoretical attempt to determine whether these experimental results may be quantitively explained by the action of the earth's field on secondary electrons (positive or negative) ejected by primary photons in the earth's atmosphere or whether it is necessary to postulate primary charged particles coming from outside the earth's atmosphere.

When an electron which has fallen through a potential of V volts passes normally through a magnetic field H the radius of curvature of its path r in cm is given by[1]

$$V=510{,}000[\{1+(0.00059\,Hr)^2\}^{\frac{1}{2}}-1]. \quad (1)$$

With cosmic-ray particles V is very large, usually of the order of several hundreds of millions of volts. Indeed if the energy of the particle is less than a million volts it is unable to penetrate most measuring instruments. Consequently the expression for r may be simplified to

$$r=V/300\,H. \quad (2)$$

Furthermore by direct counts it is found that a high energy particle dissipates its energy approximately uniformly along its path by the production of about 32 P ions per cm of its path in air at a pressure of P atmospheres. Since this requires about 1000 P electron-volts per cm the range (R) of such a particle is $V/1000\,P$. Since r and R are both proportional to V it follows at once that the radius of curvature (r) at any point on the path is proportional to the length of path (R) remaining before the particle is brought to rest. If the origin is placed at the end of the path this condition is satisfied by the equiangular spiral of the form

$$\rho=e^{r\theta/R}. \quad (3)$$

[1] Bull. Nat. Research Council 10, p. 85 (1925).

TABLE I. *Comparison of observed and calculated east-west dissymmetry.*

Location	Fractional excess west over east E	Observed angular shift φ	Pressure P	Horizontal component H	Calculated shift $\psi=3H/10P$	Excess of positives Q
Swarthmore[2]	0.028±0.006	0.43±0.09	0.98	0.18	3.2	0.13±0.03
Colorado[3]	.022± .005	.34± .08	.71	.22	5.3	.06± .02
Flagstaff[4]	.020± .018	.31± .28	.67	.26	6.7	.05± .04
Mexico City[5]	.084± .013	1.29± .20	.76	.31	7.0	.18± .03
" " [6]	.082± .006	1.26± .09				.18± .01
Peru[7]	.086	1.3	.97	.30	5.3	.25
	.112	1.7	.66	.30	7.8	.22
	.123	1.9	.58	.30	8.9	.21

I. MEAN DEVIATION OF PARTICLES

Since in an equiangular spiral the radius vector maintains a constant angle with the tangent to the path, the change in direction of the path in passing from one point to another equals the difference in position angles of the two points.

$$\theta_0-\theta=(R\log\rho_0/\rho)/r=(R\log R_0/R)/r. \quad (4)$$

As in direction measurements with Geiger counters there is an equal probability of observing the particle at any point in its path the observed dissymmetry in the east-west counts will correspond to the average deviation ψ.

$$\psi=\frac{\int_0^{R_0}(R/r)\log(R_0/R)dR}{\int_0^{R_0}dR}=\frac{R}{r}=\frac{3H}{10P}. \quad (5)$$

Both theoretical and experimental evidence indicates that these very high energy particles occasionally suffer very large losses by ejecting other charged particles with high energy thus cutting down the range of the original particle to a small fraction of the above value of R. However, it can easily be shown that the mean deviation averaged over the paths of the original particle and of all particles ejected by it, is exactly that given in (5) for the single particle. In all of these derivations it is necessary to assume that the initial energy of all particles is large compared to that required to pass through the walls of the counters. Otherwise the counters cannot be considered as giving all parts of the paths equal weights, a condition which was assumed in taking the above averages.

ψ as given by Eq. (5) represents the mean deviation of a single particle or of any group of particles provided they are all of the same sign. If particles of both signs are present ψ must be multiplied by a factor Q which is equal to the excess in the number of one sign over that of the other divided by the total number of particles.

The east-west dissymmetry in Geiger counts has been measured at the locations given in the first column of Table I. In the second column an attempt has been made to place the readings of all observers on a common basis by listing the value of the quantity E which is the average, for all angles between 30° and 50° inclusive, of the ratio of the difference between west and east to the mean of west and east. A study of the complete curve of count frequency as a function of altitude angle for the cases where it has been determined, indicates that a shift in the center of symmetry of the curve of φ degrees from the vertical corresponds to a value of E of about 0.065φ. Assuming this relationship holds for all localities we obtain the values of φ in the third column. The sixth column gives the value of ψ (in degrees), i.e., the mean deviation of a secondary electron, corresponding to the values of P and H given in the fourth and fifth columns. The last column lists the value of $Q=(\varphi/\psi)$, i.e., the excess of positives, necessary to explain the observed dissymmetry if this is caused solely by the deflection of secondaries.

From the table it is at once evident that the deflection of secondaries is adequate to account for the observed dissymmetry provided we can

[2] T. H. Johnson and E. C. Stevenson, Phys. Rev. **44**, 125 (1933).

[3] E. C. Stevenson, Phys. Rev. **44**, 855 (1933).

[4] S. A. Korff, Phys. Rev. **44**, 515 (1933).

[5] L. Alvarez and A. H. Compton, Phys. Rev. **43**, 835 (1933).

[6] T. H. Johnson, Phys. Rev. **43**, 834 (1933).

[7] T. H. Johnson, Phys. Rev. **44**, 856 (1933).

assume an appropriate value for the excess of positives over negatives at each latitude.

Anderson's direct counts of positive and negative tracks in a Wilson expansion chamber give $Q=0.0\pm0.04$. Since however most of these secondary particles are ejected from the metal parts of the surrounding magnet it is not certain that this value of Q can be applied to the Geiger counter experiments in which the secondary particles are ejected from air.

If these secondary electrons are ejected by primary photons Q should have the same value at all latitudes since the earth's field has no effect on the intensity or quality of the incoming photons. Furthermore even though we assume that all of the dissymmetry at Flagstaff or in Colorado is caused by the deflection of secondaries the largest value of Q that we can justify is not much more than 0.06. This value of Q is, however, too small to explain all of the dissymmetry near the equator.

Dr. Korff of this Institute is now making experiments in Peru to determine just what fraction of the observed dissymmetry may be assigned to the deflection of secondaries. In these experiments the east-west dissymmetry, when the secondaries come from a 30 cm lead block placed directly above the counters, is compared with the dissymmetry when there is an equivalent amount of air above them. Since R, the range of the secondaries, in the lead is negligible, the part of the dissymmetry produced by the deflection of secondary electrons is largely eliminated in the first arrangement.

II. Decrease in Ionization Near the Equator[8]

If an electron is ejected vertically downward and if it ionizes uniformly along its range (R) then the average vertical distance between the ions formed and the point of ejection is $R/2$ if the path is straight. If the path is the equiangular spiral discussed above a simple calculation shows that the average vertical component of the distance between ions and the point of ejection is reduced to $R/2(1+R^2/4r^2)$. Therefore, on the average, the secondary particles passing through an ionization chamber are ejected at a point $(R/2)(1-1/[1+R^2/4r^2])$ lower than when the magnetic field is not present. Consequently if the intensity of the primary photons is given by $I_0e^{-\beta z}$ the intensity of ionization will be decreased in the ratio

$$e^{-(\beta R/2)(1-1/[1+R^2/4r^2])}.$$

This reduces to $1-\beta R/8(r^2/R^2)$ approximately. If we make the usual assumption that the range of the secondary electron is small compared to that of the primary photon and insert the value of r/R deduced above this ratio differs from unity by at most a few tenths of a percent. As has generally been assumed, this mechanism is therefore entirely inadequate to explain the observed effect of about ten percent at sea level and about thirty or forty percent at the highest elevations investigated.

[8] This section merely confirms the conclusions reached by R. M. Langer by a different method. Phys. Rev. **43**, 215 (1933).

The Mechanism of Cosmic-Ray Counter Action

CARL D. ANDERSON, R. A. MILLIKAN, SETH NEDDERMEYER AND WILLIAM PICKERING, *Norman Bridge Laboratory of Physics, California Institute of Technology*

(Received December 26, 1933)

A study of photographs taken in a very powerful magnetic field with the aid of a cloud chamber activated by counter responses shows (1) that such an arrangement has a strong selective action on showers; (2) that showers so selected have an exceptional multiplicity of tracks; (3) that the two counters show simultaneous responses when no single particle can pass through both of them; (4) that in general these showers consist of a mixture of positive and negative electrons rather than of electrons and protons, no effects certainly attributable to neutrons being observed; (5) that these electrons in getting out of the nucleus some times produce an intense photon spray of the nature of "brems strahlung"; (6) that these photon sprays are increasingly responsible for the simultaneous activation of the two counters the thicker the intervening lead; (7) that a light element like carbon has little effect in producing either showers or sprays; (8) that the total energy of a shower is not larger than that of single electrons (+ or −); (9) that the Dirac theory encounters certain difficulties in accounting for the observed effects.

1. HISTORICAL

AS pointed out by Millikan[1] in 1932, coincidences in the responses of two counters placed on a vertical line and separated by considerable thicknesses of heavy matter, such, for example as a meter of lead, cannot in general be due to the passage of one charged particle through both counters and the intervening lead, but *must rather be due to some mechanism by which a photon can release successively along, or in the general neighborhood of, its path a number of different particles whose separate but practically simultaneous action on the two or more counters is responsible for the observed coincidences.* The evidence advanced for this view was as follows: Anderson, Millikan and Neddermeyer had measured (1) the actual energy distribution among the particles whose passage through a gas-filled chamber is responsible for practically all the ionization therein produced, and had found that 75 percent of these particles have energies under a billion (10^9) volts, while a negligible fraction have energies as high as 3×10^9 volts.[2] They had (2) measured *directly* the energy loss of these particles in passing through lead and had found it about 35 million volts per cm of Pb[2]. This meant that a billion volt particle could not pass through more than 30 cm of lead and that practically no particles of those existing at sea level could pass through a meter of lead. (3) Guided by these facts Pickering had actually changed the number of coincidences observed in three counters without changing the intervening lead, but rather by merely changing the distribution of lead about the line joining the three counters. He had also shown that with large quantities of lead intervening between both the upper and lower pairs of the three counters displacing the counters from a straight line did not necessarily reduce the number of coincidences.

The present experiments not only confirm the foregoing viewpoint, but they show clearly what is the actual mechanism of counter action when considerable amounts of heavy material intervene between the counters. In order to appreciate the nature of the evidence the following previously established facts, obtained by the method of random exposure, must be borne in mind.

2. SUMMARY OF RESULTS WITH RANDOM CLOUD-CHAMBER EXPANSIONS

In all our preceding measurements on the energies of the cosmic-ray ionizing particles, we have obtained about one good track for every thirty exposures, but since an exposure can be made about once every ten seconds, a successful

[1] R. A. Millikan, Phys. Rev. **43**, 661 (1933); Institut Poincarè Proceedings (1933).

[2] C. D. Anderson, Phys. Rev. **44**, 406 (1933); Millikan and Anderson, Phys. Rev. **40**, 325 (1932).

exposure can be obtained about once every five minutes. This is more rapidly than the tracks can be measured and analyzed any way, and the motion picture film used is inexpensive so that for rapidity of work there was no advantage in arranging to have the passage of the rays themselves produce the cloud-chamber expansions and the photographic exposures. Further, for the accurate measurement of cosmic-ray energies the random method has very great advantages. For when the passage of the particle itself precedes the expansion, as it obviously must do if it produces it, this expansion may, and often does, seriously distort the track, but when the random method is used the sharpest tracks are obtained, and without distortion, when the particle passes at the instant at which the expansion is completed or very shortly thereafter. Out of a group of 815 cosmic-ray photographs taken by this method on which a good track or tracks were obtained, about 708, or 88 percent, corresponded to single isolated tracks; 82, or 10 percent, corresponded to double tracks or pairs; 7 photographs showed three tracks, i.e., two positives and a negative or two negatives and a positive; 7 photographs showed four tracks; 3 showed 5 tracks; while 7 showed between 5 and 10 tracks; all the tracks on a given photograph being *associated* in a sense that they are produced by particles passing through the chamber at the same instant as revealed by the identity in sharpness or diffuseness of them all, but not always emanating from a single center; and finally, but one photograph out of the 815 revealed more than 10 tracks. In other words, 88 percent of all the photographs reveal single "electron-shots," while 12 percent reveal "showers," a shower being defined as two or more tracks associated in time. So far as we can now see, from our energy measurements in our powerful magnetic field as well as from our ion-counts, all the electron shots are due to free positive electrons (positrons), or to free negative electrons (negatrons),[3] practically none to protons. As to energies, a third of the tracks taken at sea level show energies under 350 million volts, 75 percent show energies under a billion volts, while 98 percent show energies under 3 billion volts, *the highest energies so far obtained being shown by single tracks*, not by the summation of the energies in a shower.

Practically all of the showers are certainly due to photon encounters with an atomic nucleus for though we have had a bar of lead, a centimeter thick, across the middle of the cloud chamber, and have observed the tracks of a great number of free electrons, both positive and negative, passing through this lead, only in two cases out of say a thousand, have we seen a pair of tracks one of which was a positron produced from the passage of an electron, positive or negative, through the lead. This kind of an encounter—that of an electron with a nucleus, yielding a positron or a pair—is then a very rare event, while in a great many cases a pair emerges from the lower side of the lead when no ionizing ray is seen entering the upper side. This must, so far as we can see, be the result of the encounter of a photon with a nucleus.

3. Geiger-Counter Controlled Exposures

Having obtained, from our method of photographing random cosmic-ray shots, the foregoing statistical information as to the normal behaviors of cosmic-ray nuclear encounters and normal cosmic secondary particles, and having deduced

[3] To remove the ambiguity in the definition of the term "electron" existing at the present time because of the double sense in which it is used in the literature, namely, to denote on the one hand—as for example in the universally used expression electron-volts—*the magnitude of the elementary quantity of electric charge*, and on the other hand, the name of a *particle* of a particular mass, the terms "negatron" and "positron" are here used. These terms are used merely as convenient contractions for the fully descriptive *particle* designations, "free negative electron" and "free positive electron." The term electron then retains its historical, derivative, and logical meaning as the name of the elementary unit of charge, and the present ambiguity no longer remains. It is pointed out that this suggestion is not at all in conflict with the tradition and usage of the term electron. Even today probably nine-tenths of the usage has reference in the mind of the author to charge rather than to mass, as to take but a single example, in all cases in which the number of electrons going to a given electrode is under consideration. The usage we are suggesting is merely for the sake of removing the ambiguity, the bad effects of which are becoming increasingly felt since the discovery of the "free positive electron," and since the discussion of nuclear processes has become more common. In this usage there is no difficulty in speaking of electrons as existing in the nucleus since one has then in mind only the number of units of electric charge.

therefrom the foregoing theory as to the nature of cosmic-ray counter action, it was clear that if our reasoning were correct, the use of a pair of counters above and below a cloud chamber for the purpose of letting the simultaneous response of these two counters activate a trip, which, in turn, produced the expansion and took the photograph. would not only throw new light on the mechanism of counter action, but would select showers for special study in our 20,000 gauss field. *For Anderson[4] had published in August, 1932 photographs which showed a group of tracks associated in time, not all of which emanated from the same center, and therefore, which must have involved some non-ionizing mechanism to connect the tracks so associated.* Blackett and Occhialini's photographs (March, 1933) present similar evidence.[5] These observers had not, however, a sufficiently strong magnetic field to measure the total energies of their showers, nor to differentiate in many cases positive and negative electron tracks, and this measurement and differentiation are vital for some of the conclusions at which we arrive herewith.

A cloud chamber actuated by tube-counters is effective only if the time-lag between the passage of the particle through the counters and the completion of the expansion is made extremely small, so that only a negligible diffusion of the ions along the path of the particle occurs before the vapor-track is formed.

Our apparatus was designed for particularly rapid operation, and the tracks obtained are comparable in sharpness with the very sharpest obtained by the random method of photographing. The apparatus is wholly self-operating, all the resetting operations being made automatically, placing the apparatus in a sensitive state 14 seconds after an exposure. The tube-counters and the vacuum-tube circuit for selecting the simultaneous responses of the two counters situated just above and below the expansion chamber were built, along new lines too, by one of us, Mr. Pickering. Just above the upper counter is placed a bar of lead about 1×1 inch in cross section (the same as that of the counters) so as to facilitate photon-encounters with the nuclei of lead atoms. Secondary electron-shots resulting from such encounters, if they pass through both counters and thus produce simultaneous counter responses, must also pass through the expansion chamber and appear there as a track in the plane defined by these two counters.

[4] Anderson, Phys. Rev. **41**, 409 (1932).

[5] Blackett and Occhialini, Proc. Roy. Soc. **A139**, 699 (1933).

4. Results Obtained with Geiger Counter Controlled Exposures

Figs. 1 to 15 show photographs obtained with Geiger counter controlled cloud chamber. The effective diameter of the chamber is 14 cm and its effective depth 1.5 cm. Two views of the chamber are shown; in each case the one on the left is the direct central view, the right-hand one a mirror image of the central view. It is thus possible to view the tracks stereoscopically and reproduce the effects in space.

Figs. 1 to 6 and 9 to 14 show a plate of lead 1 cm thick across the center of the chamber. In Fig. 15 a plate of graphite of 1.4 cm thickness replaces the lead. A plate of lead of 2 mm thickness across the upper part of the chamber was present in all cases. In the left-hand or direct view particles of positive charge are evidenced by a counter-clockwise sense of rotation in the magnetic field.

(1) The first result appearing from our photographs thus taken, is that as earlier suggested by Blackett and Occhialini this arrangement has a very marked selective action on showers, since these appear very much more frequently than in photographs taken with the aid of the random method described above.

(2) The second result is that the showers caught with the present arrangement show in many cases very many more tracks than do the showers heretofore photographed. This again shows the selectivity, for showers, of this method.

(3) The third result is that not infrequently the *two counters show simultaneous responses when no electron shot appears which can possibly pass through both counters and the expansion chamber.* This behavior is very fully shown in photographs 1 to 6, and 10, 11 and 15 (see also legends). These photographs are all illustrations of the situation in which the counters were clearly set off, not by a single particle going through both counters, but,

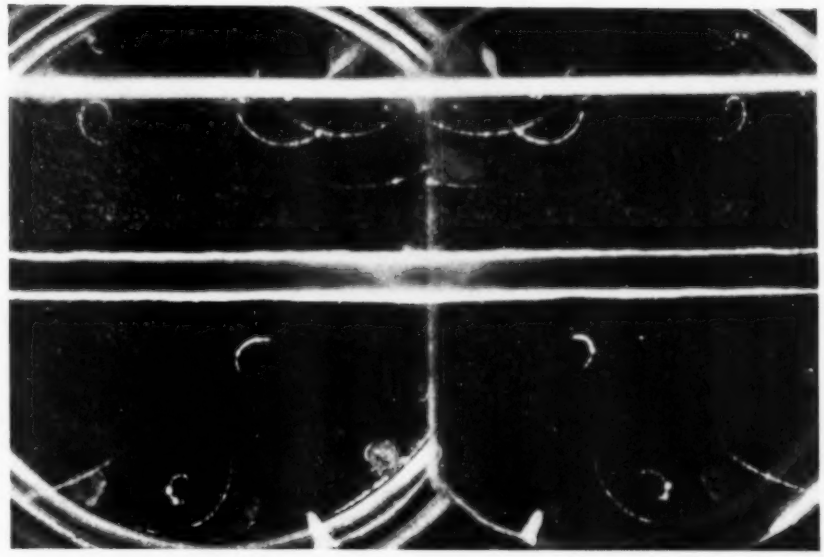

FIG. 1. 17,000 gauss field. The left-hand exposure is the direct photograph, the other the reflection taken for stereoscopic purposes. Six low energy electrons are seen between the two lead plates and four below the lower one. Stereoscopic vision shows that eight of these ten come from the wall and two from the upper lead plate. The short, very heavy track above the top plate, probably not associated in time with the others, may be a recoil nucleus.

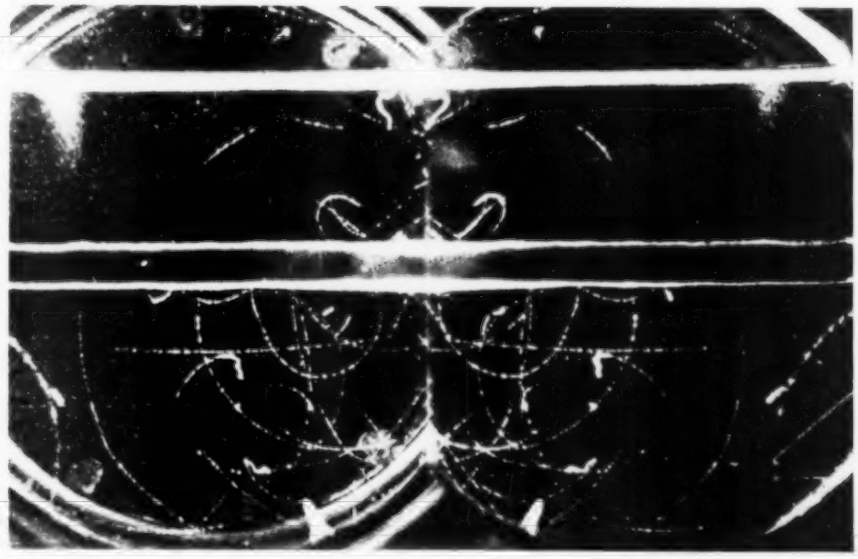

FIG. 2. 825 gauss field. This photograph shows eight electron tracks between the two plates and 15–20 below the central one, mostly of the order of but a million electron-volts. Stereoscopic vision shows two pairs produced within the central plate and emerging from its lower face. Most of the remaining electrons come from the walls. Their distribution in direction is extremely various, indicating that they arise from the absorption of a spray of photons, probably originating in the lead bar above the upper counter. The horizontal track cutting across all the others is particularly interesting.

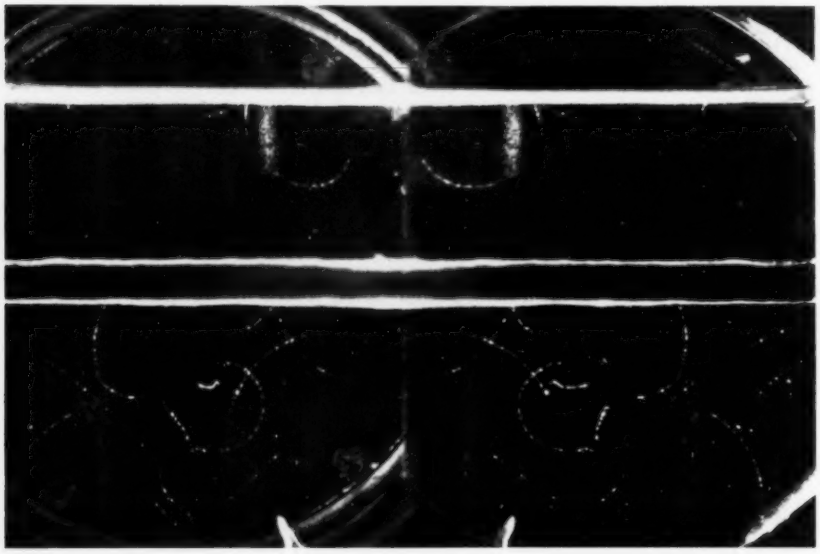

FIG. 3. 825 gauss field. A pair ejected from the upper lead plate and another from the central lead plate; also a group of some fifteen tracks of irregular distribution all ejected by soft photon rays, probably originating in the lead bar above the upper counter.

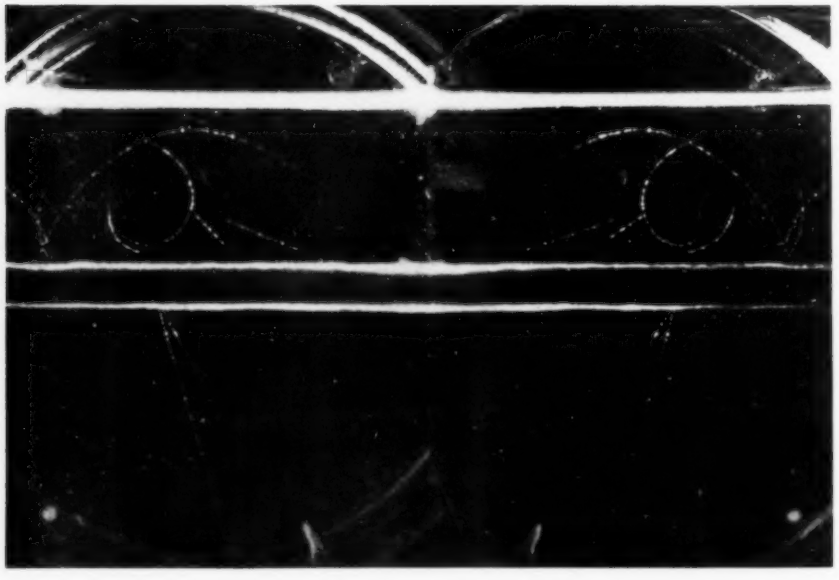

FIG. 4. 825 gauss field. A rather high energy pair is ejected from the lead plate by the absorption within it of a photon. The signs and energies of the components cannot be determined because of the weakness of the field.

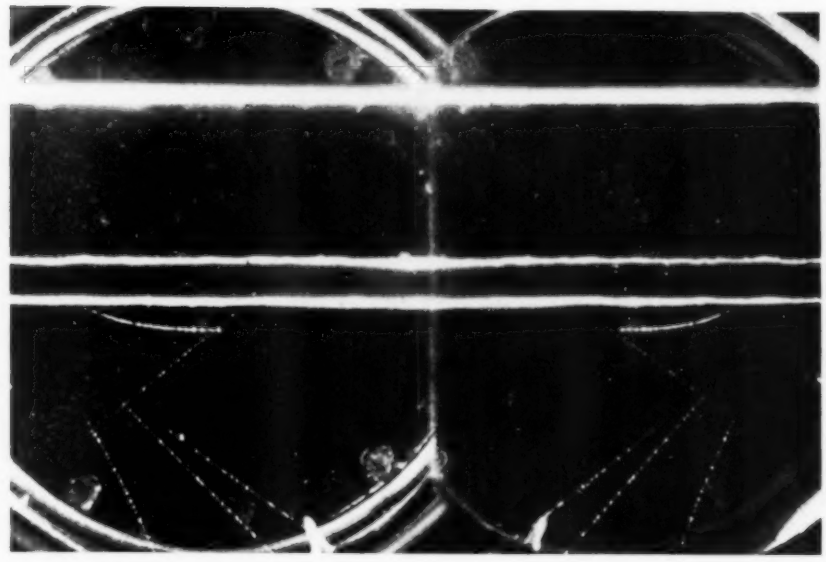

FIG. 5. 17,000 gauss field. Four tracks come from a common region behind the chamber. The fifth is definitely associated with them in time but has a totally different origin. We again postulate a secondary photon spray.

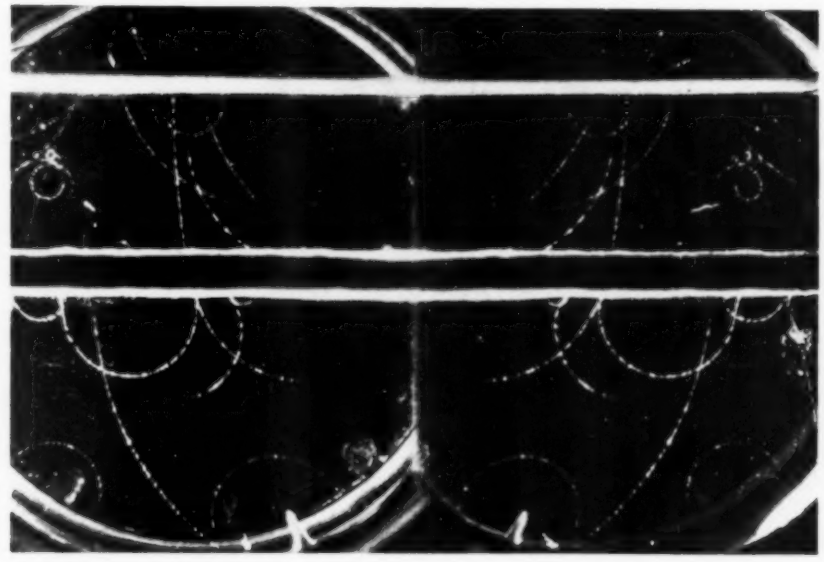

FIG. 6. 17,000 gauss field. Here again no single particle goes through the counters and the cloud chamber, but a secondary photon spray originating above ejects from the lead plates and the walls several pairs and a number of single electrons. A positron of energy 140×10^6 electron-volts penetrates the central 1 cm lead plate and emerges with an energy of 13×10^6 electron-volts after giving by a close encounter 6.7×10^6 electron-volts to a negatron.

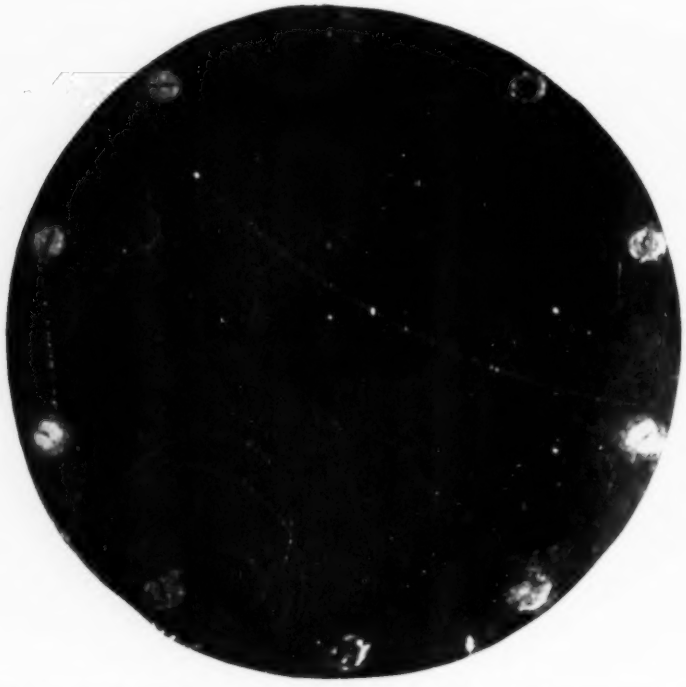

FIG. 7. 17,000 gauss field. An electron pair, positron 75 million electron-volts, negatron 290 million ejected presumably from the nucleus of a lead atom above the upper counter. These electrons in getting through or out of the nucleus presumably collided with its mass, and produced thereby "brems-strahlung." This photon spray shot downward and its absorption in the gas of the chamber, or the surface layer of its wall, produced the four secondaries seen between the electron tracks of energies in millions of electron-volts 9, 9, 4, 1.

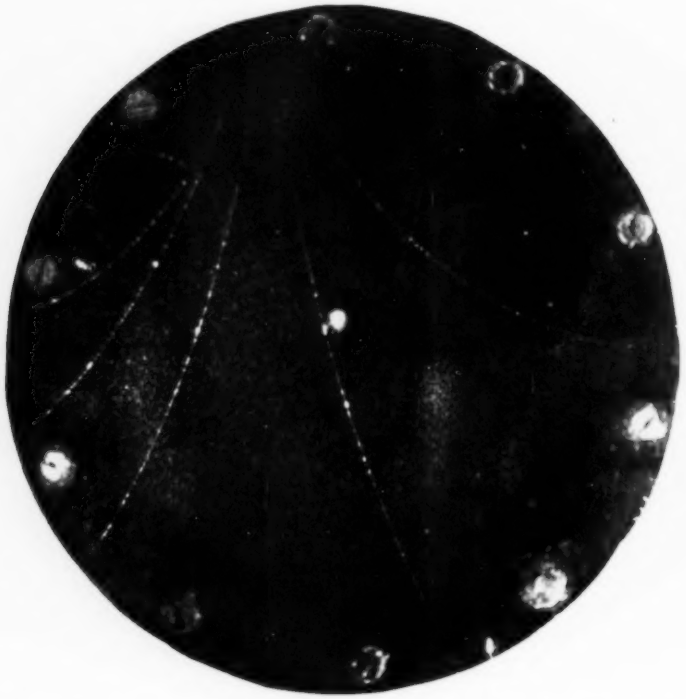

FIG. 8. 17,000 gauss field. A shower presumably originating in the impact of a cosmic-ray photon upon the nucleus of an atom of lead in the bar just above the top counter. Energies in millions of e.v.; positrons, 145, 38, negatrons 104, 65, 28; sum of all 380. Again the presence of secondary photons is demonstrated by the tracks of low energy particles at the left; their energies are: 6.7, 4, 2, 0.1.

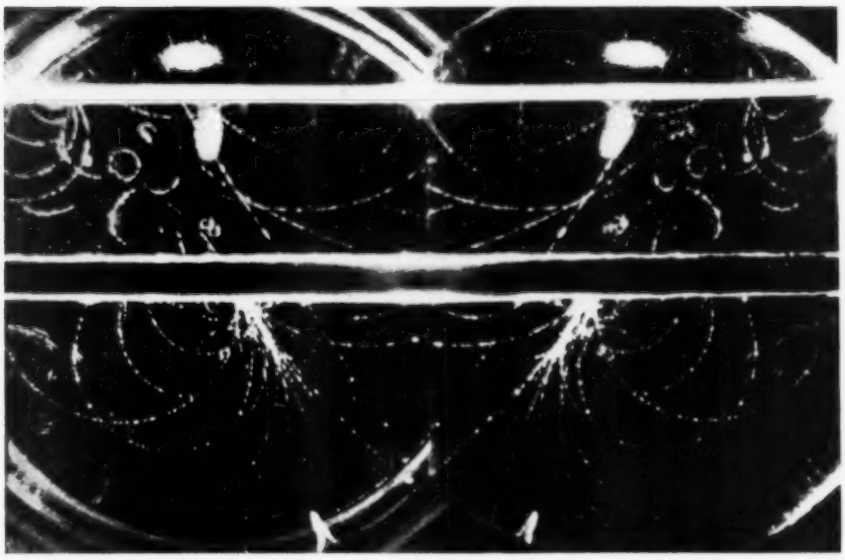

FIG. 9. 17,000 gauss field. The tracks in the upper part of the photograph, at least three of which converge to a region in front of the chamber, indicate the occurrence of a shower above the chamber. A second shower of 22 particles 7 positives, 15 negatives is seen to originate in the lead plate, the initial directions of the particles indicating that the photon (or photons) producing it passed through a point very close to the origin of the upper shower. The high energy positron (520 million electron-volts) passing through both lead plates probably has its origin at the point above the chamber through which passed the photon which gave rise to the showers. There are other tracks not in line with the main shower, as, for example, a group of three tracks from the upper lead plate at the left, which we attribute to the absorption there of secondary photons. The two heavy white patches just above and just below the upper lead plate cannot be associated in time with the shower. Their diffuse appearance may be explained by the assumption that they are due to recoil nuclei released *before* the expansion. The total energy of all the tracks is about a billion volts. All this suggests that a high energy photon may knock out one or many electrons from several nuclei which it may encounter along its path.

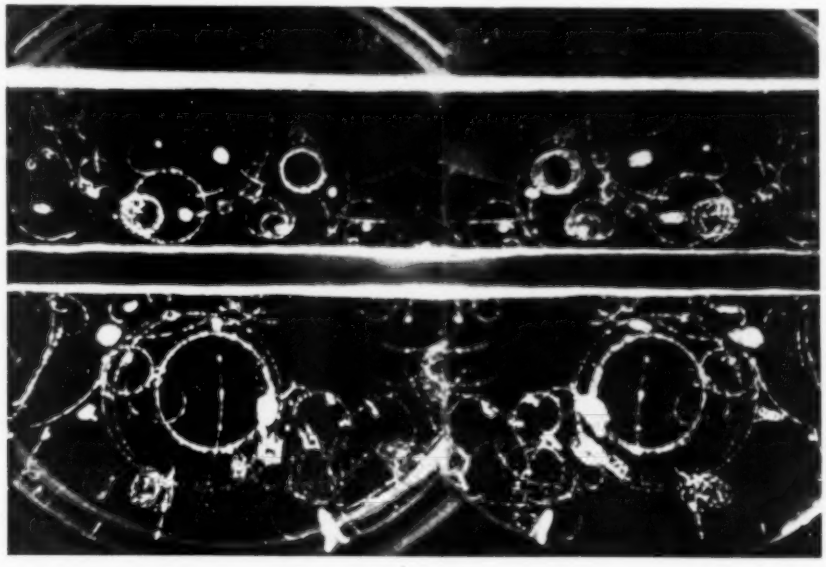

FIG. 10. 17,000 gauss field. More than 80 low energy tracks. A stereoscopic study of the orientations and directions of these tracks shows that in most instances their motions are nearly in the plane of the chamber so they could not have originated except from a considerable number of separate centers, hence indicating a large number of secondary low energy photons (100,000 to 10 million electron-volts) presumably resulting from the collision of a primary photon with a lead nucleus above the upper counter. It is this shower that must set off both counters, as well as produce the cloud-chamber effects.

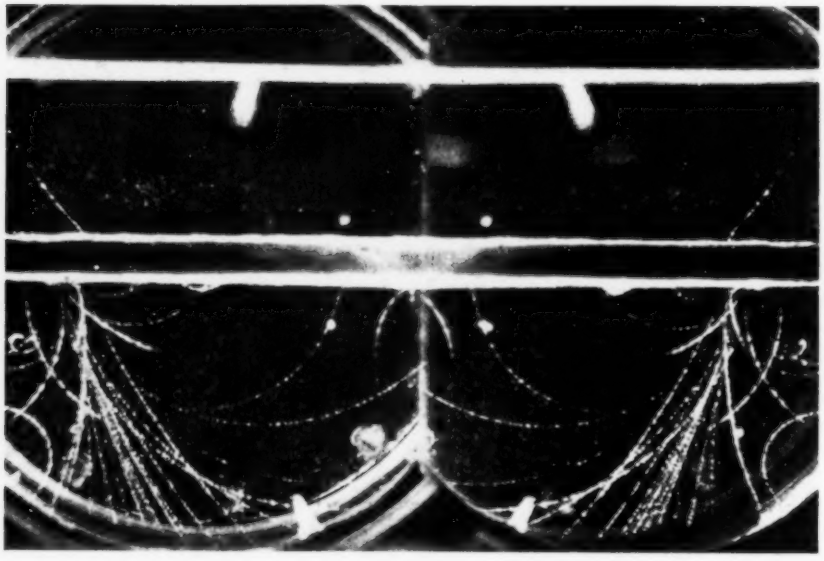

FIG. 11. 17,000 gauss field. Shower of 28 electron tracks resulting presumably from the absorption of a very high energy primary photon in the central lead bar. From one main center at the left there diverge 15 positrons and 10 negatrons, while the three remaining tracks may arise from the photon spray. The total energy is about 2.5×10^9 volts, slightly less than that of the highest energy single tracks we have observed.

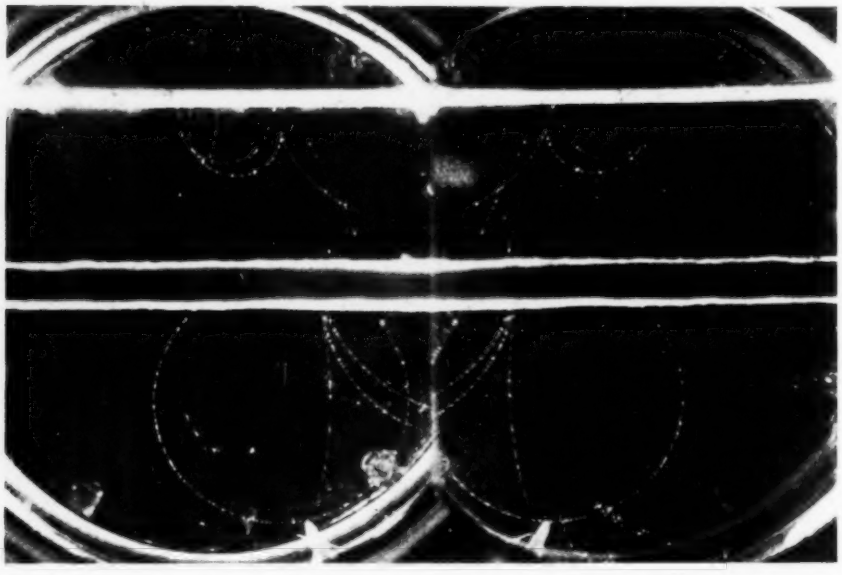

FIG. 12. 17,000 gauss field. An example, like Fig. 9, of associated showers. A pair from the upper sheet of lead and a group of three from the lower are ejected in the same general direction along the same straight line, and the pair which enters the top of the chamber originates not far from the line joining the centers of the two foregoing showers.

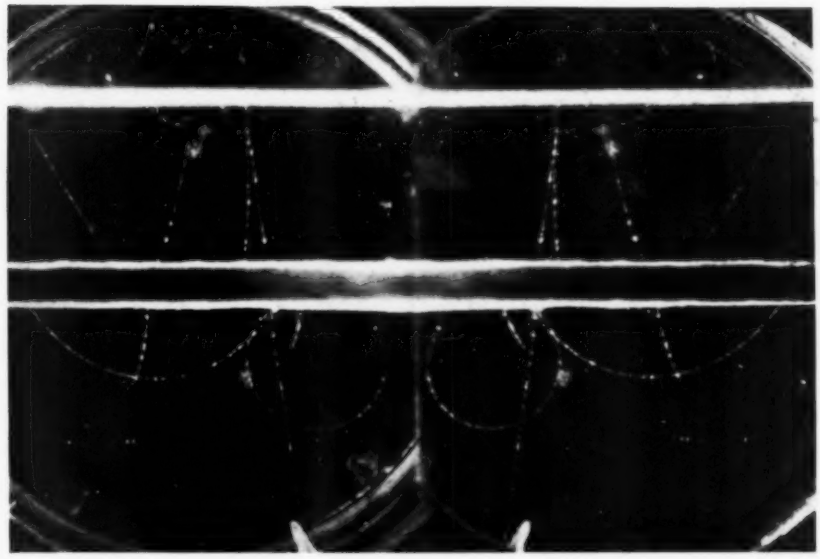

FIG. 13. 17,000 gauss field. One of the two observed cases of formation of a pair by a charged particle. Energies: (−) 16; (+) 7.6.

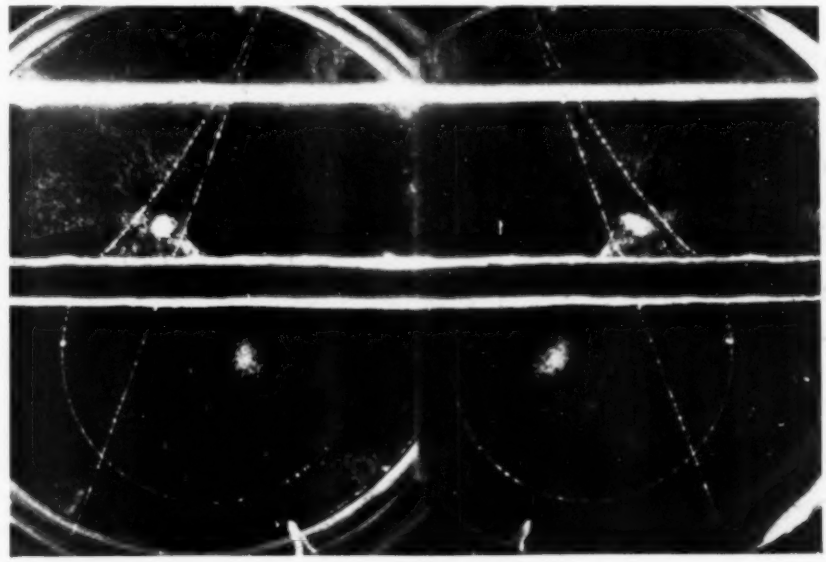

FIG. 14. 17,000 gauss field. At the left an electron passes into the middle lead plate and either transfers its energy to a positron or else forms a pair, both the negatron-component of the pair and the original negatron being absorbed in the lead. The former interpretation seems more likely. The difference in energy above and below the plate is consistent with observed values of the specific energy loss for electrons in lead, inasmuch as the fluctuations are rather large. Energies: (−) above, 90; (+) below, 26. (Specific energy loss 49×10^6 e.v./cm.)

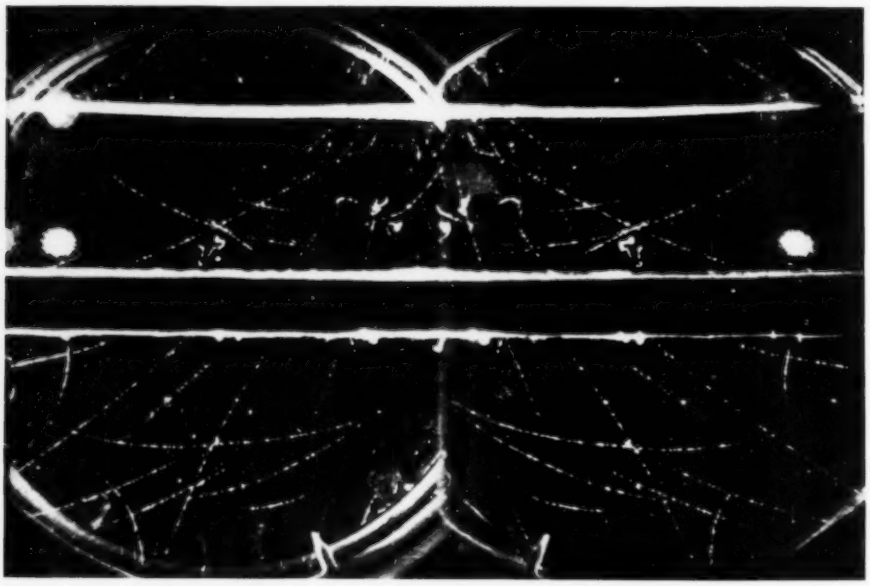

FIG. 15. 17,000 gauss field. The upper plate is lead, 2 mm thick; the center one, carbon 1.4 cm thick. A shower occurs in the upper right-hand part of the chamber, sending particles downward into the central slab of carbon. The absence of a shower from the carbon in this photograph, as well as in several other similar ones in which a second shower should certainly have been observed had the carbon been replaced by lead, demonstrates the relative inability of a carbon nucleus to absorb a photon by shower formation. There are, however, indications of extranuclear absorption of low energy photons generated in the shower.

by a multitude of separate particles all accurately associated in time as shown by identity in the sharpness or diffuseness of the tracks, but in general of low energy as revealed by the very strong curvatures of the tracks, since the field is here, for the first time, strong enough when the counter controlled method is used, *to produce measureable curvatures in all the tracks.* A common characteristic of these photographs is the wide and irregular distribution of the tracks, presumably due to a secondary photon spray (see (4) below).

(4) The fourth result is that there is clear photographic evidence that by a photon encounter with a nucleus in the lead or other solid matter above the upper counter, there is sometimes produced not only a shower of positrons and negatrons, but also a copious spray of relatively soft gamma-rays or photons presumably arising, precisely as in the case of the general gamma-radiation resulting from cathode-ray impacts upon the anticathode, from the impact of the electrons (+ and −) against the heavy parts of the exceedingly dense nucleus as these electrons, energized by the colliding photon, strive to escape from that nucleus. That these are not in general fluorescence gamma-rays is shown by the fact that these photons in general, though not always, appear *below* the point of encounter of the primary photon with a nucleus, not above it. Millikan and Neher have proved this by taking an electroscope to high altitudes in an airplane and finding that the ionization in that electroscope is essentially the same whether the electroscope rests upon a very heavy mass of lead or upon a very thin wooden support. The photographs, however, seem to furnish good evidence that *occasionally* a gamma-ray photon as well as an electron, shoots upward from the point of collision as well as downward. That the foregoing spray consists of gamma-rays or photons, rather than of neutrons, is proved by the fact that, in being absorbed by the surrounding matter, this spray apparently throws out many extranuclear electrons with energies from below 100,000 volts up to 20 or 30 million electron-volts—a behavior foreign to the nature of neutrons, which can impart high energies only to bodies of nuclear mass. None of our photographs taken thus far with this apparatus reveal the tracks of protons or of heavier nuclei, associated in time with the tracks

of the shower. We have, however, two or three isolated tracks which seem to be those of recoil nuclei.[6] These results are particularly evident from the photographs 7 to 15. Our interpretation of these photographs is set forth in the captions.

(5) The fifth result is that when no lead is inserted in the middle of the cloud chamber, out of 145 track photographs 141 show one track that at least may go through both counters, while 4 show no apparent possibility of a single track traversing both, but do show the characteristic photon-spray tracks. When, however, the strip of lead one centimeter thick is placed across the middle of the cloud chamber, out of 397 track photographs there are 358 in which one track may go through both counters, while there are 39 cases in which both counters are definitely set off by low energy sprays. In other words, 4/145 or 2.8 percent of the coincidences obtained with no intervening lead, do not represent a track through both counters. While when one centimeter of lead intervenes between the counters, 39/397 or 9.8 percent do not represent one single track going straight through both counters. It is then most significant for the theory of counter action that a piece of lead only one centimeter thick, between the counters, increases the number of coincidences which do not represent a straight track, from 2.8 to 9.8 percent. For thick lead plates between the counters, the differences would of course be higher. *Here is, then, very direct photographic evidence for the correctness of the foregoing theory of counter action when large amounts of heavy matter intervene between the counters.*

(6) The sixth result of these studies of counter-action is that when a slab of carbon, 1.4 cm thick, replaces the slab of lead in the middle of the chamber (see Fig. 15), very few showers or sprays appear, and as yet no evidence of neutron encounters. Out of 441 successful track photographs taken this way, while they show many showers coming in from above, nine of which have more than five tracks, there is no evidence of any secondary centers whatever formed within the carbon by secondary photons. There are in this case 29 photographs which show no apparent possibility of a single track traversing both counters, but do show the characteristic photon spray tracks, as compared to 412 cases where one track did pass through both counters; in 6.6 percent of the cases, therefore, a photon spray was responsible for the simultaneous responses.

(7) The seventh result of these studies is to show that when a shower occurs, the total energy in the shower is thus far never higher than the energy appearing in single electron shots. In other words, the energy of the incident photon may apparently be largely transferred to a single positron or negatron, or it may be divided between many such, and the accompanying spray of gamma-ray photons. Since 88 percent of the photographs show single electron shots even when materials of large atomic weight surround the chamber, the production of a shower is apparently a relatively rare event.

(8) The eighth result of these studies is to indicate that the simplest interpretation of the nature of the interaction of cosmic rays with the nuclei of atoms, lies in the assumption that when a cosmic-ray photon impinges upon a heavy nucleus, electrons of both signs are ejected from that nucleus and appear in the form of the positrons and negatrons shown in our photographs. The large, and the, in general uneven number of positrons and negatrons appearing in such photographs as those shown in Figs. 9 and 11, for example, seem difficult to reconcile with the Dirac theory, as interpreted by Blackett and Occhialini, of the creation of electron-pairs out of the incident photons, and point strongly to the existence of nuclear reactions of a type in which the nucleus plays a more active rôle than merely that of a catalyst. The essential difference between the two points of view is that in one case the nucleus changes its character and in the other it does not do so.

[6] While diffuse patches of ionization such as those reported by Locher (Phys. Rev. **44**, 779, 1933) occasionally appear in our photographs, it does not seem certain that they represent nucleus tracks produced by neutron encounters as he suggests. In fact, such patches of ionization occur more frequently immediately after the chamber has been filled with fresh air, and at least a part of their number therefore cannot represent cosmic-ray effects.

Widths of X-Ray Lines from Alloy Targets

LYMAN G. PARRATT,* *Cornell University*†

(Received January 22, 1934)

The widths of the $K\alpha$ x-ray lines have been found to depend upon the physical or chemical state of the target. Several alloys of Ni, Fe, Mn, Cr and Ti have been used. The widths of the lines of element A when alloyed with element B may be increased or decreased, depending on element B. Targets of Mn-Ni show an approximately linear increase in the width of $K\alpha_1$ with relative increase of Ni, reaching, at 50–50 atomic concentration, a maximum width of 23 percent greater than the width from pure Mn, then, with further addition of Ni, an approximately linear decrease with the same slope as before. In general the width of $K\alpha_1$ is more susceptible than of $K\alpha_2$ to changes in the atomic environment but the ratio of peak intensities varies in a compensating manner to allow the ratio of integrated intensities of α_1 to α_2 to remain constant, 2 to 1, within the estimated error of ± 4 percent. All the lines are asymmetrical.

IN the present study of the contour of the $K\alpha$ x-ray doublet a dependence of the line breadth and shape on the physical or chemical state of the emitting target has been observed. The widths of the lines of element A when alloyed with element B may be greater or less, depending on element B, than the widths of the lines of pure A. It seems possible that the effect is akin to the "pressure broadening" of lines in the optical region.

APPARATUS

The double-crystal vacuum spectrometer with which the ionization curves of these lines were taken has been previously described,[1] and the crystals, slits, method of recording readings, etc., discussed in an earlier paper.[2] The voltage with all the present targets was 15 kv and currents from 3 to 25 m.a.

With the removable target of the x-ray tube, the various alloy specimens of a given element were inserted without disturbing the settings or geometrical alignment of the instrument, thus allowing the rocking curves of the element in pure and in alloy states to be observed in more or less rapid and alternate succession. Since we are interested in comparing contours of lines of the same wave-length, the uncertain distortions due to the instrument itself (crystals and slits) are constant and of little or no importance.

TARGETS

All the targets, except the Mn_2O_3 (?) and Ti-Si, were produced[3] by an aluminothermic reduction from their oxides, thus assuring a relatively high degree of accuracy in their composition. The Mn_2O_3 was formed by oxidizing the surface of a pure Mn target by heating in air with a blow torch until a heavy layer of dark oxide had formed, probably a mixture of MnO, Mn_2O_3 and MnO_2. After completing the curves the oxide layer was visually examined and found to be imperceptibly altered by the uncertain physical conditions of the focal spot. The Ti-Si was obtained commercially and is of unknown preparation.

Unless otherwise designated the alloy liquidus was allowed to cool in air in the clay crucible in which it was prepared. The pure Mn was slowly cooled in a large sand bed, giving supposedly the α-phase. The α-Fe (single crystal) was produced by very slow cooling over a period of 1000 hours, and the γ-phase, with a trace (about 2 percent) of carbon present, by quenching. After the γ specimen had been used as a target it was polished, etched with alcohol and HNO_3, and

* National Research Fellow.

† Experimental part done at Ryerson Physical Laboratory, University of Chicago.

[1] Parratt, Phys. Rev. **41**, 553 (1932).

[2] Parratt, Phys. Rev. **44**, 695 (1933).

[3] The author is indebted to Mr. L. G. Hall, metallurgist of Ryerson Physical Laboratory, University of Chicago, for the preparation of most of the alloy specimens in this work.

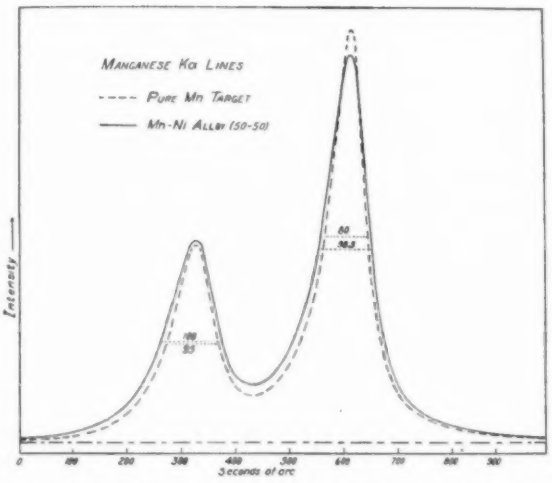

FIG. 1. Double-crystal ionization curves of the Mn $K\alpha$ doublet from targets of Mn-Ni alloy (50–50 atomic concentration) and pure Mn.

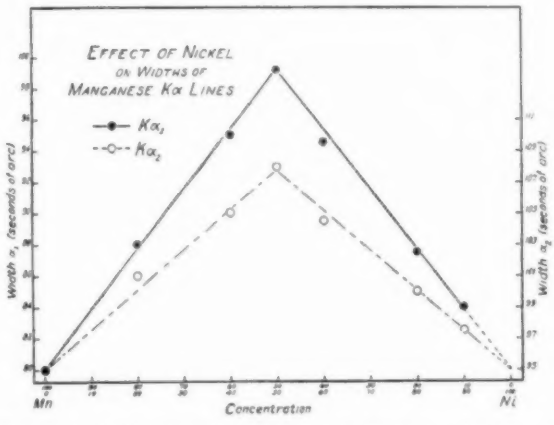

FIG. 3. Variations in widths of the Mn $K\alpha$ lines with concentration of Ni in Mn-Ni alloys.

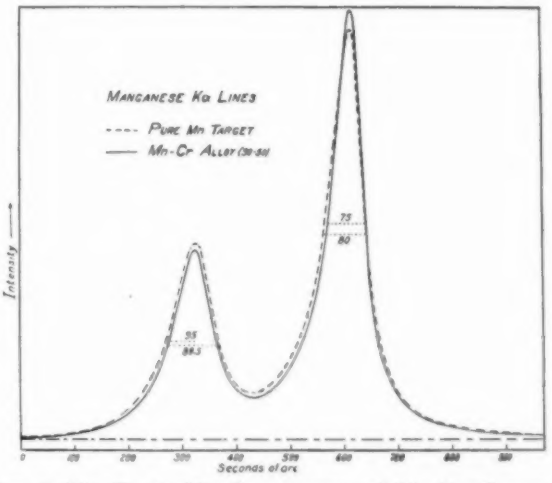

FIG. 2. Mn $K\alpha$ doublet from targets of Mn-Cr alloy and pure Mn.

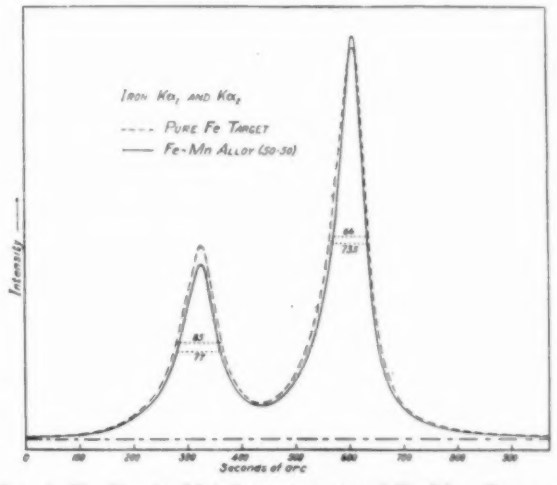

FIG. 4. Fe $K\alpha$ doublet from targets of Fe-Mn alloy and "pure" Fe.

microscopically examined. Both austenite, which is undercooled γ-Fe, and martensite, whose structure is now a controversial subject—possibly a strained α or a tetragonal lattice, were observed. Sufficient martensite was present to cause the sample to be ferromagnetic. We shall refer to this target as γ-Fe with the understanding that other forms of Fe were present and that the perturbing influence of the carbon on the x-ray line widths may not be negligible. Consequently, the data on "γ-Fe" in this paper should not be considered as quantatitive except, perhaps, for the particular alloy specimen used.

The concentration ratio of the alloys refers to atomic concentrations except in the cases marked (wt) where the basis is that of weight.

RESULTS

In Table I are presented the data obtained from Mn (25) and several Mn alloys. Figs. 1 and 2 give curves of Mn alloys superposed on the curve of pure Mn, showing a relative increase and decrease in the breadth of each of the $K\alpha$ lines. For just one alloy, the Mn-Ni series,[4] has the change in width been studied as a function of concentration. These data are shown in Fig. 3.

Measurements of the curves of pure Fe (26)

[4] The alloy system of Mn-Ni is reported in the literature as a continuous series of solid solutions, but many systems so reported have been found by careful x-ray analyses to have more than one solid phase. It has been suggested that the structure of the Mn-Ni alloys is also more complex than previously assumed.

and of Fe alloys are listed in Table II. The change in the Fe $K\alpha$ doublet due to the presence of Mn is indicated in Fig. 4. The difference between the two allotropic forms of Fe, the α- and γ-structures, is felt to be greater than experimental error and introduces an ambiguity as to which form should be used, for purposes of comparison, as characteristic of Fe. Fig. 5 shows graphically the widths of both irons in relation to the widths of neighboring pure elements. In Fig. 4 the quenched or γ-Fe is arbitrarily taken as representing "pure" Fe for the reason that the lattice structure of the Fe-Mn alloy is that of γ-Fe, face-centered cubic. Supposedly the α-phase of Mn and Cr is the one present in the "pure" targets of each of these elements.

Table III gives the data from a few other alloys and Fig. 6 the perturbing influence of silicon on the titanium atoms.

Certainly one or more molecular layers of oxide had formed on most of these targets in the few minutes between the final cleaning, by filing, and the pumping out of the x-ray tube. The effect of this oxide is probably small in all cases except calcium which oxidizes rather readily. Consequently the widths of the $K\alpha$ lines of Ca given in Fig. 5 may include the effect of the oxygen. A slight amount of tungsten was sputtered on the targets from the filament of the tube but the effect of these foreign W atoms is probably negligible due to the relatively great average depth in the target at which the x-rays are generated.

The width of $K\alpha_1$ is, in general, more susceptible than that of $K\alpha_2$ to alterations in the atomic environment. In just one instance, that of the Ti-Si target, were the changes in widths of α_1 and α_2 of opposite sign. Except for the two pure

TABLE I. *Rocking curves of Mn Kα lines not corrected for overlapping.*

Target	Full Width at Half Max.				Ratio of peak intensities α_1/α_2
	X. Units		Pure Mn taken as 1.00		
	α_1	α_2	α_1	α_2	
Mn pure annealed	1.10	1.31	1.00	1.00	2.15
Mn_2O_3 (?) compound	1.27	1.46	1.15	1.12	2.10
Mn-Cu 30–70	1.30	1.45	1.18	1.11	2.00
Mn-Cr 50–50	1.03	1.22	0.94	0.93	2.17
Mn-Fe 50–50	1.15	1.33	1.05	1.02	2.13
Mn-Ni 80–20	1.21	1.39	1.10	1.06	2.05
Mn-Ni 60–40	1.31	1.45	1.19	1.11	2.00
Mn-Ni 50–50	1.36	1.49	1.23	1.14	1.98
Mn-Ni 40–60	1.30	1.44	1.18	1.10	2.06
Mn-Ni 20–80	1.21	1.38	1.09	1.05	2.07
Mn-Ni 10–90	1.16	1.34	1.05	1.03	2.13

TABLE II. *Rocking curves of Fe Kα lines not corrected for overlapping.*

Target	Full Width at Half Max.				Ratio of peak intensities α_1/α_2
	X. Units		γ-Fe taken as 1.00		
	α_1	α_2	α_1	α_2	
Fe quenched γ-Fe	1.02	1.18	1.00	1.00	2.07
Fe pure annealed α-Fe	1.06	1.23	1.04	1.04	2.17
Fe-Cr 50–50	1.00	1.15	0.98	0.98	2.05
Fe-Cr 40–60 (wt) annealed	1.01	1.17	0.99	0.99	2.09
$FeAl_2$ compound	0.97	1.18	0.95	1.00	2.15
Fe-Mn 50–50	0.92	1.07	0.90	0.91	2.20
Fe-Ni 50–50	1.06	1.23	1.04	1.04	2.00
Fe-V 50–50	0.96	1.14	0.94	0.96	2.14

TABLE III. *Rocking curves of Ni, Cr and Ti Kα lines not corrected for overlapping.*

Target	Full Width at Half Max.				Ratio of peak intensities α_1/α_2
	X. Units		Pure taken as 1.00		
	α_1	α_2	α_1	α_2	
Ni pure	0.71	0.91	1.00	1.00	2.30
Ni-Mn 40–60	0.77	0.97	1.07	1.06	2.32
Cr pure	1.09	1.40	1.00	1.00	2.26
Cr-Fe 60–40 (wt) annealed	1.11	1.43	1.02	1.02	2.15
Ti pure	1.24	1.58	1.00	1.00	2.19
Ti-Si 83–17 (wt) compound excess Ti	1.14	1.63	0.92	1.03	2.43

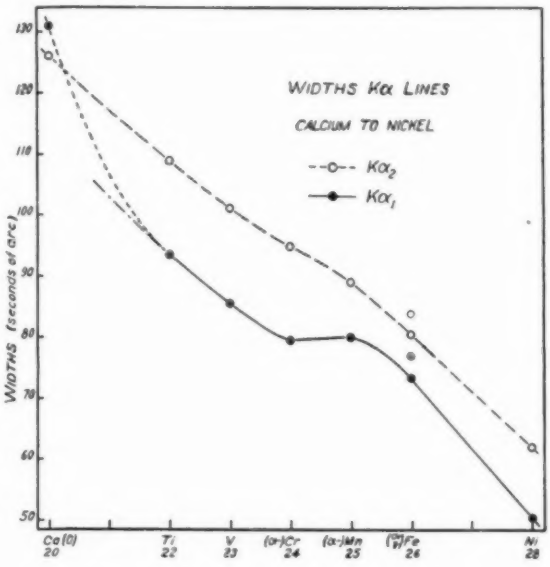

FIG. 5. Widths in seconds of arc of $K\alpha$ lines of pure elements. The two allotropic forms of Fe, α and γ, are given, the lower values those of γ-Fe. The α-phase of Cr and Mn is supposedly present in these two targets. An oxide layer on the surface of the Ca target may have an effect on the widths of the lines of Ca.

irons, a decrease in width is attended by an increase in the ratio of peak intensities[5] and *vice versa*. This is to be expected in view of the relative changes in widths of α_1 and α_2 *if* the ratio of the integrated intensities of the two (component) lines be supposed constant.

An attempt has been made to resolve the observed overlapping curves into the two components, α_1 and α_2, but the method is one of trial and error[2] since the components are asymmetrical and of different degrees of asymmetry. The ratio of the areas under the component curves may be defined as the ratio of intensities of the two lines, and this areal ratio, measured with a planimeter, remains constant irrespective of the alloy composition of the target within the error of drawing

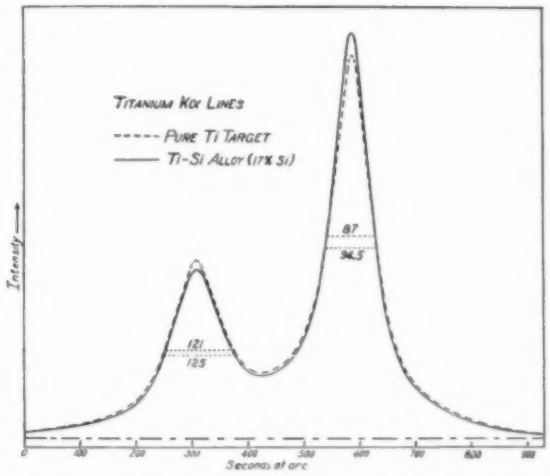

FIG. 6. Ti $K\alpha$ doublet from targets of Ti-Si alloy and pure Ti.

the component curves, estimated as less than 4 percent. The values of widths and peak intensity ratios listed in the tables are in description of the observed contours, uncorrected for overlapping.

There is a suggestion in the curves that the alterations in widths are not entirely symmetrical, possibly a greater effect being present on the long wave-length side. Part of this difference may lie in the error of superposing the alloy curves on those of the pure elements.[6]

The experimental error in the width measurements as estimated from the consistency of several curves for each target is less than ± 2 percent.

DISCUSSION

The information available in regards to the structures of alloy systems is as yet meager. Temperature equilibrium diagrams, many of them lacking in detail, of certain alloys and a few x-ray analyses of crystal structure comprise our knowledge to date.

[5] The ratio of peak intensities as given in the tables is subject to several corrections one of which is the absorption of the x-rays in the target. As Williams (Phys. Rev. **44**, 146 (1933)) has shown this correction is usually very small, entirely negligible for the wave-length difference (4 X.U.) between α_1 and α_2 excited with tube voltage as low as 15 kv. With the Fe-Cr target, and a similar relation applies with a few other targets, the wave-length of Fe $K\alpha$ radiation is shorter than the wave-length corresponding to the K absorption limit of Cr. Consequently the absorption of Cr for the region of Fe $K\alpha_1$ and α_2 varies much more rapidly with wave-length than does the absorption of Fe. However a simple calculation (after Williams) shows that the difference in the ratio of peak intensities due to the differential absorption of the Fe and Cr is less than the experimental error in the electrometer readings.

[6] The wave-length of α_1 or α_2 (or the separation $\alpha_1 \rightarrow \alpha_2$) differed with alloying, if at all, by less than 0.14 X.U. or, in angular measure, by less than 10 seconds of arc. The spectrometer, because of the action of the stopcock grease in the bearings of axis B, would not repeat angular positions with certainty within this range of ± 5 seconds. Angular distances, however, could be repeated within 1 or 2 percent.

When two metals, A and B, are mixed together to form an alloy the atoms of B either replace atoms of A in the A lattice structure or enter the interspaces of the A lattice. When the atoms are more or less the same size, as is the case in most of the alloys considered in this paper, the former, the replacement process, is the one in effect, and the resultant lattice of A appears to be stretched or shrunk according, apparently, to whether atom B is greater or smaller than atom A. With further addition of atoms B, the limit of this homogeneous distortion of the A lattice may be reached, and, if so, the structure changes to that of another allotropic form of A or assumes the lattice of B. In the latter case the A atoms become the invaders. The region of concentration in which these lattice structures occur may overlap, with resultant mixed crystals. In case a definite compound of A and B is formed the picture can be somewhat more complicated by the addition of the third unit of structure, and much more so if a different type of internal binding is introduced. These relations have been ascertained[7] directly by x-ray crystal analyses and, to a certain extent, may be inferred from the temperature equilibrium diagrams.

One of the characteristics of a metallic element is its apparent constancy of atomic volume, irrespective of the alloy structure. The atomic volumes of elements V to Cu are given in Table IV, calculated by Bernal[8] from Goldschmidt's[9] atomic radii.

TABLE IV. *Atomic volumes* ($\times 10^{-24}$).

V	Cr	Mn	Fe	Co	Ni	Cu
14.25	11.9	14.85	11.6	11.35	10.9	11.8

Mn-Cu[10]

The addition of Mn to Cu from 0 to 30 percent Mn increases the Cu lattice constant from 3.6 to 3.7A. Further additions of Mn cause the lattice of Cu to give way to that of Mn. The temperature equilibrium diagram of this alloy shows a strong minimum at about 30 percent Mn, evidence, perhaps, that at this concentration the homogeneous distortion of the lattice is at its limit. For alloys not strictly isomorphous, the melting-point curve of the equilibrium diagram is of less importance than the changes in the solid phases. For example, at approximately 400°C the alloy of 30 percent Mn changes, upon further slow cooling, from the Cu lattice to that of β-Mn. The temperature of the emitting part of the target is of course unknown. The region of the focal spot as a whole is probably less than 400°C for this and most of the other targets concerned in this paper, but the neighborhood conditions of those individual atoms bearing the brunt of the enormous electron impacts are a matter of pure conjecture. No curves of the Cu $K\alpha$ doublet were taken for this target but the widths of the Mn lines are considerably increased as compared with the lines from pure α-Mn. No targets of pure β-Mn were attempted.

Mn-Fe[11]

Alloys of from 40 to 60 percent Mn have the lattice of γ-Fe, face-centered cubic, with the lattice constant, at 50–50 concentration, 3.63 as compared with 3.58A for pure γ-Fe. No minimum is observed in the complex equilibrium diagram. The Fe lines are narrowed and the Mn lines broadened.

Mn-Ni[4, 12]

There exists a greater difference between the atomic volumes of Mn and Ni than any other pair of metals studied. The equilibrium diagram shows a very marked minimum at approximately 50–50 concentration, very similar in form, when inverted, to the variations in the widths of the Mn lines, Fig. 3. Both the Mn and Ni lines are increased in widths.

α-Fe and γ-Fe

Goldschmidt[13] has pointed out that a change in coordination number from 8 to 12, that is, a

[7] *Strukturbericht*, 1913–1928, Zeits. f. Kristallographie.

[8] Bernal, Trans. Faraday Soc. **25**, 367 (1929).

[9] Goldschmidt, Trans. Faraday Soc. **25**, 253 (1929).

[10] Patterson, Phys. Rev. **23**, 552 (1924); Persson, Zeits. f. physik. Chemie **9**, 25 (1930); Bain, Chem. Met. Eng. **28**, 21 (1923); Zemczuzny, Urasow and Rykowskow, Zeits. f. anorgan. Chemie **57**, 253 (1908).

[11] Bain, reference 10; Ohman, Zeits. f. physik. Chemie **B8**, 81 (1930).

[12] Zemczuzny, Urasow and Rykowskow, reference 10.

[13] Goldschmidt, Zeits. f. physik. Chemie **133**, 397 (1928).

transformation of the α-lattice, body-centered cubic, into the γ-form, close-packed, is associated with an increase in the atomic diameter of about 3 percent. The lines from the more compact atoms of the α-Fe are wider than from the γ-structure.

Fe-Cr[14]

α-Fe and α-Cr have the same crystal lattice and very nearly equal atomic volumes. The Fe curves from the alloy are somewhat narrower than those from pure α-Fe, while the Cr lines are unaltered or slightly broadened.

Fe-Ni[15]

Over a large intermediate range of concentrations both the body- and face-centered Fe lattices are present, the relative amounts depending on the heat treatment. The equilibrium diagram is not simple, showing both a maximum and a minimum. The Fe and Ni atoms have similar atomic volumes. The widths of the Fe lines are the same as those obtained from pure γ-Fe.

Fe-V[16]

The equilibrium diagram of this alloy system has a pronounced minimum, and there is a large difference in atomic volumes. Both elements have body-centered cubic crystals, and the narrowed Fe lines should perhaps be compared with the α-form of pure Fe.

The data are too fragmentary to permit explanations or correlations. Little is known of the forces involved in the metallic bond and even less as to the factors responsible for x-ray line widths. Just how the effects of alterations in the atomic environment, usually supposed to affect the outer or valence electrons only, can penetrate to the inner electrons involved in the $K\alpha$-radiation is not obvious. Perhaps by changing the values of the energy levels by altering the field potential of certain atoms more than others due to their particular positions in the space lattice relative to the invading atoms. Perhaps by subdividing the energy states according to a Stark or Zeeman effect. Perhaps by altering the emission probability coefficients.

In conclusion the author expresses with pleasure his indebtedness to Professor S. K. Allison, Ryerson Physical Laboratory, University of Chicago, for the privileges of working in his laboratory where the data of this paper were taken.

---

[14] Kreutzer, Zeits. f. Physik **48**, 556 (1928); Oberhoffer and Esser, Stahl Eissen **47**, 2021 (1927); Bain, reference 10.

[15] McKeehan, Phys. Rev. **21**, 402 (1923); Bain, reference 10.

[16] Asawa and Oya, Sci. Rep. Tohoku Imp. Univ. **18**, 727 (1929).

Characteristic X-Rays from Metals in the Extreme Ultraviolet

H. M. O'BRYAN, *Massachusetts Institute of Technology*
AND
H. W. B. SKINNER, *Wills Physical Laboratory, Bristol, England*

(Received December 4, 1933)

Soft x-ray bands in region 50–500A from Li, Be, C, Na, Mg, Al, Si and Ba targets. A 2-meter grazing-incidence spectrograph was used. The bands (except those for Ba) correspond to transitions of outer (or conduction) electrons into a vacant K- or L-shell. The diffuseness of the bands is associated with the energy spread of the filled conduction electron levels. The Ba band is an $O \rightarrow N$ transition. The other metal bands extend over a fairly wide wave-length region and each has a sharp short wave-length edge which corresponds to the sharp "surface" of the filled conduction electron levels. The bands of C and Si have a more diffuse head which is connected with their semiconducting property. The energy spread of the metal bands may be calculated approximately from the Sommerfeld theory of metals; this provides a method of determining uniquely the number of conduction-electrons per atom in a metal. But the explanation of the precise shapes of the bands will require a more detailed theory and in particular an investigation of the transition probability of a conduction electron into a K- or L-shell. Some discussion is added on the absolute energies involved in the transitions which give rise to the bands.

THE radiation emitted when free electrons in a metal make transitions into the relatively sharp K- or L-levels which have been ionized by electron impact furnishes one of the most direct sources of information about the energy states of conduction electrons in the unexcited metal. DuMond[1] has recently published results on the breadth of the Compton scattered band from beryllium and carbon and has been able to make inferences about the momentum of the electrons in the metal. However, since the electrons of even a free atom have a finite momentum spread, these results are not very sensitively affected by the actual lattice-binding. In working with the soft x-ray emission-bands, one has the advantage that the actual energy levels of the electrons in the metal are directly involved; and also the dispersion of the spectrograph used (in the region 50 to 500A) is easily able to show fine details within the actual energy-spread of the conduction electrons (of the order of 10 volts). An attempt to use the K-band of beryllium, as measured by Söderman,[2] was made by Houston.[3] He was led to the conclusion that the conduction electrons were badly represented by a theory of the Sommerfeld type. In a recent note[4] we have shown that this conclusion is not supported if our measured band of beryllium is used in place of Söderman's. The discrepancy between his result (and also that of Prins[5]) and ours may probably be traced to the question of cleanness of the beryllium surface. Simultaneously with our note, Osgood[6] has published a photometer trace of the aluminum L-band; his result agrees fairly well with ours, except that he has missed an interesting structure effect. We have also observed the bands of lithium, magnesium and silicon, and rather inadequately, those of carbon and sodium. The carbon results agree reasonably with observations of Söderman[7] and Renniger.[8] Since our note, Siegbahn and Magnusson[9] have published in a brief preliminary note the wave-lengths of the bands of Mg, Al and Si. These agree closely with our wave-lengths.

[1] DuMond, Rev. Mod. Phys. **5**, 1 (1933).
[2] Söderman, Zeits. f. Physik **65**, 656 (1930).
[3] Houston, Phys. Rev. **38**, 1791 (1931).
[4] O'Bryan and Skinner, Phys. Rev. **44**, 602 (1933).
[5] Prins, Zeits. f. Physik **69**, 618 (1931).
[6] Osgood, Phys. Rev. **44**, 517 (1933).
[7] Söderman, Zeits. f. Physik **52**, 795 (1929).
[8] Renniger, Zeits. f. Physik **38**, 510 (1932).
[9] Siegbahn and Magnusson, Nature **132**, 750 (1933).

Experimental Method

The soft x-ray bands were photographed on a 2-meter glancing-incidence vacuum spectrograph of the same general construction as those used in Siegbahn's Laboratory. The glass grating ruled by Professor R. W. Wood with 30,000 lines per inch was lightly etched with hydrofluoric acid as previously described by O'Bryan.[10] The extreme astigmatic property of the concave grating at angles near grazing incidence made possible a direct comparison of the spectra from narrow strips of the grating surface perpendicular to the ruled lines, and in this way it was shown that the first-order spectrum was increased in intensity at least twenty times by the proper amount of etching.

The incident radiation made a mean angle of about 6° with the grating surface. The slit-width was normally 0.3 mm but was reduced to 0.075 mm for certain exposures. A system of diaphragms was inserted between the grating and the slit to prevent scattered light or localized fogging of the plate. The light from the direct image was trapped effectively, and diffused light from the inside of the spectrograph was prevented as far as possible from reaching the plate.

The purity of the metal surface from which the radiation is emitted is of great importance, since metals have a high absorption coefficient both for radiation in this wave-length range (50 to 500A) and for the bombarding electrons (of 2000 volts energy). With the exception of carbon, all the elements we have tried were evaporated onto a copper anode in a high vacuum; the surface could thus be renewed at suitable intervals during the exposure. In this way, surfaces were obtained which we believe give x-rays characteristic of the pure metal and in fact in one case (beryllium) evidence will be given of the effect of the inevitable fouling of the surface after a period of electron bombardment. The carbon surface used was one produced accidentally by the decomposition of hydrocarbons in a good vacuum. From this surface seven orders of the carbon K-line were obtained on one plate. The absence of this line from all other plates is good evidence of freedom from other contaminations such as oxygen and nitrogen which are often present.

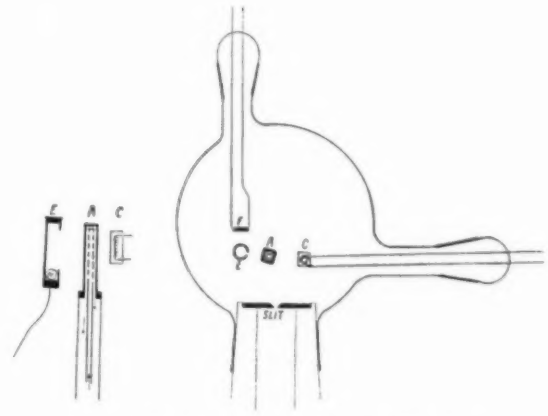

Fig. 1. X-ray tube and evaporating oven.

The x-ray tube was a one liter glass bulb fitted to a cone around the spectrograph slit as shown in Fig. 1. Into it are fitted, by means of cones in side tubes, the hot cathode C, the oven E used for evaporating the metals, the auxiliary filament F used for heating E, and the target A. The latter was a square sectioned copper rod about 6 mm thick, drilled for water cooling so that the minimum thickness of wall was about 1/10 mm. The rod was placed parallel to the slit (at about 2 cm from it) and was carefully lined up optically with the spectrograph by slight bending of the glass tube holding it. It could be rotated so that any of the four sides could be put in place for the exposure. The position chosen was one in which the radiation entering the spectrograph made an angle of about 10° with the surface. In this way, a fairly large area of the anode was effective in spite of the narrow angle (about 2°) taken in by the spectrograph. When the apparatus was satisfactorily evacuated, the anode was heated to a dull-red by discontinuing the water cooling and bombarding with electrons to free it as far as possible from gas. The cathode C was a dull-emitter consisting of a nickel box coated with barium oxide, indirectly heated by a tungsten filament. It was placed about 3 mm from the anode, and with a 2000 volt acceleration, a current of 500 m.a. was possible. A focussing cylinder (not shown in the diagram) was mounted around the filament. The evaporating oven E was a hollow molybdenum cylinder

[10] O'Bryan, Phys. Rev. **38**, 32 (1931).

closed at the ends with a slit in the side which faces the anode. It was heated to a suitable temperature by electron-bombardment from the filament *F*. To get a steady evaporation of clean metal, it was necessary to overheat *E* for some time to drive out the occluded gases. One side of *A* was sacrificed for this purpose. When all signs of gas discharge had ceased, a fresh side of *A* was turned towards the oven and a coating was slowly put on at a gas pressure of less than 10^{-5} mm. Generally all four sides of *A* were coated since this appeared to prevent gas-liberation by electrons which had strayed around the anode. This method of evaporation worked well even for a substance with so low a vapor pressure as silicon which required a temperature of at least 1500°C for evaporation. The temperature of the target surface under electron bombardment is rather difficult to estimate. For good heat conductors, it was probably less than 200°C; but with carbon there were glowing particles visible on the surface.

The spectrograph was exhausted to a pressure of about 10^{-4} to 10^{-5} mm by continued pumping by a Gaede 4-stage steel mercury pump and liquid air trap. A fast multi-jet glass mercury pump kept the pressure in the x-ray tube down to 10^{-6} mm at which pressure exposures were made. The pressures were measured by ionization gauges. Liquid air traps were placed in the lines of both pumps and a glass bulb inside the body of the spectrograph was usually filled with liquid air to remove vapors. In this way the time necessary before the spectrograph vacuum was sufficiently good for use was considerably shortened. The good vaccum was required partly to prevent surface contamination of the anode and partly to increase the temperature efficiency of the dull-emitter. If the pressure were allowed to get high, it became necessary to overheat the filament to get sufficient electron current; then it was found that barium was distilled on to the target and barium lines appeared on the plate. In a bad case, the barium might mask the element to be investigated; but it was quite possible by paying attention to the vacuum to avoid the barium lines completely. The tube was kept free from carbon vapors by the use of a mixture of the low vapor-pressure Apiezon grease with powdered graphite on the cones. In fact the carbon *K*-line only appeared on a single plate taken early in the series of exposures.

Eastman "Spectroscopic" plates were used coated with Apiezon oil. This combination was found fairly satisfactory for photometry provided the oil was carefully applied by a soft leather pad. With a beryllium target, a good exposure was taken in 15 minutes with an applied potential of 2000 volts and a current of 400 m.a. This represents the shortest exposure; often several hours were necessary. With lithium surfaces, for example, we had to work with a considerably lower current and to recoat frequently because of the tendency to melt and to acquire obvious contamination under the electron bombardment. With sodium, the metal tended to flow away from the spot bombarded leaving a very foul surface, and the problem was not adequately solved. For all the other metals, it was easy to keep the surface spotless during the course of the exposure by redistillation at about half-hourly intervals.

The standard voltage chosen was 2000 volts supplied by a 60 cycle transformer rectified by two 866 mercury vapor tubes. No smoothing was used. The power input was limited by the boiling of the water cooling. Spectra of beryllium were also taken with accelerating voltages of 700 volts and 10,000 volts. They showed no essential differences as far as the structure of the line was concerned but the general continuous background seemed to increase with the voltage. There was no evidence of any great alteration in the exposure time for different voltages with equal power input; but this could not be maintained at its maximum value for the lowest voltage.

The wave-lengths were determined by placing the spectrum of a vacuum hot spark on the same plate as the x-ray spectrum. Electrodes of aluminum and beryllium were used and the wave-lengths were taken from a paper by Soderquist and Edlen.[11] The metal spark chamber fitted on the cone around the spectrograph in the place usually occupied by the x-ray tube. It was necessary to admit air to the spectrograph during the change of sources but the photographic plate was not touched. The Be, Li, Mg and Ba wave-

[11] Soderquist and Edlen, Zeits. f. Physik **69**, 356 (1931).

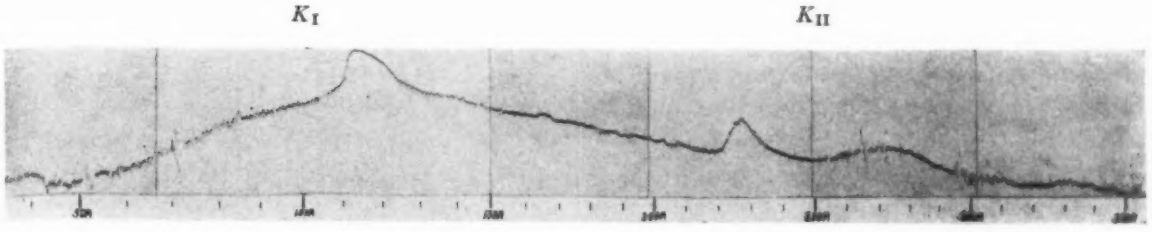

FIG. 2. Photometric curve of a heavy Be exposure.

lengths were compared directly with spark lines. The accuracy of measurement was limited entirely by the difficulty of fixing a definable characteristic of the radiation band; but a precision of a few tenths of an Angstrom could be attained. The other x-ray bands (of C, Al, Si) were determined by using these known x-ray bands as standards. Only for Si, which had no standard sufficiently near, was the loss in accuracy serious.

RESULTS

Fig. 2 shows a photometric curve of a heavy exposure with a beryllium target over an extended range of the spectrum. The humps near 115 and 230A are the Be K-radiation in the first and second orders. Besides these, there is a strong continuous background which is not due to scattered visible or near ultraviolet radiation. It is hard to be sure that it is a genuine continuous spectrum, but there was some indication from the intensity distribution that this is really the case. If so it may possibly be partly due to contamination. The faint broad band at about 137A is certainly due to contamination of the target; that at 270A is perhaps the second order of the other although its intensity seems at first sight too great.

Fig. 3 shows (a) a good Be exposure in the first order of suitable density for photometry. The slit width was 0.075 mm and the target was frequently recoated. Also (b) an exposure from a target which had been run for two hours without recoating. There was an obvious brownish spot on the surface, almost certainly due to oxidation. Originally the surface had given a spectrum like (a), but the band has become broadened to the long wave-length side. The sharp edge of (a) is missing and two extra bands are to be seen, one at about 117A and the other at about 137A. The generally broadened band looks somewhat similar to those found by Söderman and Prins who worked at considerably higher gas-pressures than we have and without distillation. Some faint but (on the original plate) quite definite signs of structure are to be found even on (a) on the long wave-length side of the maximum. These are perhaps due to residual contamination.

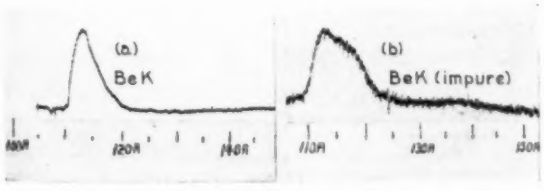

FIG. 3. Structure of beryllium K.

Fig. 4 shows (a) a lithium exposure in which slight hump on the short wave-length side is probably genuinely present, if so it may be due to impurity; (b) a magnesium exposure in which the main features have been carefully verified, in particular the curious minimum and sudden rise near the head; (c) an aluminum exposure showing rather similar characteristics; (d) a silicon exposure in which the main feature is the unsharpness of the band-head; (e) a barium exposure showing a quite different form from the remaining bands.

To obtain the actual energy distribution of the emitted radiation, the plate was calibrated with a quartz spectrograph in the region below 3800A (the approximate region of the oil fluorescence under the action of soft x-rays). A series of photometric screens[12] was kindly lent by Professor Harrison. To obtain the energies, it is necessary to assume that the wave-lengths in a given band are equally efficient in producing fluorescence in the oil, but as the bands are not

[12] Harrison and Leighton, Phys. Rev. **38**, 899 (1931).

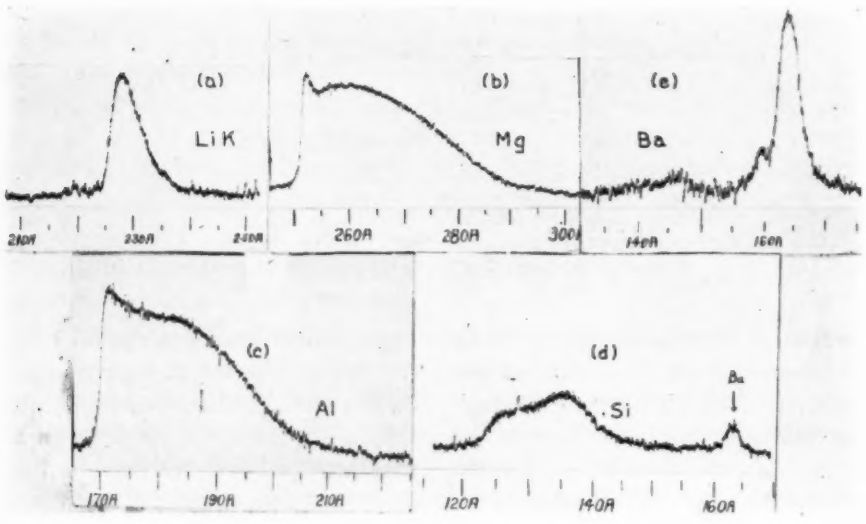

FIG. 4. Photometer curves of x-ray lines.

very wide compared with their absolute frequency, this is probably legitimate. Corrected curves of the intensity of the radiation (on an arbitrary scale) plotted against the energy of the quanta (in volts) are shown in Fig. 5 for the elements Li, Be, Mg and Al. It is worth noting that, besides characteristic differences in the forms of the curve near the band-head, there is a definite difference in the tail-shapes of the bands of Li and Be compared with those of Mg and Al.

In Table I, certain numerical characteristics of the bands are tabulated. The bands of C and Na were not satisfactorily investigated; only one plate of each was taken and these were not suitable for photometry. The band of Na appeared to have a suggestion of a minimum of intensity in the middle, but this was possibly due to surface contamination of which there was a strong suspicion. The wave-lengths for Na and Si were not directly compared with standards and the possible error is difficult to assess.

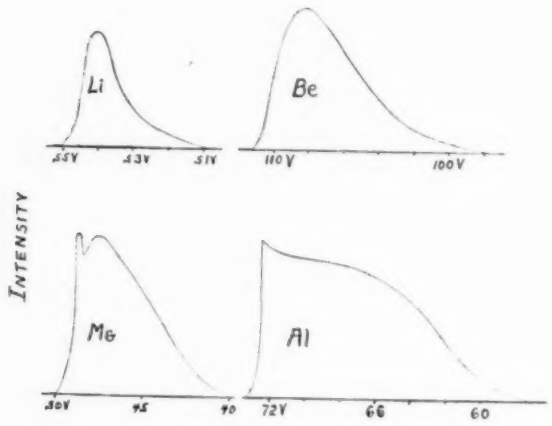

FIG. 5. Intensity against energy in electron-volts of soft x-ray emission.

TABLE I. *Numerical characteristics of the bands.* λ_0 is the wave-length of the band-head obtained by extrapolating the straight portion of the sudden fall in intensity to the level of the uniform background and applying a correction for slit width. V_0 is the voltage corresponding to λ_0. δV is the voltage range from λ_0 to the maximum intensity of the band. ΔV is the total estimated width of the band.

Element	λ_0	V_0	δV	ΔV (exp.)	ΔV (theor.)
Li	225.3±0.2	54.8	0.6	4.2±0.6	4.6
Be	110.9±0.2	111.2	2.7	13.5±2.5	13.8
C*	45.4±0.3	272	—	5	20.8(?)
Na	405 ±2	30.5	—	3.5±1	3.2
Mg	251.0±0.2	49.2	0.6	9.0±1.5	7.2
Al	169.8±0.2	72.7	0.4	16.0±2	12.0
Si	123 ±1.5	100.3	5	19.2±2.5	13
Ba*	164.6±0.3	74.9	—	3.0±0.3	—
Ba*	159 ±0.5	77.6	—	—	—

* Measurement to the center of band.

IDENTIFICATION OF THE BANDS

For Li, Be and C, the observed bands are obviously *K*-bands. They represent transitions from the outermost (or conduction) levels into

the K-level. For Na, Mg, Al, Si the bands are L-bands. The question arises in the latter case which of the three L-levels is concerned.

The separations between the L-levels may be estimated from the laws of x-ray doublet separation. It is found that the $L_{II}-L_{III}$ $(2p_{\frac{1}{2}}-2p_{\frac{3}{2}})$ separation is negligible for us; but that the $L_I-L_{II}(2s-2p)$ separation is quite large. The $L_{II,\,III}$ term values for these elements are known within a few percent and tabulated.[13] These are sufficient to determine the observed bands unambiguously as due to transitions into the $L_{II,\,III}$ levels. The agreement is as follows:

	Mg	Al	Si
V_0 (obs.)	49.2	72.8	101 (inaccurate)
V_0 (Siegbahn)	49.9	71.5	97.5

We are left to explain why there are not two bands instead of only one. Evidently the transitions (conduction$\rightarrow L_I$) do not occur with any probability. This at first sight is rather strange since they seem of the same type as the transitions (conduction$\rightarrow K$) which are found for Li and Be. But it may be that these (conduction$\rightarrow L_I$) transitions are extinguished through the higher probability of ($L_{II,\,III}\rightarrow L_I$) transitions. To obtain an estimate of the wave-length at which the radiation from these transitions should be found we have to make an extrapolation by the screening-doublet formula, since the energies of the L_I-levels have not been evaluated. We find in this way that the ($L_{II,\,III}\rightarrow L_I$) transitions should have been in the region of our observations; but the extrapolation necessary is very long, and we suggest that it would be worth while to look for them in the region above about 500A which was not covered in our experiments.

Finally there remains the interpretations of the barium bands (Fig. 4e). Their different form suggests immediately that they are not due to transition from conduction electron levels, but from underlying "atomic" levels. Actually these bands were observed by Osgood[14] and were correctly assigned by him as $O\rightarrow N$ transitions. He did not make accurate wave-length determinations; also he reports the λ165 band as a doublet and an extra line at a much shorter wave-length, neither of which features we observed. Table II gives a comparison of our values of V_m, the mean voltage of the band and that calculated from x-ray data.[13] (The last column can be neglected for the present.) The agreement is poor, and since our determination is accurate, an error in the x-ray data is suggested. The faint band of radiation visible on Fig. 4e at around 145A represents probably the transitions (conduction)$\rightarrow N_{IV}$ and (conduction)$\rightarrow N_V$, that is to say two broad superposed bands. If we assume a band-head at 145A, we are able to obtain a (ν/R) value for the $O_{II,\,III}$ level of Ba of 1.40 as compared with Siegbahn's value of 0.7. This value when used in conjunction with Siegbahn's values for N_{IV} and N_V gives a much better agreement with the values of V_m, as is shown by the last calculated column of Table II. This gives one confidence in the identifications. However, more experimental data on pure Barium targets are needed to complete these interpretations.

TABLE II. *Observed and calculated values of V_m for Ba band.*

Transition	V_m (obs.)	V_m (calc. 1)	V_m (calc. 2)
$O_{II,\,III}\rightarrow N_{IV}$	75	84	73
$O_{II,\,III}\rightarrow N_V$	77.6	88	77

DISCUSSION OF BAND-FORMS

Except in the case of barium, the soft x-ray bands observed are all due to transitions from the filled outer (or conduction) electron levels into a vacant K- or L-shell. In the excited state, a K- or L-electron is missing but all the conduction levels are filled and thus the energy of the system is well defined. On the other hand, after the radiation has been emitted, we have a normal metal in which an arbitrary level of the conduction electron system lacks an electron. The structure of the filled conduction levels therefore plays an important part in determining the structure of the bands. If E is the energy, n_E the number of occupied conduction levels per unit energy range, and f_E the transition probability into a K- or L-shell of an electron from a level of energy E, the intensity distribution in the band is given by

$$I_E = n_E f_E. \qquad (1)$$

[13] Siegbahn, *Spektroskopie der Rontgenstrahlen*, p. 348 (1931).

[14] Osgood, Phys. Rev. **30**, 567 (1927).

The form of f_E is indeterminate at present but some characteristics of the bands can be obtained from that of n_E.

It is well known that a good conductor of electricity is a substance for which there exist a large number of unoccupied levels within a small energy range above the highest occupied level. A rough sketch of some possible curves of n_E for metals, semiconductors and insulators is given in Fig. 6, in which the unoccupied levels

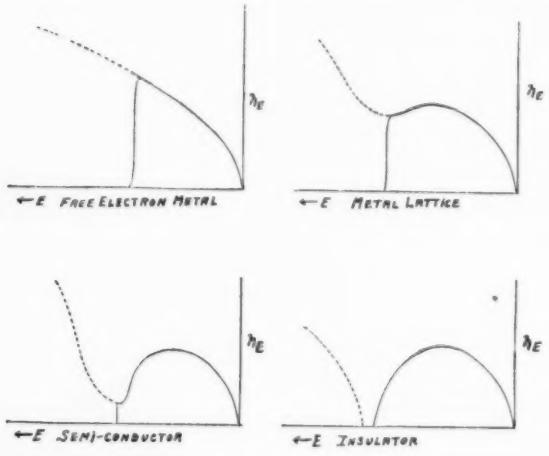

FIG. 6. Energy states in solids.

are represented by dotted curves. It follows that, for metals, I_E must drop suddenly to zero from some finite value; and so the bands must have a high-energy head, just as is observed (Fig. 4a, b and c). For insulators, on the other hand, no sharp edge is to be expected. We have no observations for such substances but the case is actually exemplified by the Ba $O \rightarrow N$ band, since the O-levels are certainly nonconducting. We find a band which is symmetrical about its center (Fig. 4e). It is also interesting that the bands of the semiconductors C and Si (Fig. 4d) do not show any appreciable sharp edge, thus demonstrating that the valence-electrons in these substances form almost self-contained groups, as might be expected.

The actual energy range δV (in volts) of the intensity drop from a maximum to zero for the metals has been given in Table I. Apparently this should be dead sharp except for the obvious temperature-diffusion (of the order of 1/10 volt) of the "surface" of the filled conduction electron levels. Actually we have to take into account the finite slit-width which increases in effect for decreasing wave-length. This would account for an unsharpness of about 0.3 volt for Li and Mg and 0.4 volt for Al. These are certainly smaller than the observed values δV but the difference can probably be accounted for by photographic spreading of the image. The case of Be is exceptional; the apparent diffusion of the edge is much more than could be accounted for. But a close examination of the Be curve (Fig. 3a) suggests that I_E is beginning to diminish before the edge is reached.[15]

An elementary conclusion from (1) is that the energy-spread of the bands is equal to the energy spread of the filled conduction electron levels. If we adopt the Sommerfeld (or free-electron) model of the metal, this spread ΔE is calculated in terms of the number of atoms per cc ρ and the number of electrons per atom N is

$$\Delta E = (h^2/2m)(3\rho N/8\pi)^{\frac{2}{3}}. \qquad (2)$$

On the assumption that N is 1 for Li and Na, 2 for Be and Mg, 3 for Al, and 4 for C and Si, the result of the calculation of the corresponding voltage-range ΔV is given in Table I, and may be compared with the experimental values. The agreement for the true metals is good, and, in spite of the fact that the discrepancy for Al seems to be outside the limits of error, one is able to determine unambiguously in all cases the number of conduction electrons per atom. For C and Si one could not expect the Sommerfeld theory to hold; but the great breadth of the Si band is perhaps unexpected. For Ba, the relative sharpness of the $O \rightarrow N$ bands is due to the sharpness of the O-level which lies at about 20 volts below the surface of the conduction electron levels.

Even for metals, the formula (2) involves all the consequences of the elementary theory which neglects completely the lattice-structure of the metals. We know that in fact n_E does not increase continuously as $E^{\frac{1}{2}}$ as would be required; the curve of n_E against E breaks up into separate zones which, for metals with two conduction electrons must overlap somewhat. This is probably unimportant in the case of alkali-metals with only one conduction electron per atom, and in fact no evident breach of the theory

[15] Jones, Mott and Skinner, Phys. Rev. **45**, 379 (1934).

occurs for Li. Preliminary calculations by means of Bragg's law for the de Broglie wave-lengths reflected by the metallic lattice give fair agreement with the most obvious structures noted in the photometer curves shown in Fig. 4. These are the breadth of the short wave-length edge of Be, the minima of intensity near the short wave-length edge of the Mg band and possibly a similar effect for Al but not as close to the edge. To discuss the meaning of the curious shapes of these bands involves a detailed and much more careful consideration of the functions f_E and n_E which will be left to a subsequent paper.[15] But here we may note that there is a certain similarity between the shapes of the K-bands of Li and Be (Fig. 5) when compared with the L-bands of Mg and Al. This may be ascribed to the fact that the first are transitions into an s-level, while the second are transitions into a p-level.

We may sum up in saying that the characteristic properties of metals, semiconductors and insulators are reflected in the sharpness of the soft x-ray band-heads and that the breadths of the bands allow one to fix the number of free electrons per atom in a metal.

Comparison with Critical Potential Measurements

In two recent papers,[16] Skinner has described photoelectric measurements of the intensity distribution in the K-bands of Li and Be, using an exciting voltage of 300. These agree as well as could be expected with the results of the present experiments; the band-heads were found correctly to within one volt. In the same papers, direct measurements were also described of the K-excitation voltages. The method employed was to vary the energy of the bombarding electrons and measure photoelectrically the intensity of the radiation emitted. Thus curves were obtained showing breaks when the region of K-excitation is reached. In this way, the values 53.7 and 92 volts were obtained for the minimum K-excitation potentials of Li and Be metals. It follows from what has been said that the minimum K-excitation voltage must be equal to the voltage V_0 of radiation corresponding to the band-head. From Table I values of V_0 of 54.9 and 110.3 volts for Li and Be are obtained. The agreement for Li is fair; but there is no agreement for Be. However, the voltage 92 agrees reasonably with the limit of the faint band at about 140A (Fig. 3b) which has been definitely ascribed to contamination of the surface. A further strong break at 107 volts appears to correspond with the hump at 117A which also appears with an impure surface. One seems therefore to be forced to the conclusion that the results of the excitation-potential measurements were spoiled by surface contamination.[17] This was in spite of great precaution taken to ensure purity. It is possible that a very slight contamination will have a serious effect for electrons with energy of the order of 100 volts; the results of experiments using higher exciting voltages will be much less sensitively affected. It is hoped to investigate this question further.

It is of some interest to compare the energy corresponding to the radiation emitted with the energy values for $L \rightarrow K$ transitions in the corresponding free atoms. The energy difference between $\mathrm{Li}(1s \cdot 2s^2)$ and the normal atom, $\mathrm{Li}(1s^2 \cdot 2s)$, may be obtained from the experimental value of the energy[18] of $\mathrm{Li}^+(1a \cdot 2s)$ by subtracting a rough estimated value of 7.5 volts for the work gained in replacing the second $2s$ electrons. The value for $\mathrm{Be}(1s \cdot 2s^2 \cdot 2p)$ was similarly found from a calculated value for $\mathrm{Be}^+(1s \cdot 2s^2)$ kindly supplied by Professor P. M. Morse. The values so obtained are better than those given previously by Skinner.[16] The following table shows (a) the maximum energy V_0 of the radiation emitted from the metals, (b) an approximate estimate of the mean energy V_m of the radiation bands and (c) the energy V_a for the $L \rightarrow K$ transition in the free atom.

	V_0	V_m	V_a
Li	54.9	53	56.6 ± 1
Be	111.2	105	117.5 ± 4

It is seen that, as might be expected, the metallic binding has the effect of depressing the value of V.

[16] Skinner, Proc. Roy. Soc. **A135**, 84 (1932); and **A140**, 277 (1933).

[17] We are indebted to Dr. D. R. Bhawalkar for the information that he has obtained by a similar method the low value of 63 volts for Al. The value of V_0 from Table I is 72.8 volts.

[18] Bacher and Goudsmit, *Atomic Energy States*.

The value of 170.5A for the L absorption edge given by Siegbahn[19] agrees well with our measurement of the short wave-length edge of the conduction band for aluminum. The experiments of R. W. Wood[20] on the absorption in the near ultraviolet and those[21] started at this laboratory should add much information about the filled levels and the transition probabilities to the empty levels in solids.

The experiments were carried out during the tenure by one of us (H.W.B.S.) of a Rockefeller Fellowship at the Massachusetts Institute of Technology. A grant by the Rumford Committee made possible the construction of the vacuum spectrograph.

Note added in proof. More recently we have photographed the boron K line at 67.5A emitted by bombardment of an evaporated surface. In a recent report (Siegbahn, Proc. Phys. Soc. **45**, 689, 1933) on some of the same elements from Siegbahn's laboratory there are a few differences which are worthy of comment.

Our curves (Fig. 3) for beryllium show the vast differences which a slight contamination may produce. Hence their curves (Fig. 3) for this element are probably not characteristic of the pure metal since nearly all spectra and photometer curves in this and a preceding article (Siegbahn and Magnusson, Zeits. f. Physik **87**, 291, 1934) show intense carbon lines and even oxygen and nitrogen lines. The carbon lines were present only on one of our plates and yet plates which showed no trace of this commonest of contaminations gave spurious structure when the target surface was not renewed frequently. The surfaces prepared and recoated frequently by evaporation in high vacuum are the most satisfactory, for these lines are due to transitions from the conduction electron states which are very sensitive to the effect of chemical combination.

The boron line is almost symmetrical with a width at half-maximum intensity of 7.8 volts. The wave-length is that reported by Siegbahn and Magnusson but the shape more symmetrical. The boron shape resembles what is expected of semiconductors on the short wave-length side of the line. The edge at 169.9A due to the Al L_{II} level is not as distinct in our Fig. 4c as in theirs. There is an indication of a similar structure for Mg in our Fig. 4b. Their photometer curve Fig. 6 for aluminum shows structure at 212.4A and 198.5 obviously due to Al_2O_3 present in the target.

[19] Siegbahn, Proc. Phys. Soc. **45**, 689 (1933).
[20] Wood, Phys. Rev. **44**, 353 (1933).
[21] Liben and O'Bryan, Phys. Rev. **44**, 952A (1933).

A Theory of the Form of the X-Ray Emission Bands of Metals

H. JONES, N. F. MOTT AND H. W. B. SKINNER, *Wills Physical Laboratory, Bristol, England*

(Received December 11, 1933)

It is shown that the optical transition probabilities for transitions from the conduction levels in metals to the K- and L-levels may vary strongly within the lowest allowed zone, and will also depend on the azimuthal quantum number of the final state. An explanation is given of the form of the x-ray emission bands observed by O'Bryan and Skinner for Li, Be, Mg, Al.

IN a recent paper, O'Bryan and Skinner[1] have determined the intensity distribution in the x-ray bands emitted by light metals when electrons make transitions from the conduction levels to the K- or L-levels. To interpret their results, they denote by $n_E\,dE$ the number of conduction electron levels with energy between E and $E+dE$, and by f_E the optical transition probability from a state with energy E (measured from the bottom of the conduction electron band) to the K- or L-level. If the conduction states up to a certain maximum energy E_{max} are filled, the intensity of the x-ray band is given by

$$\begin{aligned} I_E &= n_E f_E \qquad E<E_{max} \\ &= 0 \qquad\quad E>E_{max}. \end{aligned} \tag{1}$$

They find a striking difference in the intensity distribution in the bands of beryllium and magnesium, two metals of the same structure which both have two valence electrons per atom. In this paper, we give a theoretical explanation of some of the effects observed, and show that the difference between the bands in Be and Mg is due to the fact that in the former metal a transition to the K-level ($1s$) is observed, in the latter a transition to the L_{II} and L_{III} levels ($2p$). Thus f_E is different in the two cases.

Houston[2] attempted the calculation of f_E using Sommerfeld wave functions and came to the conclusion that f_E should be proportional to E. But he neglected the fact that the important region for transitions into inner shells is that just around the nucleus and that here the wave functions calculated on a free-electron model (which omits the lattice-structure completely) can have no relation to the actual case. A more detailed investigation than his is therefore required.

In the theory developed by Bloch, Brillouin and others, each state of the electron in the metal is denoted by a vector $\mathbf{k}$; the direction of $\mathbf{k}$ is the direction of motion of the electron, and $2\pi/k$ is its de Broglie wave-length. Bloch has shown that the wave function for each individual electron takes the form

$$\psi_k(x, y, z) = u_k(x, y, z)e^{2\pi i(\mathbf{k}\cdot\mathbf{r})}, \tag{2}$$

where $u_k(x, y, z)$ has the periodicity of the lattice. The energy is a function of $\mathbf{k}$; for the values of k_x, k_y, k_z for which Bragg reflection takes place, a discontinuity in the energy occurs. Thus the states of an electron in the metallic lattice may be divided into zones, separated by planes in k-space across which the energy is discontinuous. If we plot n_E for each zone as a function of E, we obtain curves such as those shown in Fig. 1a. If the energy gaps at the surfaces of discontinuity are small enough, the zones will overlap. We know that this must occur in Mg and Be, since the number of states in the first zone is two per atom, and, if there were no overlap, the first zone would be full, and the crystals would be insulators instead of being rather good conductors. We also know that, on account of the similar lattice-structures, these two metals must have (on different energy scales) rather similar n_E curves.

[1] O'Bryan and Skinner, Phys. Rev. **45**, 370 (1934).
[2] W. V. Houston, Phys. Rev. **38**, 1791 (1931).

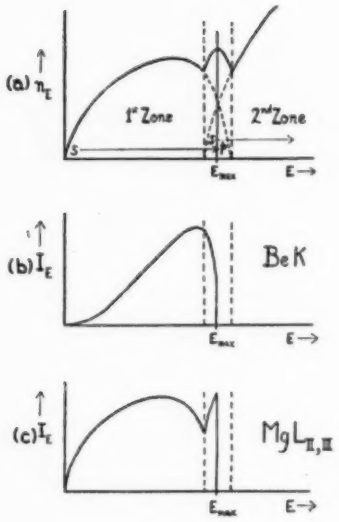

FIG. 1.

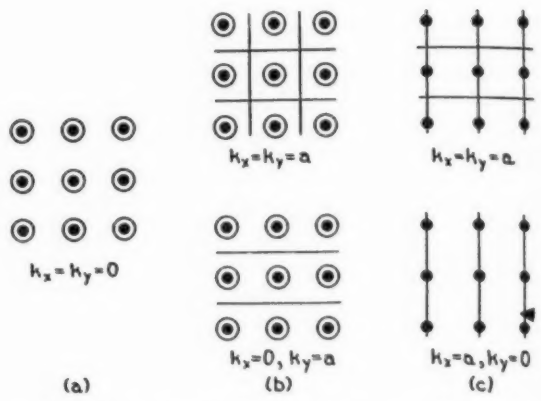

FIG. 2. Wave functions ψ_k for a two dimensional cubic lattice. The dots denote atomic nuclei, the circles and lines denote nodes of the wave function, and a is the lattice constant. (a) shows the lowest state, (b) are the wave functions which, near the nuclei, have the form of a $2s$ electron, and (c) have the form of a $2p$ electron.

§1

We shall now consider the transition probability f_E. If $\Phi(x, y, z)$ denotes the wave function of an electron in the K- or L-state, f_E will be proportional to the quantity

$$\nu^3\left|\int \Phi^*(x, y, z)[\partial\psi_k(xyz)/\partial x]dx\,dy\,dz\right|^2 \qquad (3)$$

where ν is the frequency of the emitted radiation. The factor ν^3 may vary by as much as 2 over an emission band; since, however, we shall use the formula only to obtain the form at the head and tail of the band, the factor ν^3 may be neglected. Thus f_E depends on the form of the wave function of the conduction electron near the nucleus, where Φ is not small.

Let us expand ψ_k, in the region near to one nucleus, as a series

$$\psi_k = \sum_n a_n\phi_n(x, y, z), \qquad (4)$$

where the ϕ_n are the wave functions of an electron in the free atom. In this expression, let a_s denote the coefficient of the lowest s-state, a_p that of the lowest p-state ($2s$, $2p$ in Be, $3s$, $3p$ in Mg). Then in Be the transition probability f_E to the K-level will be approximately proportional to a_p^2, whereas in Mg the transition probability to the L_{II}, L_{III} levels will be proportional to a_s^2, since Δl must change by unity.

The nodes of the wave function for the *lowest* state of the first zone are shown in Fig. 2a. In the neighborhood of the nucleus, ψ_k is slightly perturbed from its form ($2s$ in the figure) for the free atom. Nevertheless, it is clear from symmetry that a_p vanishes, for the wave function for a p-state has a node through the origin; thus if a_p did not vanish ψ_k could not reach a maximum value at each nucleus. In the *higher* states, however, a wave of wave-length $2\pi/k$ must be superimposed on a function having the periodicity of the lattice (cf. Eq. (2)). Thus it is no longer true that a_p vanishes. In §2 we show, using a perturbation method, that when the atoms are far apart, then, for small E, $a_p \propto E^{\frac{1}{2}}$. If this result is true in general, we have, for small E

$$f_E \propto E \qquad \text{(Beryllium } K\text{)}$$

$$f_E \propto \text{const.} \qquad \text{(Magnesium } L_{II,\,III}\text{)}.$$

Since for any metal, for small E, $n_E \propto E^{\frac{1}{2}}$, we have as shown in Fig. 1 (b and c), for the bottom of the bands

$$I_E \propto E^{\frac{1}{2}} \qquad \text{(Beryllium } K\text{)}$$

$$I_E \propto E^{\frac{1}{2}} \qquad \text{(Magnesium } L_{II,\,III}\text{)}.$$

As was pointed out by O'Bryan and Skinner, the tail-forms of the bands of Li and Be metals are certainly different from those of Mg and Al. It can be seen from Fig. 5 of their paper that the first are entirely concave upwards until the maximum is reached, and appear to be increasing about as E^2; while the second pair are concave

downward except at the extreme low-energy limit of the bands. Here, it is true, the intensity appears to increase more rapidly than E; but if we can regard this extreme tail (about the last 2 volts) of these bands as incidental (by which is meant that they are due either to spurious spreading of the photographic image perhaps by light-reflection along the acutely inclined plate, or at any rate to some cause not taken into account by the present theory) then a general increase of the intensity proportional to $E^{\frac{1}{2}}$ at the tails of the Mg and Al bands might be taken as correct; and for similar reasons an increase proportional to $E^{\frac{1}{2}}$ (instead of the apparent E^2) for Li and Be might be postulated. Unfortunately it is not feasible at present to make any more exact statement of the facts than this.

We shall now consider the values of f_E near the *head* of the emission band. Figs. 2b and 2c show the type of wave function ψ_k that we shall expect to find in this region. In the type 2b, the form of ψ_k near a nucleus is similar to that of a $2s$ wave function of the free atom; as before, the coefficient a_p vanishes exactly, by symmetry. In the type 2c, the wave function near a nucleus is similar to that of the $2p$ state of the free atom, and a_s vanishes. If, in the free atom, the difference between the energy of the $2s$ and $2p$ states is large compared to the breadth of the allowed zones, it is clear that all wave functions ψ_k in the first zone will be similar to $2s$ functions near the nucleus; in this case the wave functions near the top of the first zone will be of the type 2b, and a_p will rise to a maximum in the middle of the first zone, and be zero at either end. At the bottom of the second zone the wave function will be of the form 2c, and a_p will take a maximum value. If, on the other hand, the energy difference between the $2s$ and $2p$ states is small, wave functions of the type 2c will have *lower* energy than the type 2b. The behavior of the coefficient a_p is discussed from a mathematical point of view in the next section, and it is shown that in this case wave functions of the type 2c occur at the top of the first band, and functions of the type 2b at the bottom of the second band. Thus a_p^2 increases from 0 to 1 in the first band, whereas a_s^2 decreases from 1 to 0. At the bottom of the second band a_s^2 is equal to unity, and a_p^2 vanishes. In order to account for the experimental results we must assume that the wave functions behave in this second way. This is reasonable since the energy separation of the $2s$ and $2p$ states for the Be and Mg atoms is considerably smaller than the energy-spread of their filled conduction-electron bands.

The observed characteristics of the soft x-ray bands of beryllium and magnesium[3] near the heads are: (1) The slow fall of I_E in the Be K-band from a maximum to zero; it appears that I_E has already started to diminish before the sudden drop due to the fact that there are no more conduction electrons. (2) The curious minimum which is found in the Mg, $L_{II,\,III}$ band and the very sharp rise just before the sudden drop at the head.

We have seen that Be and Mg, on account of their like lattice-structure must have similar n_E curves of somewhat the type shown in Fig. 1a. Applying the preceding ideas about transition probabilities, we may regard $n_E|a_s(E)|^2$ and $n_E|a_p(E)|^2$ as the numbers of s- and p-electrons respectively corresponding to the energy E. We observe that for Be the introduction, as the energy rises, of electrons from the second zone does not affect I_E, since they are s-electrons and cannot make transitions to the K-level. The shape of the I_E curve therefore depends only on the variation of $n_E|a_p|^2$ in the range of the first zone; and thus, since a_p is steadily increasing, I_E reaches a maximum later than n_E, then begins to diminish till the limit $E_{\max}$ of the filled levels is reached and there are no more transitions. On the other hand, I_E for the Mg $L_{II,\,III}$ band depends on the variation of the quantity $n_E|a_s|^2$, which gives the number of transitions into a p-level. Thus with increasing E, since a_s is steadily diminishing, I_E reaches a maximum earlier than n_E and begins to fall. But then the introduction of the overlap with the second zone brings into action a fresh set of s-electrons. So at this point I_E rises rapidly until the value $E_{\max}$ is reached. An attempt is made to show this qualitatively in Fig. 1. It seems that the assumptions made allow one to interpret accurately the characteristic differences of the K- and L-spectra from the same type of n_E curve. From the Mg

[3] See O'Bryan and Skinner, Phys. Rev. **45**, 370 (1934), Figs. 4 and 5.

curve we may infer that the overlap of the first two zones is of the order of $1\frac{1}{2}$ volts.

When passing finally to Al, the different lattice structure does not allow one to make any precise comparison with Mg, but the x-ray bands are actually very similar. The main difference is that the minimum is considerably further from the edge than is the case with Mg (4 volts instead of 0.7). This difference would certainly be anticipated since, in Al, there are 3 conduction electrons per atom (i.e., more than enough to fill the first zone). The energy range over which we obtain transitions from *s*-electrons in the second zone is therefore much greater than for Mg.

§2

In this section we consider a three-dimensional cubic lattice of atoms, and calculate the splitting of the energy levels by treating the interaction between the atoms as small, by the method first given by Bloch.[4] Our calculation differs from Bloch's in that we take the ground state of the atom to be an *s*-state, and consider the next *p*-state to have nearly the same energy, so that the "zero order" wave function for the lattice will contain both *s*- and *p*-states, as explained in the last section. Results obtained for the cubic lattice may be expected to apply qualitatively to more complicated structures, such as the hexagonal close-packed lattices of Be and Mg.

The three independent wave functions associated with the degenerate *p*-state of an atom may be written $xf(r)$, $yf(r)$, $zf(r)$; r being the distance from the nucleus. We shall denote these functions by $\varphi_1(\mathbf{r})$, $\varphi_2(\mathbf{r})$, $\varphi_3(\mathbf{r})$, respectively, and the single spherically symmetrical wave function belonging to the *s*-state by $\varphi_0(\mathbf{r})$. If the interaction between the *s*- and *p*-states is neglected, the wave functions for the electrons in the lattice can be expressed in the form originally given by Bloch,[4] *viz.*,

$$\psi_{nk}=\sum_{g} e^{2\pi i(\mathbf{g}\cdot\mathbf{k})/G}\varphi_n(\mathbf{r}-a\mathbf{g}), \qquad (5)$$

where a is the lattice constant, G the number of atoms along the side of a unit cube, and each component of $\mathbf{g}$ may have any positive or negative integral value. The components of $\mathbf{k}$ will be written k_1, k_2, k_3.

The question to be answered in this section is how the functions ψ_{nk} derived from *s*- and *p*-atomic states combine to form the true 'zero' order wave functions for the electrons in the lattice.

We write in the usual way for the zero-order function Ψ

$$\Psi_{nk}=\sum_{m=0}^{3} a_{mk}\psi_{mk} \quad n=0,\ 1,\ 2,\ 3, \qquad (6)$$

where the coefficients a_m are subject to the normalizing condition

$$\sum_m |a_m|^2=1.$$

The wave equation which these functions must satisfy is

$$(H-E)\Psi=0,$$

where

$$H=-(h^2/8\pi^2m)\nabla^2+\sum_v v(\mathbf{r}-a\mathbf{g})$$

and $v(\mathbf{r})$ is the self-consistent potential field due to a single atom.

The diagonal elements of the matrix H with respect to the functions of Eq. (5) have been calculated by Wilson[5] and may be denoted by $A_n(\mathbf{k})$. For a simple cubic lattice they take the following values

$$A_0(k)=\alpha_0+2\gamma_0\{\cos(2\pi k_1/G)+\cos(2\pi k_2/G)+\cos(2\pi k_3/G)\}$$

$$A_n(k)=\alpha_n+2\gamma_n\cos(2\pi k_n/G)+2\gamma_n'\{\cos(2\pi k_l/G)+\cos(2\pi k_m/G)\} \qquad n=1,\ 2,\ 3.$$

where l and m are the two remaining numbers other than n, and

$$\alpha_n=\int \phi_n^*(r)H\phi_n(r)d\tau \qquad n=0,\ 1,\ 2,\ 3.$$

$$\gamma_0=\int \phi_0^*(x+a,\ y,\ z)H\phi_0(x,\ y,\ z)d\tau$$

$$\gamma_1=\int \phi_1^*(x+a,\ y,\ z)H\phi_1(x,\ y,\ z)d\tau,$$

[4] F. Bloch, Zeits. f. Physik **52**, 555 (1928).

[5] A. H. Wilson, Proc. Roy. Soc. **A133**, 458 (1931).

with similar expressions for γ_2 and γ_3. In γ_2 for instance the first term of the integrand is $\phi_2^*(x, y+a, z)$. Finally

$$\gamma_1' = \int \phi_1^*(x, y+a, z) H \varphi_1(x, y, z) d\tau,$$

again with similar expressions for γ_2' and γ_3'. The first term of the integrand in γ_2' is $\varphi_2^*(x, y, z+a)$, and in γ_3', $\varphi_3^*(x+a, y, z)$.

For the nondiagonal elements we have

$$H_{0n} = \int \psi_{0k}^* H \psi_{nk} d\tau$$

$$= \sum_{g, g'} e^{2\pi i(\mathbf{g}-\mathbf{g}', k)/G} \int \phi_0^*(\mathbf{r}-a\mathbf{g}) H \phi_n(\mathbf{r}-a\mathbf{g}) d\tau.$$

If we restrict ourselves to a simple cubic lattice, and consider only the integrals which correspond to nearest neighbors, then, since

$$\int \phi_0^*(x+a, y, z) H \phi_n(x, y, z) d\tau$$

$$= -\int \phi_0^*(x-a, y, z) H \phi_n(x, y, z) d\tau,$$

we have

$$H_{0n} = 2i\beta \sin (2\pi k_n/G),$$

where

$$\beta = \int \phi_1^*(x+a, y, z) H \phi_0(x, y, z) d\tau.$$

The nondiagonal elements H_{nm} vanish if neither n nor m is zero, for it is clear that a field with cubic symmetry will not raise the degeneracy of the states associated with the wave functions ϕ_1, ϕ_2, ϕ_3.

The secular equation for the energy of an electron in the lattice thus becomes

$$\begin{vmatrix} A_0(k)-E, & 2i\beta \sin (2\pi k_1/G), & 2i\beta \sin (2\pi k_2/G), & 2i\beta \sin (2\pi k_3/G) \\ -2i\beta \sin (2\pi k_1/G), & A_1(k)-E, & 0, & 0 \\ -2i\beta \sin (2\pi k_1/G), & 0, & A_2(k)-E, & 0 \\ -2i\beta \sin (2\pi k_3/G), & 0, & 0, & A_3(k)-E \end{vmatrix} = 0. \quad (7)$$

In order to calculate the transition probability between a deep lying x-ray level and states described by the wave functions in Eq. (6), it is essential to know the relative amounts of s- and p-atomic states which these functions contain, i.e., we must know the values of a_{nm} as functions of k. It will be sufficient for the present purpose if we consider only the states which lie along a line in the k space from the origin perpendicular to one face of the first cube across which the energy is discontinuous. For such states the functions in Eq. (6) reduce to

$$\Psi_{0k} = a_{00}\psi_{0k} + a_{01}\psi_{1k},$$

$$\Psi_{1k} = a_{10}\psi_{0k} + a_{11}\psi_{1k}.$$

Eq. (7) gives readily

$$|a_{00}| = |a_{11}| = \cos \tfrac{1}{2}\theta,$$

$$|a_{01}| = |a_{10}| = \sin \tfrac{1}{2}\theta,$$

where

$$\cot \theta = [A_1(k) - A_0(k)]/4\beta \sin (2\pi k/G).$$

The wave functions Ψ_{0k} will refer to states lying in the first zone, Ψ_{1k} to states lying in the second zone, and the coefficients a_{00} and a_{01} will then become identical with the coefficients a_s and a_p of the previous section. It follows that we must always have $A_1(0) > A_0(0)$, but when $k = \frac{1}{2}G$ (i.e., the value of k at the surface of energy discontinuity in k space) there are two possibilities.

(a) $A_0(\frac{1}{2}G) > A_1(\frac{1}{2}G)$,

(b) $A_0(\frac{1}{2}G) < A_1(\frac{1}{2}G)$.

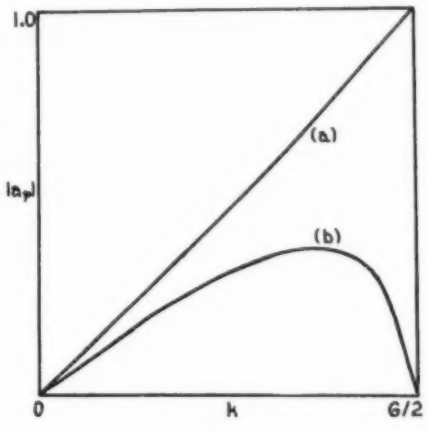

FIG. 3.

In case (a) as k goes from 0 to $\frac{1}{2}G$, θ increases from 0 to π, so that a_p increases steadily from 0 to 1. In case (b), as k goes from 0 to $\frac{1}{2}G$, θ increases from 0 to some maximum value less than π, and then falls again to 0. Hence in this case a_p increases from 0 to some maximum value less than 1 and falls again to zero as k reaches $\frac{1}{2}G$. These two possibilities are illustrated in Fig. 3 where a_p is plotted against k, showing the amount of p-state for each case. Since $|a_{01}| = |a_{10}|$, the curves also show the amount of s-state contained in the functions Ψ_{1k} associated with states in the second zone.

It was shown in §1 that in order to explain the experimental results it is necessary to suppose that for the metals Be and Mg it is the case (a) which actually exists.

For small values of k

$$\tan\theta = 8\beta\pi k/G[A_1(0) - A_0(0)].$$

Hence for small k, a_s is proportional to k, i.e., to $E^{\frac{1}{2}}$ and a_s as approximately constant.

Faint Lines in the L Spectrum of the Elements 73 Ta to 90 Th. I.

SIDNEY KAUFMAN, *Cornell University*

(Received January 17, 1934)

Numerous weak L lines in the x-ray spectra of the heavier elements are reported. The majority are diagram lines attributable to quadrupole radiations. The non-diagram lines are satellites of $L\beta_2$. Measurements were made with a modified Siegbahn-Thoraeus high vacuum spectrometer having a dispersion, with calcite in first order and at $\lambda = 1080$ X.U., of 4.5 X.U./mm.

WITHIN the last decade several investigators[1, 2, 3, 4, 5] have reported faint lines in x-ray spectra which cannot be explained as normal dipole radiations. These lines are of two classes. First, "forbidden" lines which fit into the energy level diagrams but involve transitions violating the dipole selection rules. Second, those lines which as yet have no place in the energy level schemes, known variously as "non-diagram" lines, "satellites" or "spark" lines. This paper is an experimental report on both types of faint lines observed in the region of the $L\beta_2$ line for nine and the $L\gamma_1$ line for four of the heavier elements. Italics in the tables below indicate lines not reported before.

The spectrometer used was of the high vacuum type described by Siegbahn and Thoraeus[6] with slit width of 0.04 mm, slit-crystal distance of 27.15 cm and crystal-plate distance of 105.61 cm. This arrangement gives a large dispersion; at the wave-length of Au β_1 it is about 4.5 X.U./mm with a calcite crystal in first order. Plates were exposed from 10 to 30 hours at 29 kv and 10 to 25 m.a. with the crystal stationary during each exposure.

Wave-length measurements for each element except Pb are relative to Friman's[7] and Wennerlof's[8] values for the β_1, β_2 or γ_1-lines. Idei's[9] value of β_3 for Pb was used as a standard for the β region of that element. The β_1 and β_2-lines, measured as a single line by Friman, were partially resolved in the present work. The error in the wave-lengths given below is estimated to be less than 0.4 X.U.

The "computed" values of ν/R in the tables are from data on the strong lines of the L series by Idei[9] and from the M series measurements of Lindberg.[10]

I. DIAGRAM LINES

Dipole radiation

The dipole selection rules for the quantum numbers l and j allow transitions between energy states for which $\Delta l = \pm 1$; $\Delta j = 0, \pm 1$ except $j = 0$ to $j = 0$. Table I gives the weak lines in the γ region obeying these rules.

Quadrupole radiation

The quadrupole selection rules[11, 12] for l and j are $\Delta l = 0, \pm 1, \pm 2$ except $l = 0$ to $l = 0$; $\Delta j = 0, \pm 1, \pm 2$ except $j = 0$ to $j = 0$ and $j = 1/2$ to $j = 1/2$. Observed lines obeying these quadrupole rules are given in Tables II–XVI.

β_9 and β_{10} are the strongest of the quadrupole lines observed in this work. Richtmyer and Barnes,[13] in this laboratory, find the ratio of

[1] Data reported before 1931 are tabulated in M. Siegbahn, *Spektroskopie der Röntgenstrahlen*, second edition (1931).

[2] P. A. Ross, Phys. Rev. **39**, 536 and 748 (1932).

[3] S. Kaufman, Phys. Rev. **40**, 116 (1932).

[4] E. Carlsson, Zeits. f. Physik **80**, 604; **84**, 119 (1932).

[5] H. Claësson, Zeits. f. Physik **85**, 231 (1933).

[6] M. Siegbahn and R. Thoraeus, J. Opt. Soc. Am. and Rev. Sci. Inst. **13**, 235 (1926).

[7] E. Friman, Zeits. f. Physik **39**, 813 (1926).

[8] I. Wennerlof, Zeits. f. Physik **41**, 524 (1927).

[9] S. Idei, Tohoku Imp. Univ., Sci. Rep. **19**, 559 (1930).

[10] E. Lindberg, Nova Acta Reg. Soc. Sc. Upsala **7**, No. 7 (1931).

[11] E. Segrè, Rend. Accad. Naz. dei Lincei, **16**, 9 (1932).

[12] H. C. Brinkman, Dissertation, Utrecht (1932).

[13] Unpublished preliminary data on relative intensities and widths of Au lines. Double crystal spectrometer used.

TABLE I. *Dipole transitions.* Claësson[5] gives ν/R values for W γ_4' 887.8, W γ_4 888.6, Au γ_4' 1052.5, Au γ_4 1052.9.

Transition	Line	λ	ν/R	ν/R (comp.)
$L_{II}O_I$	Pb γ_8	821.7	1109.0	1108.9
	Bi γ_8	*795.6*	*1145.4*	1145.6
L_IO_{II}	W γ_4'	1026.4	887.8	887.4
	Pb γ_4'	*785.3*	*1160.4*	
	Bi γ_4'	760.4	1198.5	1198.4
L_IO_{III}	W γ_4	1025.7	888.5	
	Au γ_4	865.6	1052.8	1053.2
	Pb γ_4	783.9	1162.5	1162.1
	Bi γ_4	759.2	1200.3	
$L_IP_{II,\ III}$	Bi γ_{13}	755.3	1206.5	

TABLE II. $L_{III}N_{II}$ ($\Delta l=0$, $\Delta j=+1$).

Element	λ	ν/R	ν/R (comp.)
73 Ta	*1313.5*	*693.8*	693.5
74 W	*1273.9*	*715.4*	715.4
77 Ir	*1162.8*	*783.7*	783.6
78 Pt	*1129.1*	*807.1*	806.9
79 Au	*1097.7*	*830.2*	830.4
82 Pb	*1008.2*	*903.8*	904.0
83 Bi	*980.8*	*929.1*	929.0
90 Th	*817.6*	*1114.6*	1114.5

TABLE III. $L_{III}N_{III}$ ($\Delta l=0$, $\Delta j=0$).

Element	λ	ν/R	ν/R (comp.)
73 Ta	*1306.0*	*697.7*	697.9
74 W	*1264.6*	*720.6*	720.4
77 Ir	*1153.6*	*790.0*	789.8
78 Pt	*1120.1*	*813.5*	813.6
79 Au	*1087.7*	*837.8*	837.8
81 Tl	*1026.3*	*887.9*	887.4
82 Pb	*997.8*	*913.2*	912.7
83 Bi	*970.3*	*939.1*	938.5

TABLE IV. $L_{III}N_{VI}$ ($\Delta l=-?$, $\Delta j=-1$). Also reported by Croffut[14] for W and by Dauvillier[15] for Pt and Au.

Element	λ	ν/R	ν/R (computed)	ν/R, Idei[9]
73 Ta	1255.3	726.0	725.7	725.4
74 W	1216.3	749.2	749.0	749.3
77 Ir	1109.0	821.7	821.3	821.6
78 Pt	1076.3	846.7	846.4	846.2
79 Au	1045.4	871.7	871.5	871.9
81 Tl	986.4	923.9	923.3	923.3
82 Pb	959.2	950.0	949.5	949.8
90 Th	775.2	1175.5	1175.3	1175.5

[14] C. B. Croffut, Phys. Rev. **24**, 9 (1924).

[15] A. Dauvillier, J. de Physique et Radium **3**, 230 (1922).

TABLE V. $L_{III}O_{II,\ III}$ ($\Delta l=0$, $\Delta j=+1$, 0).

Element	λ	ν/R	ν/R (comp.)
73 Ta	*1257.6*	*724.6*	724.3
74 W	*1218.6*	*747.8*	747.9
77 Ir	*1107.3*	*823.0*	
78 Pt	*1073.9*	*848.5*	848.1
79 Au	*1043.4*	*873.3*	873.8
81 Tl	*984.1*	*926.0*	
82 Pb	*956.6*	*952.6*	
	955.8	*953.5*	953.9
83 Bi	*930.0*	*979.9*	979.6
	927.7	*982.3*	
90 Th	*769.8*	*1183.7*	1183.0
	767.5	*1187.3*	

TABLE VI. $L_{III}P_{II,\ III}$ ($\Delta l=0$, $\Delta j=+1$, 0).

Element	λ	ν/R
83 Bi	*922.2*	*988.1*
90 Th	*760.5*	*1198.3*

TABLE VII. $L_{II}M_{III}$ ($\Delta l=0$, $\Delta j=-1$). Reported for Ta, W, Ir and Pt by Dauvillier,[15] for Tl by Idei[9] and for Au by Claësson.[5]

Element	λ	ν/R	ν/R (comp.)
74 W	1335.9	682.1	682.4
78 Pt	1164.7	782.4	782.8
81 Tl	1053.5	865.0	865.0
83 Bi	*987.5*	*922.8*	923.1

TABLE VIII. $L_{II}M_V$ ($\Delta l=-1$, $\Delta j=-2$).

Element	λ	ν/R	ν/R (comp.)
73 Ta	*1316.3*	*692.3*	692.5
74 W	*1270.2*	*717.4*	717.0
77 Ir	*1146.4*	*794.9*	794.4
79 Au	*1072.9*	*849.4*	849.2
82 Pb	*972.5*	*937.0*	936.8
83 Bi	*942.2*	*967.2*	967.2
90 Th	*756.4*	*1204.8*	1205.2

TABLE IX. $L_{II}N_{III}$ ($\Delta l=0$, $\Delta j=-1$). Claësson has reported $L_{II}N_{III}$ for W and Au. He gives for Au $\nu/R=972.1$.

Element	λ	ν/R	ν/R (comp.)
79 Au	938.6	970.9	971.5
82 Pb	*849.9*	*1072.2*	1072.3
83 Bi	*823.3*	*1106.8*	1107.3

TABLE X. $L_{II}N_{VI}$ ($\Delta l=-2$, $\Delta j=-2$). Reported for W by Croffut,[14] for W and Ir by Idei[9] and for W and Au by Claësson.[5] Idei gives ν/R for W 847.5; Claësson gives for W 847.5, for Au 1005.3.

Element	λ	ν/R	ν/R (comp.)
74 W	1075.1	847.6	847.6
79 Au	906.7	1005.0	1005.2

TABLE XI. $L_{II}O_{III}$ ($\Delta l=0$, $\Delta j=-1$). Claësson gives ν/R for W 846.0, for Au 1007.0.

Element	λ	ν/R	ν/R (comp.)
74 W	1076.7	846.4	
79 Au	904.5	1007.5	1007.5
82 Pb	*818.5*	*1113.4*	1113.5
83 Bi	*792.3*	*1150.2*	

TABLE XII. L_IM_{IV} (β_{10}) ($\Delta l=-2$, $\Delta j=-1$).

Element	λ	ν/R	ν/R (computed)	ν/R, Idei[9]
73 Ta	1251.1	728.4	728.3	728.7
74 W	1209.7	753.3	753.3	753.4
77 Ir	1094.3	832.7	832.5	832.4
78 Pt	*1059.4*	*860.2*	860.0	
79 Au	1025.9	888.2	888.5	888.2
81 Tl	961.6	947.7	947.4	947.7
83 Bi	903.3	1008.8	1009.1	1008.6

TABLE XIII. L_IM_V (β_9) ($\Delta l=-2$, $\Delta j=-2$).

Element	λ	ν/R	ν/R (computed)	ν/R, Idei[9]
73 Ta	1243.9	732.6	732.6	732.6
74 W	1202.2	758.0	757.9	758.0
77 Ir	1087.2	838.2	838.1	838.0
78 Pt	1051.9	866.3	865.8	865.9
79 Au	1018.7	894.6	894.9	894.4
83 Bi	896.4	1016.6	1017.1	1017.0

TABLE XIV. L_IN_{IV} ($\Delta l=-?$, $\Delta j=-1$). L_IN_{IV} has been observed for W by Croffut,[14] for Pb and Bi by Eddy and Turner,[16] and for Au and W by Claësson. The last named gives for W 872.3, for Au 1031.5.

Element	λ	ν/R	ν/R (comp.)
74 W	1044.4	872.5	872.1
79 Au	884.0	1030.9	1031.3
82 Pb	802.0	1136.2	1136.2
83 Bi	777.0	1172.8	1172.9

[16] C. E. Eddy and A. H. Turner, Proc. Roy. Soc. **A114**, 605 (1927).

TABLE XV. L_IN_V ($\Delta l=-2$, $\Delta j=-2$). This transition has been found by Dauvillier[15] for W, Ir, Pt and Au; by Idei[9] for W, Ir, Au, Pb and Th; by Claësson[5] for W and Au. Claësson gives ν/R for W 873.2, for Au 1033.1.

Element	λ	ν/R	ν/R (comp.)
74 W	1043.5	873.3	873.2
79 Au	882.6	1032.5	1032.7
82 Pb	800.6	1138.2	1137.6
83 Bi	*775.6*	*1175.0*	1174.6

TABLE XVI. $L_IO_{IV, V}$ ($\Delta l=-2$, $\Delta j=-1$, -2). Claësson[5] has reported these lines resolved for W and Au. His measurements for W are λ=1022.8 and λ=1022.4; for Au, λ=862.0 and λ=861.7.

Element	λ	ν/R
74 W	1023.0	890.7
79 Au	862.2	1056.9
82 Pb	*780.9*	*1167.0*
83 Bi	*756.4*	*1204.8*

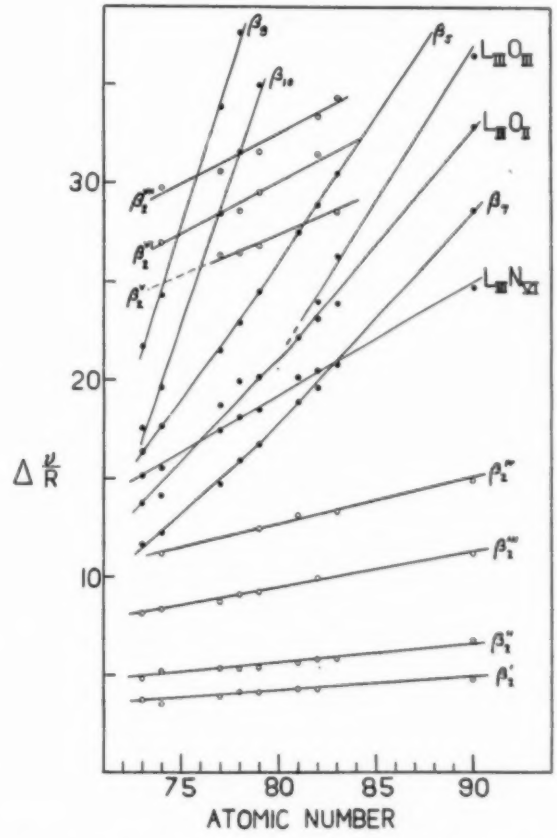

FIG. 1. ν/R from β_2 for lines on short wave-length side of β_2 as a function of atomic number. Diagram lines indicated by solid circles; non-diagram lines by open circles.

TABLE XVII. β_2^{I}.

Element	λ	ν/R	$(\nu/R)^{\frac{1}{2}}$
73 Ta	1275.2	714.6	26.732
74 W	1236.1	737.2	27.152
77 Ir	1127.5	808.3	28.430
78 Pt	1094.2	832.8	28.858
79 Au	1062.9	857.4	29.281
81 Tl	1003.4	908.2	30.136
82 Pb	975.9	933.8	30.558
90 Th	788.6	1155.6	33.994

TABLE XVIII. β_2^{II}.

Element	λ	ν/R	$(\nu/R)^{\frac{1}{2}}$
73 Ta	1273.3	715.7	26.752
74 W	1233.2	738.9	27.183
77 Ir	1125.4	809.7	28.456
78 Pt	1092.6	834.0	28.879
79 Au	1061.3	858.7	29.303
81 Tl	1001.9	909.5	30.158
82 Pb	974.3	935.3	30.583
83 Bi	947.4	961.8	31.013
90 Th	787.3	1157.5	34.022

TABLE XIX. β_2^{III}.

Element	λ	ν/R	$(\nu/R)^{\frac{1}{2}}$
73 Ta	*1267.4*	*719.0*	*26.815*
74 W	*1228.0*	*742.1*	*27.241*
77 Ir	*1120.8*	*813.1*	*28.515*
78 Pt	*1087.8*	*837.8*	*28.944*
79 Au	*1056.6*	*862.5*	*29.368*
82 Pb	*970.0*	*939.5*	*30.651*
90 Th	*784.3*	*1161.9*	*34.087*

intensities of Au β_5 to Au β_9 and Au β_{10} to be 10 and 16, respectively.

II. NON-DIAGRAM LINES

The non-diagram lines in Tables XVII–XXIII are those observed on the short wave-length side of the β_2-line. The measurements of the strong satellites β_2^{I} and β_2^{II} are believed to be superior to those reported before.[1, 17]

The assignment of these lines as satellites of β_2 appears from Fig. 1 in which the ν/R differences between β_2 and the lines on the short wave-length side of β_2 are plotted as a function of the atomic number. The diagram lines, besides fitting the energy level schemes, have slopes independent of that of β_2 whereas the slopes of the satellite curves ($\beta_2^{I}-\beta_2^{VII}$) increase regularly with respect to the slope of β_2.

TABLE XX. β_2^{IV}.

Element	λ	ν/R	$(\nu/R)^{\frac{1}{2}}$
74 W	*1223.5*	*744.8*	*27.292*
79 Au	*1052.7*	*865.7*	*29.422*
81 Tl	*993.8*	*917.0*	*30.281*
83 Bi	*940.1*	*969.3*	*31.134*
90 Th	*781.8*	*1165.7*	*34.142*

TABLE XXI. β_2^{V}.

Element	λ	ν/R	$(\nu/R)^{\frac{1}{2}}$
77 Ir	*1097.0*	*830.7*	*28.821*
78 Pt	*1065.7*	*855.1*	*29.242*
79 Au	*1035.4*	*880.1*	*29.666*
83 Bi	*925.6*	*984.6*	*31.378*

TABLE XXII. β_2^{VI}. Claësson[5] reports for Au, λ = 1032.3 and λ = 1031.3.

Element	λ	ν/R	$(\nu/R)^{\frac{1}{2}}$
74 W	*1198.0*	*760.6*	*27.580*
78 Pt	*1063.1*	*857.2*	*29.278*
79 Au	1032.3	882.7	29.711
82 Pb	*948.3*	*961.0*	*30.999*

TABLE XXIII. β_2^{VII}.

Element	λ	ν/R	$(\nu/R)^{\frac{1}{2}}$
74 W	*1193.7*	*763.4*	*27.630*
77 Ir	*1091.5*	*834.9*	*28.895*
79 Au	*1029.9*	*884.8*	*29.746*
82 Pb	*946.4*	*962.9*	*31.031*
83 Bi	*920.1*	*990.4*	*31.470*

The work is being continued in regions of the x-ray spectra not included in the present report. It is a pleasure to acknowledge the advice and criticism which Professor F. K. Richtmyer has offered in the course of this research.

[17] F. K. Richtmyer and S. Kaufman, Phys. Rev. **44**, 605 (1933).

Probability of Double Jumps in X-Ray Spectra

E. G. RAMBERG,[1] *Heckscher Research Assistant, Cornell University*

(Received October 19, 1933)

By a suitable perturbation method, two-electron transition probabilities are computed for a number of double jumps, such as $2p, 4s \rightarrow 1s, 3s$ and $2p, 3d \rightarrow 1s, 3s$, in Na and Cu atoms. It is found that these probabilities are too small to account for the observed intensities of the x-ray satellites $K\alpha_{3,4}$. As a more general argument against the correctness of the double-jump hypothesis for the origin of the short wave-length x-ray satellites it is pointed out that the line structure due to two-electron transitions of the kind considered would consist of a symmetrical grouping of faint lines about the parent line, the stronger components being on the long wave-length side.

A NUMBER of considerations,[2] in particular the disagreement between the ionization potentials of x-ray satellites as predicted by the double ionization theory of Wentzel and Druyvesteyn with the experimental results of DuMond and Hoyt,[3] have lent support to the alternative view advanced by Richtmyer[4] that these satellites were due to transitions between the outer orbits of the atom taking place simultaneously with the inner transition normally producing the parent line. Conclusions reached in the present work are not in agreement with this view.

To test the last-mentioned hypothesis the strong satellites of $K\alpha_{1,2}$, $K\alpha_{3,4}$, were singled out for closer scrutiny. The parent line $K\alpha_{1,2}$ is known to be due to jumps of a $2p$ electron into a vacant $1s$ state. Now the outer field of an atom (atomic number Z) having lost a $1s$ electron resembles that of a singly ionized one of the next higher element (atomic number $Z+1$) very closely. Hence, assuming the double-jump hypothesis to be correct, we have to expect for the frequency of the satellite:

$$\nu_s(Z) \cong \nu_p(Z) + \nu_0(Z+1)^+,$$

where ν_p is the frequency of the parent line and ν_0 that corresponding to a transition in the outer atomic layers. Comparing, with due regard of the selection rules for multiple jumps, transitions in the optical term system of the ion of atomic number $Z+1$[5] with the observed frequency separations of satellite and parent line for element Z, we find that only transitions ending in a $3s$ or $3p$ level could yield separations of the right order of magnitude. Of these, again, we can expect the lowest members of the series, such as $4s \rightarrow 3s$, $4p \rightarrow 3p$, $3d \rightarrow 3s$ to occur most frequently, so that we can confine our attention to them.

If we suppose the satellites to originate in the above manner, the intensity ratio W of satellite and parent line is given by the product of two probability ratios, W_1, that for the excitation process necessary in each case, and W_2, that for the emission process. Thus we have for the line corresponding to $2p, 4s \rightarrow 1s, 3s$:

$$W = W_1 \cdot W_2 = \left\{ \text{Probability of } \begin{pmatrix} 1s \rightarrow \infty \\ 3s \rightarrow 4s \text{ or } \infty \end{pmatrix} \Big/ \text{Probability of } (1s \rightarrow \infty) \right\}$$
$$\times \left\{ \text{Probability of } \begin{pmatrix} 2p \rightarrow 1s \\ 4s \rightarrow 3s \end{pmatrix} \Big/ \text{Probability of } (2p \rightarrow 1s) \right\}.$$

[1] The present note gives results obtained in a thesis presented to the University of Munich.

[2] F. K. Richtmyer, J. Frank. Inst. **208**, 325 (1929); J. W. M. DuMond, Phys. Rev. **36**, 1015 (1930).

[3] J. W. M. DuMond and A. Hoyt, Phys. Rev. **36**, 799 (1930). For contrary evidence see D. Coster and W. J. Thijssen, Zeits. f. Physik **84**, 686 (1933).

[4] F. K. Richtmyer, Phil. Mag. **6**, 64 (1928).

[5] Optical terms refer to free atoms, x-ray observations to atoms bound in a crystal lattice; their comparison is justified below.

Both W_1 and W_2 depend principally on the closeness of the coupling between the electrons in the inner and outer shells of the atom, so that, if we find $W_2 \ll 1$, we are justified in assuming $W_1 \ll 1$ as well. W_2 does not depend on the nature of the excitation process and is, furthermore, easier to compute. Hence we confine our attention to it.

For the purpose of the computations the two electrons participating in the transition were thought of as moving in the centrally symmetric field of the atom core, made up of the nucleus and the remainder of the electrons of the atom and the charge of one electron distributed so as to compensate the effect of one of the moving electrons on the other. We thus treat the case of the free atom. There may be little justification for expecting results thus obtained to hold for atoms bound in a crystal lattice. However, once we assume that x-ray satellites are due to two-electron transitions of the kind considered, the experimentally observed fact that the $K\alpha$ satellite structure is only very slightly influenced by chemical combination[6] leads us to the conclusion that, as long as we are concerned only with orders of magnitude, the influence of the neighboring atoms may be left out of account. As the frequencies of satellite and parent line differ very little we can, disregarding retardation effects, regard the probability I of any transition as proportional to the square of the matrix element of the coordinates of the two electrons:

$$I \sim \left| \int U_a^*(\vec{r}_1+\vec{r}_2)\, U_b d\tau \right|^2. \tag{1}$$

Here U_a is the wave function of the initial and U_b that of the final state. To the zero approximation, i.e., with the linear combinations of products of one-electron wave functions appropriate for (j, j) coupling as wave functions of the system,[7] this matrix element vanishes for two-electron transitions. Hence, expanding U_a and U_b in terms of one-electron wave functions[8] and determining the coefficients by numerical integration, first order expressions were obtained for the matrix element in (1).

The one-electron wave functions themselves were found by numerical integration and adjustment of energy parameters from the Schrödinger equation for central field. The latter was obtained with the aid of a semi-empirical formula given by Slater.[9] Finally the probability of each of the double jumps considered as well as of the related one-electron jump were computed by summing the probabilities of all possible transitions between states making up the initial and final configurations of the atom.

Carrying out computations for the two electron transitions $2p$, $4s \to 1s$, $3s$ and $2p$, $3s \to 1s$, $4s$ in Na(11) and $2p$, $4s \to 1s$, $3s$ and $2p$, $3d \to 1s$, $3s$ in Cu(29) following results were obtained for the probability ratio W_2 of double and single jump:

Sodium:

$$I(2p, 4s \to 1s, 3s)/I(2p, 4s \to 1s, 4s) = 1 : 170, \tag{2a}$$

$$I(2p, 3s \to 1s, 4s)/I(2p, 3s \to 1s, 3s) = 1 : 320 \tag{2b}$$

Copper:

$$I(2p, 4s \to 1s, 3s)/I(2p, 4s \to 1s, 4s) = 1 : 4800, \tag{2c}$$

$$I(2p, 3d \to 1s, 3s)/I(2p, 3d \to 1s, 3d) = 1 : 18{,}000. \tag{2d}$$

As there are 10 $3d$ electrons in copper we have to multiply the ratio in (2d) by the factor 10, obtaining for the relative probability of double and single jumps the ratio 1 : 1800. The double jumps in (2a), (2c), and (2d) correspond to lines on the short wave-length side of the parent line. Here we must require the atom to be initially doubly excited, so that the probability ratio W_1 for the excitation process is itself $\ll 1$, probably of the same order of magnitude as W_2. The computed values of W_2 are themselves considerably

[6] For observations on Si(14) and S(16) see E. Bäcklin, Zeits. f. Physik **38**, 215 (1926).

[7] An analogous treatment for Russell-Saunders coupling led to the same results.

[8] See H. S. W. Massey and C. B. O. Mohr, Proc. Roy. Soc. (London) **A136**, 289 (1932), esp. Eqs. (2) and (4).

[9] J. C. Slater, Phys. Rev. **36**, 57 (1930).

smaller than the measured or estimated intensity ratio for $K\alpha_{3,4}$ and $K\alpha_{1,2}$ (1 : 180 for Cu[10]; very much larger for Na). Hence we must conclude that the relative intensity $W = W_1 \cdot W_2$ predicted by the double jump hypothesis is far too low to account for the satellites $K\alpha_{3,4}$.

The case (2b) corresponds to a long wave-length satellite of $K\alpha_{1,2}$ with a separation from the parent line equal to that of the short wave-length satellite considered in (2a). In this case—(2b)—the initial states of parent line and satellite are identical, so that the expected intensity ratio here becomes simply $W = W_2$. As W_2 for (2b) and (2a) differs by less than a factor of 2, we must hence expect the long wave-length satellite to be far stronger than the corresponding short wave-length satellite. It is generally to be expected that, for every double jump which involves the filling of a newly created vacancy in the outer shells of the atom, there is another more frequently occurring double jump with the same outer transition taking place in the reverse direction. We conclude that the line structure due to double jumps of the type here considered consists, as in the Raman effect, of a symmetrical grouping of faint lines about the parent line, the more intense ones being on the long wave-length side, while the actually observed satellites lie on the short wave-length side. This last conclusion should hold for the bound as well as the free atom, though in the former case the double jump line structure might be replaced largely or even entirely by bands due to transitions from conduction levels and thus become still less observable.

The author wishes to express his thanks to Professor Sommerfeld for his interest and encouragement of this work, and Drs. K. Bechert and H. Bethe for many valuable suggestions. He is also greatly indebted to Professor F. K. Richtmyer, to whom he owes his interest in the subject, and Professor E. H. Kennard for many clarifying discussions.

[10] J. W. M. DuMond and A. Hoyt, Phys. Rev. **36**, 799 (1930).

Raman Spectrum of Heavy Water

R. W. Wood, *The Johns Hopkins University*
(Received January 22, 1934)

The Raman spectra of two samples of heavy water, one 18 percent and the other 80 percent, were excited by the 2536 line of mercury. The 18 percent heavy water gave the usual band ($\Delta\nu=3445$) and a new band ($\Delta\nu=2623$). The new band is probably due to the molecule H^2OH^1. With 80 percent heavy water the new band was much stronger than the 3445 band but was shifted slightly towards shorter wave-lengths. With the 80 percent sample the 3445 band was shifted slightly toward the red with respect to ordinary water. From the amount of shift it is concluded that molecules containing only one atom of heavy hydrogen give two bands, $\Delta\nu=2623$ and $\Delta\nu=3500$, while the molecules made of two heavy hydrogen atoms give a single band $\Delta\nu=2517$. These bands have been photographed as lines in the case of heavy water vapor.

THE Raman spectrum has been obtained of two samples of heavy water, one of 18 percent prepared by John W. Murray of the Chemistry Department and the other of 80 percent loaned by Professor Hugh Taylor of Princeton University. The irradiation tube was of fused quartz 6 mm internal diameter and 35 cm long with a circular disk of the same material, optically worked, and fused within the slightly widened end of the tube, the oxy-hydrogen flame being played against the outer wall only and never making contact with the disk. In this way all distortion of the optical surface was avoided. The other end was drawn down in an oblique direction and painted black. It was clamped in close contact with a vertical Hanovia high potential quartz mercury vapor tube 50 cm long, and the light issuing from the irradiation tube reflected to the spectroscope by means of a quartz total reflection prism. The vertical position has two advantages. It abolishes a temperature gradient across the diameter of the tube which, if present, causes curvature of the rays, the interior of the tube appearing bent into an arc when viewed through the window. This prevents the light from the further end of the fluid column from reaching the spectroscope and enables parasitic light from the fluorescent walls of the tube to enter the instrument. Gas bubbles are sometimes set free by the ultraviolet radiations which accumulate along the upper side of the tube if it is mounted in a horizontal position.

With a tube of such large ratio of length to diameter very careful lining up with respect to the collimator is necessary if full efficiency and complete absence of fluorescence light from the tube wall are to be secured.

As it appears likely that the introduction of heavy hydrogen into organic chemistry will be accompanied by an intensive study of Raman spectra of materials obtainable only in small quantities, a brief description of an easy and rapid method of securing this adjustment may be worth putting on record.

We shall require a double concave lens of the same focus as that of the lens employed for forming an image of the window of the quartz tube on the slit of the spectrograph, preferably a quartz fluorite achromat of about 20 cm focus, if we are operating with ultraviolet excitation. By holding the concave lens before the eye, we can view the window of the Raman tube through the center of the achromat and make sure of its proper orientation. A candle is mounted at a distance of about two meters from the slit of the spectrograph and brought into such a position that it appears at the center of the field of the camera lens when the latter is viewed from the position of the photographic plate. A cardboard screen, perforated with a hole slightly smaller than the window of the tube is next mounted close against the flame on the side facing the spectrograph and an image of the illuminated aperture focussed on the slit of the spectrograph with the achromat. The candle is now removed, the prism mounted against the hole and the ir-

radation tube brought over the prism. We now have to so adjust the prism and tube that the reflected image of the tube is exactly parallel to the axis of the collimator.

A pin is mounted at a distance of about 30 cm from the aperture in such a position that its head appears over the center of the aperture when we view it through the center of the achromat and the concave lens. We now view the aperture with the pupil of the eye immediately behind the pinhead, and by adjusting the prism and Raman tube bring the reflected image into such a position that we are looking directly down its axis at the circular black background at its further end. The pin is now removed and the adjustment checked by again viewing the aperture through the two lenses, moving the eye over the whole area of the lens to make sure that no part of it receives light from the fluorescent wall of the tube. If the aperture is too large one sees also a thin ring of blue light surrounding the black background, and the Raman spectrum will be photographed with a line of continuous spectrum at the top and bottom, punctuated at points with black dots which mark the mercury lines and are useful for distinguishing the latter from the true Raman lines. If the blue ring is exactly focussed on the slit, these horizontal lines will be blurred and partially obscure the Raman spectrum because of the astigmatism of the spectrograph.

To secure the correct position of the projecting lens back the aperture with the mercury tube and mount a narrow horizontal wire across it. Focus this on the slit (which can be lightly smoked by burning magnesium wire), and then make a trial photograph. The wire will probably be found to be out of focus all along the spectrum (for the same reason that dust on the slit is never in focus when the lines are sharp). We now move the lens a millimeter or two away from the slit and make another photograph. If this has made matters worse, move it nearer to the slit, and continue until a sharp image of the wire is obtained.

The spectrograph employed in the present work was furnished with a large Cornu prism and lenses of 100 cm focus by Hilger and was constructed in the laboratory shop. It was found that both samples of heavy water were slightly fluorescent at first, the continouus spectrum almost blotting out the Raman band characteristic of ordinary water, but after a twelve hour exposure the fluorescence disappeared, the background appearing quite black. The 18 percent heavy water gave the usual band $\Delta\nu = 3445$ and a new band $\Delta\nu = 2623$ bordering the mercury line 2700 on the long wave-length side. This sample had the composition 0.034 H^2OH^2, 0.30 H^2OH^1, and 0.66 H^1OH^1 and since the proportion of water molecules made of one atom of light and one of heavy hydrogen to those made of two heavy atoms was about 9 : 1 we can regard the new band as due largely to the former. The intensity ratio of the two bands was 4 : 1, determined by comparing photographs taken with different times of exposure.

With 80 percent heavy water the new band was much stronger than the 3445 band, and no trace of any additional band was found. By taking photographs of both concentrations of heavy water with times of exposure so regulated that the new band had the same intensity in each it was at once clear that with the 80 percent heavy water the band was shifted slightly towards the region of shorter wave-lengths with respect to the band obtained with the 18 percent sample. The faint band of longer wave-length, obtained with the 80 percent sample, was shifted slightly towards the red with respect to the band obtained with ordinary water. By estimating the amount of the two shifts, which could only be done roughly, we arrive at the following conclusions.

The molecules containing only one atom of heavy hydrogen give two bands, $\Delta\nu = 2623$ and $\Delta\nu = 3500$, while the molecules made of two heavy hydrogen atoms give a single band $\Delta\nu = 2517$. Ordinary water gives also a single band $\Delta\nu = 3445$. This band is frequently reported as double, but no trace of this appeared in any of the photographs made with the narrow tube.

On a spectrogram made last year with the same lamp and a longer and much wider tube, there was a slight indication of a region of less intensity near the center of the band. Photographs of the bands are reproduced in Fig. 1.

The exciting line, 2536 lies to the left at a distance nearly equal to the length of the spectrogram. The narrowness of the slit is indicated by the mercury lines. The percent of heavy water is

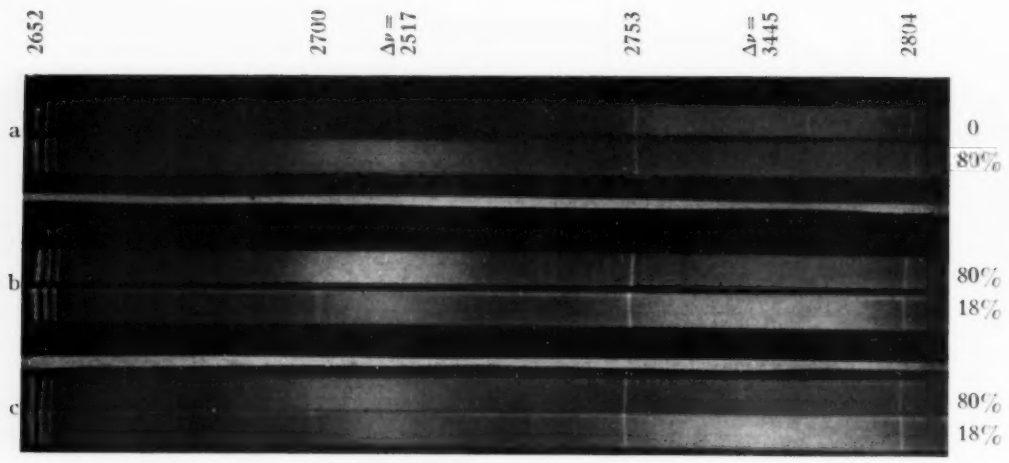

FIG. 1. Photographs of the Raman bands of 18 percent and 80 percent heavy water.

indicated at the right of each spectrogram. Each of the three enlargements were made from two negatives mounted film to film, with the spectra in coincidence. Fig. 1a, is of ordinary water and the 80 percent sample, the latter made up of 0.64 of H^2OH^2, 0.32 of H^1OH^2 and 0.04 of H^1OH^1. The band of longer wave-length, due chiefly to the half heavy molecules is seen to be shifted to the right with respect to the band due to the light water. Fig. 1b, fully exposed spectrograms of 80 percent and 18 percent heavy water and Fig. 1c, the same but with exposure times adjusted to equalize the intensities of the 2517 and 2623 bands to bring out the shift.

The Raman band of ordinary water is shifted towards shorter wave-lengths with respect to the line found by Rank[1] for water-vapor for which the $\Delta\nu = 3650$. Cross and Van Vleck[2] have calculated the values for H^2OH^1 as 3750, 2720 and 1400, the latter not having been found in the Raman spectrum. These values were for the vapor, and the values for the liquid reported in the present paper correspond to bands shifted in the same direction, i.e., towards shorter wave-lengths. Experiments are now under way on the determination of the Raman spectrum of a 66 percent sample in the vapor condition at a pressure of two atmospheres. The line $\Delta\nu = 3550$ has been obtained and also a trace of the double line of shorter wave-lengths but better spectrograms will be produced very shortly.

[1] Rank, J. Chem. Phys. **1**, 504 (1933).
[2] Cross and Van Vleck, J. Chem. Phys. **1**, 350 (1933).

A $^1\Pi \rightarrow {}^1\Delta$ Band of NH and the Corresponding ND Band

G. H. DIEKE AND R. W. BLUE,[1] *The Johns Hopkins University*

(Received December 13, 1933)

A $^1\Pi \rightarrow {}^1\Delta$ band of NH at 3240A is compared with the corresponding ND band at 3235A. The rotational constants of the two bands are related within the limits of experimental errors in the way expected theoretically. It is necessary to take into account that the lowest vibrational state has half a quantum of vibrational energy. The existence of zero point vibrational energy appears also in the fact that the zero lines of the two bands are separated by 93.39 wave numbers. In agreement with the theoretical expectations the Λ-doubling in the ND band is smaller than in the NH band by a factor 3.511.

THE discovery of the hydrogen isotope with mass two has opened up new possibilities for the study of the band spectra of hydrogen compounds. Whereas in all other cases the isotope effect is small, it may produce bands of an entirely different appearance if an H atom is replaced by its heavy isotope D.[2] Besides, the hydrogen isotopes present the additional very important advantage that they can be obtained in any ratio, whereas for the heavier elements one has to be satisfied with the mixture which is provided by nature (except for some very special cases as the Pb isotopes), and which very often gives a very unpleasant overlapping of the different bands.

The mass-ratio for the two hydrogen isotopes is approximately two, whereas it is very close to one for all other isotopes. This means that it is possible to study with ease also the isotope effect on finer points of the band structure as, e.g., the interaction between the electron movement and rotation. It hardly needs mentioning that the isotope effect will greatly help with the analysis of complicated spectra of hydrogen compounds and facilitate their interpretation.

We have, therefore, photographed besides the spectrum of the hydrogen molecule, the band spectra of several hydrogen compounds. The present paper presents the results on a band of very simple structure of the NH and ND molecule, respectively.

In a discharge in a mixture of nitrogen and hydrogen there is in the near ultraviolet, besides the well-known $^3\Pi \rightarrow {}^3\Sigma$ band at 3370A, a band of much simpler structure with a head at 3240A which apparently escaped until now the attention of band spectroscopists. We photographed and analyzed it some time ago but refrained from publishing the results, as a personal communication from Dr. Pearse informed us that he had found and studied the same band. In the meantime we were able to photograph the ND spectrum with the help of a drop of water which contained about 50 percent of the heavy isotope, for which we are greatly indebted to Professor G. N. Lewis. The photographs show clearly the ND bands equivalent both to the 3370 and 3240 NH bands. As the 3370 band is more complex there is a great deal of overlapping in the very closely spaced Q-branches so that photographs with purer ND samples are desirable.[3] We confine ourselves therefore in this paper to the much simpler short wave-length band. As Pearse's paper on the 3240 NH band had not appeared when this was written, we give also our results on this band[3a] as well as those of the corresponding ND band which has its head at 3235A.

[1] National Research Fellow.

[2] We use D as symbol for the heavy hydrogen isotope because its convenience for the typist and printer without meaning to anticipate anything about the final settlement of the nomenclature.

[3] We obtained such photographs since then and hope to report also on the $^3\Pi \rightarrow {}^3\Sigma$ bands in the near future.

[3a] *Note added with proof:* Pearse's paper has appeared in the meantime (Proc. Roy. Soc. **A143**, 112, December, 1933) and his results are in good agreement with ours. His value 30, 704.13 for ν_0 is obviously a misprint.

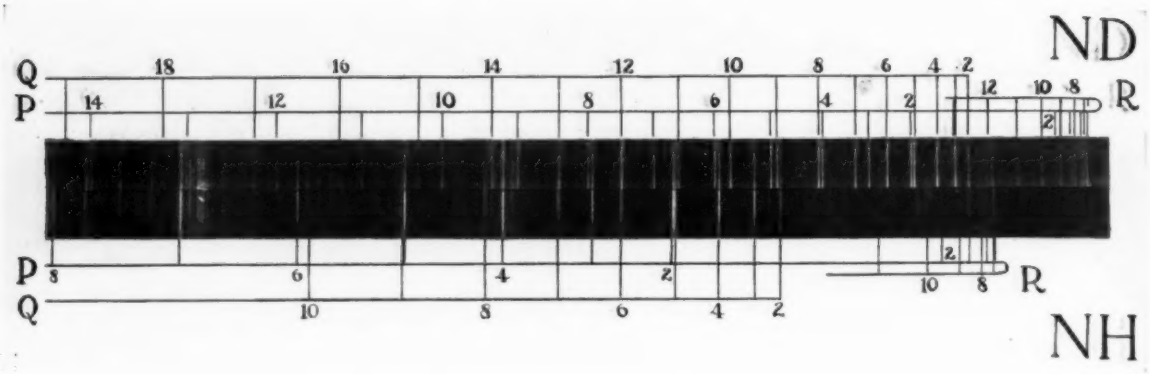

FIG. 1. Photograph of bands of NH and ND.

We can be very brief about the experimental details. For the production of the ordinary NH bands a Pyrex tube with a horizontal part of about 50 cm length and aluminum electrodes in side tubes was used. The tube was water-cooled and took a current of about 1.5 amperes at 2000 to 6000 volts. A mixture of N_2 and H_2 streamed through the tube. (Also ammonia was used but found to have no advantages.) If the percentage of nitrogen is relatively high, the NH bands are strong, but so are the nitrogen bands which obscure many of the NH lines. For this reason it is more advantageous to use a mixture with only so little nitrogen that in the visible the spectrum is almost completely the H_2 spectrum. The NH bands appear then, though much weaker, free from the nitrogen bands. The continuous hydrogen spectrum is then bothersome. It can be much weakened by employing a condensed discharge, a means which we, however, for various reasons were unable to use.

The same remarks apply to the production of the ND spectrum. Due to the small amount of heavy hydrogen at our disposal the technique was changed in several points. The discharge tube was of the same type, but smaller, with a horizontal part of 7 mm width and 50 cm length. This horizontal part was lightly silvered on the inside as the tube was primarily used for the production of the DH and D_2 spectra. The tube was made entirely of quartz and had tantalum electrodes. The heavy water was allowed to react with sodium and the hydrogen was admitted into the discharge tube through a hot palladium tube. The portion which was bound to the sodium in the form of NaOH was recovered by heating the NaOH. If a suitable amount of nitrogen was admitted the NH and ND bands appeared easily. It was found that the nitrogen disappeared quite rapidly in the tube so that the spectrum changed from a spectrum showing predominantly the nitrogen bands to a pure hydrogen spectrum. For this reason it was necessary to repeat the admission of nitrogen from time to time, and it became rather difficult to obtain the NH bands with sufficient strength without the nitrogen bands. The nitrogen must have gone into the electrodes.

Another remarkable feature of this tube was that it made apparently no difference whether nitrogen or air was used. The appearance of the spectrum was the same in both cases and in particular there was no trace of the OH bands. This seems remarkable as it was practically impossible to eliminate the OH bands from the other tube even if great care was taken to dry the gases carefully before they were admitted. We hope to be able to clear up this point with a new tube of the same design without the inside silvering and without the palladium tube.

All the plates used for the present paper were obtained in the first order of a 6 inch, 21 foot concave grating with 30,000 lines per inch and a dispersion of 1.3A per mm.

Fig. 1 shows the bands in question. The lower part is NH only, obtained with ordinary hydrogen and contains only NH lines (besides very faintly some N_2 and OH lines). The upper part was obtained with a mixture of roughly equal parts of the light and heavy isotope. The lines

which occur on the upper picture but not on the lower one are the ND lines and it is easily seen that they form a band of the same general structure as the 3240 NH band. A comparison of the two bands is the main object of this paper. (See Table I.)

The structure of each of the bands is easily recognized as that of a $^1\Pi \rightarrow {}^1\Delta$ transition. There are only three branches, which shows that the bands are singlet bands. In the P- and R-branch four lines are missing near the origin, which shows, if one takes also the position of the Q-branch into account, unambiguously that we have a $^1\Pi \rightarrow {}^1\Delta$ transition and fixes also the numbering of the lines. The fact that the R-branch is the weakest branch agrees with this.

Except for the lowest J-values all the lines show Λ-doubling. Within the limits of experimental errors the doubling is identical for $R(J-1)$, $Q(J)$, and $P(J+1)$, (see Fig. 2), and from this it follows that the doubling of the lines is entirely due to the doubling of the II-level, and that the doubling of the Δ-level is inappreciable.

The bands are both $0 \rightarrow 0$ vibrational transitions. That is made probable by the fact that no other vibrational transitions of the system are observed and confirmed by the isotope effect.

We come now to a comparison of the two bands. The rotational energy of a diatomic molecule is given by the well-known expression

$$W_r/h = BJ(J+1) - DJ^2(J+1)^2 + FJ^3(J+1)^3 - \cdots, \quad (1)$$

in which, if I is the moment of inertia and ω the frequency of the internuclear vibrations

$$B = h/8\pi^2 I; \qquad D = 4B^3/\omega^2; \qquad F = 3D^2/B. \quad (2)$$

All the constants are in general functions of the vibrational quantum number v.

Assuming the validity of a formula of the type (1) the constants were calculated from the first eight differences

$$R(J-1) - Q(J-1) = Q(J) - P(J) = F'(J) - F'(J-1)$$

$$R(J-1) - Q(J) = Q(J-1) - P(J) = F''(J) - F''(J-1)$$

respectively, and

$$F(J) - F(J-1) = 2BJ - 4DJ^3 + 2F(3J^5 + J^3). \quad (3)$$

TABLE I. The wave numbers and intensities of the bands. There are a few coincidences which are indicated in the column "Remarks." If a weak line is covered by a strong one, its wave number is not given, as it would be meaningless. The ND lines were measured on plates which showed the NH band with about the same strength, whereas the NH lines could be measured on plates free from ND, so that in this case the coincidence with a ND line does not affect the measurement. In such cases the coinciding lines are put between brackets.

	NH band at 3240A									
	P-branch			Q-branch			R-branch			
J		I	Remarks		I	Remarks		I	Remarks	
2	30 685.39	4		30 741.93	3		308 26.69	1		
3	643.45	4		728.10	4		40.85	2b		
4	597.07	4b		709.71	5		49.90	1c		
							50.36	1c		
5	545.97	3c		686.25	3c		54.08	2	R6	
	46.22	3c		86.72	3c		54.77	1		
6	490.35	3c		658.20	3	(ND Q 12)	53.15	1		
	90.88	3c		58.92	3	(ND Q 12)	54.08	2	R5	
7	430.39	2d	λ3370R	625.20	3		46.96	1		
	31.03	2		26.10	3	(ND Q 13)	48.16	1		
8	365.51	2		587.25	3		35.32	1		
	66.42	2		88.43	3		36.79	1		
9	296.09	1		544.14	2		18.05	1		
	97.35	2	λ3370R	45.74	2c	close to $P5$	19.86	1		
10				495.77	1		307 94.87	0		
				97.58	1		94.14	0		
11							65.83	0		
							68.49	0		
	ND band at 3235A									
2	30 811.28	4	(R14)	30 841.82	3		308 87.52	1		
3	788.86	5		834.61	4		95.56	2		
4	764.06	5		825.01	5		309 01.05	2		
5	736.92	5		812.99	6		04.10	2c		
6	707.40	5		798.51	6		04.57	2c		
7	675.46	5		781.59	5b		02.45	2b		
8	641.25	4b		761.96	3c		308 97.58	1c		
				62.25	3c		97.95	1c		
9	604.58	4b		739.95	3		90.16	1		
				40.34	3		90.60	1		
10	565.28	3c		715.37	2		80.00	1		
	65.64	3c		15.94	2		80.56	1		
11	523.68	2		688.23	2		67.04	1		
	24.20	2		88.81	2		67.81	1		
12	479.57	1				NH Q6	51.36	1		
	80.29	1				NH Q6	52.20	1		
13	433.08	1	Traces of head of 3285 N_2 band	626.01	3	NH Q7	32.78	0		
	33.86	2		26.73	2		33.68	0		
14	383.96	2	other line superimposed	590.85	2d	Traces of head of 3268 N_2 band				P_2
	84.92	1		91.67	2d		12.16	0		
15				552.66	1		307 86.57	0		
				53.79	1		87.87	0		
16				511.80	1					
				13.05	1					
17				467.88	1					
				69.41	1					
18				420.94	1					
				22.53	1					
19				370.97	0					
				72.72	0					

This is permissible on account of the fact that the Λ-doubling for the Δ-level is negligible. It appears that the observations can be represented within the limits of experimental errors by (3) and the constants obtained in this way are collected in Table II. In calculating the constants for NH it is necessary to take the term $FJ^3(J^3+1)$ in (1) into account. The error which is made when this term is neglected is, however, negligible for ND.

TABLE II. *Constants of the bands.*

	NH	ND	Ratio
B_a'	14.154	7.639	1.8529
B_b'	14.171	7.640	1.8555
B''	16.446	8.836	1.8614
D'	2.44×10^{-3}	6.54×10^{-4}	3.72
D''	1.74×10^{-3}	5.05×10^{-4}	3.45
			Difference
ν_0	307 55.61	308 49.00	93.39

If we distinguish the constants of the heavy isotope by a – above the symbol, and if we call, as is customary, the ratio of the reduced masses $\rho^2=\bar{\mu}/\mu$ we have the following relations

$$\omega=\rho\bar{\omega}, \qquad B=\rho^2\bar{B}, \qquad D=\rho^4\bar{D}, \qquad F=\rho^6\bar{D}, \quad (4)$$

if we assume that the only difference in the nonrotating molecules is the difference in the masses of the H and D atoms.

As the term $BJ(J+1)$ is by far the largest part of the rotational energy the effect of the substitution of an H nucleus by a D nucleus is that the rotational energies and therefore also the distance of the band lines from the origin of the band shrink by a factor ρ^2, and that this is approximately the case is immediately apparent from Fig. 1. But Fig. 1 shows also that this simple shrinking by a factor ρ^2 cannot be the complete change. For, if this were so, the relative position, except for the factor ρ^2, of all the lines should be exactly the same in both bands. A look at the position of the line $R(2)$ with respect to $R(9)$ and $R(10)$, e.g., shows immediately that this is not the case and the reason for this is that, for a given J, the centrifugal distortion is relatively bigger in NH than in ND which is expressed in that the coefficient D in (1) is multiplied by a higher power of ρ than B.

The last column of Table II gives the ratio of the constants for the two bands. If we take the value 2.01363 of Bainbridge[4] for the mass of the D atom we obtain the following values for the powers of ρ:

$$\rho=1.3684, \quad \rho^2=1.8726, \quad \rho^3=2.5625, \quad \rho^4=3.5113.$$

For D′ and D″ the agreement between the values of the ratios in Table II and the above value of ρ^4 is satisfactory, as the accuracy of the D values cannot be very great. The discrepancy between the B-ratios and ρ^2 is, however, too big to be attributed to experimental errors. In order to make sure of this we made some special calculations which showed that by no adjustment of the constants which is compatible with the observations is it possible to get ρ^2 as the ratio for the B-values.

We find the explanation for this apparent discrepancy, if we realize that the relations (4) hold only if the constants are the constants of the nonvibrating and nonrotating molecule. The constants in Table II are the constants for the nonrotating molecule in its lowest vibrational state. This lowest vibrational state has still half a quantum of vibrational energy, and in order that (4) is applicable we have to extrapolate the constants to the vibrationless state. This correction is important only for B and we have

$$B=B_e[1-\alpha(v+1/2)],$$

in which B_e is the B value for the vibrationless molecule and v the vibrational quantum number.[5] ($v=0$ for our case.) As we have only one vibrational state, the value of α is not known, and therefore it is not possible to calculate B_e. We can, however, calculate the value of α which will make $\bar{B}/B=\rho^2$. α is multiplied by ρ if H is substituted for D, and therefore we have, if R is the ratio of the *observed* B-values,

$$\alpha=2\rho(\rho^2-R)/(\rho^3-R)$$

for NH, and

$$\bar{\alpha}=2(\rho^2-R)/(\rho^3-R)$$

for ND. The values found in this way are for NH: 0.076 for Π_a, 0.066 for Π_b, and 0.044 for Δ. For ND they are 0.055, 0.048, and 0.032, respectively. These values have the right order of magnitude. We are making efforts to find some

[4] K. T. Bainbridge, Phys. Rev. **44**, 57 (1933).

[5] Usually what is called here $B_e\alpha$ is designated by α.

other vibrational transitions of the same band system from which the value of α can be calculated.[5a]

We have seen in the preceding section that the ratio of the B-values will come at least very close to its expected value ρ^2 if the constants for the nonvibrating molecule are chosen. Although in ignorance of the values for α we are not able to test now whether this value will be exactly ρ^2, it may be well to call attention to some causes which might make it deviate from this value.

There is in the first place the obvious but very unlikely effect which would occur if the internuclear distance would change by substituting D for H. We have, however, only the right to assume such a change in internuclear distance, if we are quite sure that none of the other possible causes is responsible for any deviation from the relations (4).

The expression (1) for the rotational energy together with (2) are only valid if the interaction between rotation and electronic movement can be neglected. We know that this is the case for $^1\Sigma$-levels which are far enough away from other levels with which they might interact. None of the levels involved here is a $^1\Sigma$-level. For $^1\Pi$ and $^1\Delta$ levels the interaction between rotation and electron movement has been calculated by Hill and Van Vleck[6] and the formulae of these authors apply if there are not other electronic levels near which might interact with the levels in question. The deviations from (1) are in first approximation proportional to $J(J+1)$ and the next higher term is proportional to $J^2(J+1)^2$. The formula for the rotational energy has, therefore, still the form (1) but the coefficients are no longer connected with the moment of inertia and the frequency of the nuclear vibrations by (2).

The simplest case is a $^1P\Pi$ term, i.e., a level for which the resultant angular momentum of the electron motion is one and directed along the internuclear axis. It is split up, like all levels which are not $^1\Sigma$ levels,[7] into two components (here distinguished by subscripts a and b). One of these components is exactly represented by (1) and (2), the other one has the additional terms (A is a constant)

$$(4B^2/A)J(J+1)-(16B^4/A^3)J^2(J+1)^2,$$

of which only the first one is of any significance for our case. It represents the Λ-doubling and it is multiplied by ρ^4 in going from ND to NH. Of the two B-values which are found for the Π level we see that only one can be expected to satisfy the relations (4). We cannot say in our case which of the two this is, but if the α values are known, the above fact can be used to decide about the nature of the Π level. For a $^1D\Pi$ level none of the resultant B-values will have exactly the ratio ρ^2, as both doublet components have additional terms proportional to $BJ(J+1)/A$.

In any case the Λ-doubling should be proportional to $J(J+1)$ and its transformation factor should be ρ^4. This can be tested very well with the data at our disposal. A glance at Fig. 1 shows immediately that the Λ-doubling is considerably larger for NH than for ND. That this must be the case can be seen qualitatively without any calculation if we consider the fact that the Λ-doubling is due to the interaction between electron motion and rotation and will be determined principally by the angular velocity of the rotation as the electron motion is assumed to be the same in both isotopes. As the angular velocity is proportional to J/I, for a given value of J it is larger in NH than in ND by a factor ρ^2, and therefore the Λ-doubling must be larger in the lighter isotope.

Fig. 2 gives the results of a quantitative analysis of the Λ-doubling. The upper curve represents $0.0161J(J+1)$ and the figure shows that it agrees excellently with the observed Λ-doubling for NH. The lower curve is $0.0161J(J+1)/\rho^4$ and it represents well the Λ-doubling for ND.

In a $^1\Delta$-level there are also additional terms in $J(J+1)$ and $J^2(J+1)^2$ which express the interaction between rotation and electron motion. The

[5a] *Note added with proof:* Since the present article was written we have succeeded in photographing and analyzing the 1→0 band of NH and the 1→0 and 1→2 bands of ND. From the analysis of these bands it is possible to obtain the vibrational constants and the values of α. If these values are taken into account the agreement of the value of the B_e-ratios with the theoretical value, ρ^2, becomes satisfactory. Details about these bands will be given in a subsequent paper.

[6] E. L. Hill and J. H. Van Vleck, Phys. Rev. **32**, 250 (1928).

[7] For a discussion of the properties of such terms see also G. H. Dieke, Zeits. f. Physik **57**, 71 (1929).

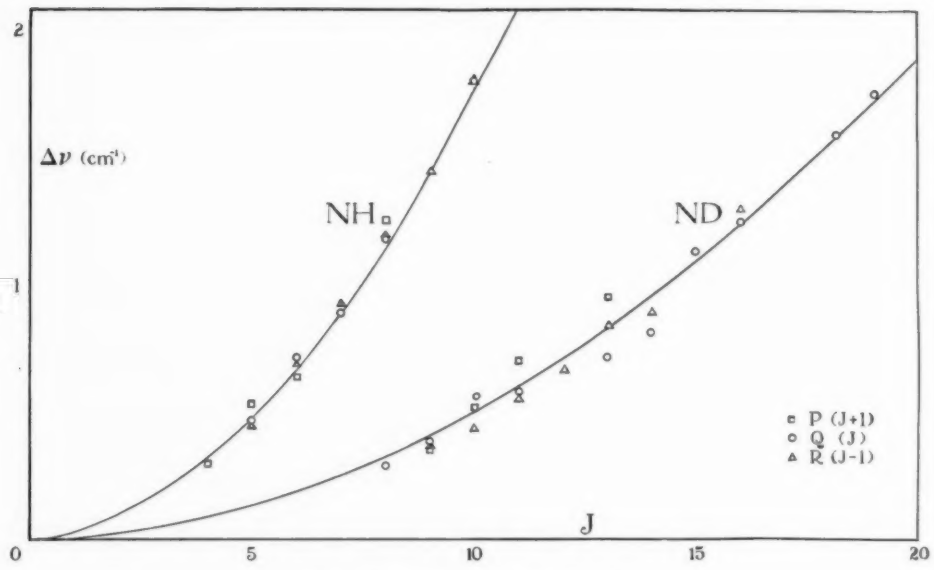

FIG. 2. Λ-doubling of the $^1\Pi$-level.

essential difference from a $^1\Pi$-term is that the terms in $J(J+1)$ have the same sign and magnitude for both doublet components so that therefore the Λ-doubling is much smaller and roughly proportional to $J^2(J+1)^2$. In our $^1\Delta$-term it is too small to be noticed. But even if the Λ-doubling is unnoticeable the term in $J(J+1)$ may be appreciable so that the observed B ratios may be different from ρ^2. There are no data which would allow an estimate of how big this difference is in our case.

The zero lines of the two bands are 307 55.61 for NH and 308 49.00 for ND. The shift of 93.39 wave numbers is due to the zero point vibrational energy of half a quantum which was also responsible for the apparent discrepancy between the observed B-ratios and the expected value ρ^2. If we neglect the anharmonic terms in the vibrational energy we have

$$\nu_0 = \nu_e - 1/2(\omega'' - \omega').$$

From which it follows that the shift is

$$[(\rho-1)/2\rho](\omega'' - \omega') = 93.39$$

or

$$\omega'' - \omega' = 694 \text{ cm}^{-1}.$$

If the transition were not a 0→0 but, e.g., a 0→1 transition we would have

$$3\omega'' - \omega' = 694,$$

which would give $\omega'' < 347$ which is much too small a value.

We wish to thank Professor G. N. Lewis and Dr. R. T. Macdonald for the heavy water which made this investigation possible.

The Spectra of Chlorine, Cl III, Cl IV and Cl V

I. S. BOWEN, *California Institute of Technology*

(Received January 25, 1934)

About 200 additional lines have been classified in Cl III. 21 of these are intercombination lines. This analysis fixes most of the doublet and quartet terms arising from the addition of a 4*s*, 5*s*, 4*p*, 3*d* or 4*d* electron to either the ^3P or ^1D state of the core. Approximately 50 new lines have been classified in Cl IV and 20 in Cl V.

THE spectrum of chlorine in the range from 200A to 600A was photographed with a grazing incidence spectrograph of two meters focus, and from 400A to 3000A with a normal incidence vacuum spectrograph of one meter focus. In both instruments the source was a vacuum spark between electrodes into which NaCl or LiCl had been fused. From 2400A to 5100A the spectrum of a condensed discharge in CCl_4 vapor was recorded with a 6.5 meter focus Rowland spectrograph. This was supplemented in the range from 2100A to 3000A with plates taken on a quartz spectrograph.

The structure of the Cl III spectrum was first investigated by the present writer[1] who classified over 80 lines, largely in the quartet system. Later Gilles[2] identified a group of lines that corresponded to transitions to the $s^2p^23d\ ^4P$ terms from the already classified quartet terms of the s^2p^24p configuration. Majumbar and Deb[3] and Murakawa[4] independently classified this same group of lines as well as another group connecting the $s^2p^24d\ ^4F$ terms with the s^2p^24p configuration. These later analyses accounted for about 30 more lines.

About 200 additional lines have been classified in the course of the present investigation. All of the lines of Cl III that have been identified by various investigators are given in Table I with the exception of the quartet lines, listed in the author's earlier paper which are omitted to save space. In a few cases in which the line was recorded on the quartz spectrograph only, the more accurate values of the wave-length determined by Jevons[5] have been substituted.

Table II lists the values of all of the terms of Cl III that have thus far been fixed. Since a large number of intercombination lines were found the relative positions of the doublet and quartet terms are accurately fixed.

Because of perturbations by the sp^4 and s^2p^24s configurations, the terms arising from the addition of a 3*d* electron to the ^3P state of the core are quite abnormal. Consequently the exact classifications of the doublet levels of this configuration are somewhat uncertain although the large number of transitions involving them leaves little doubt as to the presence of terms at the energy levels listed. One or two other terms such as the $s^2p^2(^1D)4d\ ^2D$ terms were also identified on somewhat meager evidence.

The writer's first paper also contained the classification of about 20 lines each in Cl IV and Cl V. It has now been possible to classify about 50 additional lines in Cl IV and 20 in Cl V. These are given in Tables III and V, respectively. Lines correctly identified in the earlier paper have been omitted except in a very few cases in which more accurate measurements of wave-length are now available. Tables IV and VI give all term values in Cl IV and Cl V, respectively, that have thus far been located. In Table VI the quartet and doublet term values were fixed independently as no intercombination lines were identified.

[1] I. S. Bowen, Phys. Rev. **31**, 34 (1928).
[2] M. J. Gilles, Comptes Rendus **188**, 1158 (1929).
[3] K. Majumbar and S. C. Deb, Ind. J. Sci. **3**, 445 (1929).
[4] K. Murakawa, Sci. Pap. Tokyo Inst. Phys. and Chem. **15**, 105 (1931).
[5] W. Jevons, Proc. Roy. Soc. **A103**, 193 (1923).

TABLE I. *Classified lines of Cl III.*

Int.	λ Vac.	ν	Classification	
1	406.274	246139	$s^2p^2\ ^4S$	$-s^2p^2(^3P)5s\ ^4P_{2\frac{1}{2}}$
0	407.513	245391	$s^2p^2\ ^4S$	$-s^2p^2(^3P)5s\ ^4P_{1\frac{1}{2}}$
3	411.163	243213	$s^2p^2\ ^4S$	$-s^2p^2(^3P)4d\ ^4P_{\frac{1}{2}}$
4	411.373	243088	$s^2p^2\ ^4S$	$-s^2p^2(^3P)4d\ ^4P_{1\frac{1}{2}}$
4	411.812	242829	$s^2p^2\ ^4S$	$-s^2p^2(^3P)4d\ ^4P_{2\frac{1}{2}}$
1	415.196	240850	$s^2p^2\ ^2D_{1\frac{1}{2}}$	$-s^2p^2(^1D)5s\ ^2D_{1\frac{1}{2}}$
1	415.333	240771	$s^2p^2\ ^2D_{2\frac{1}{2}}$	$-s^2p^2(^1D)5s\ ^2D_{2\frac{1}{2}}$
3	421.771	237095	$s^2p^2\ ^2D_{1\frac{1}{2}}$	$-s^2p^2(^1D)4d\ ^2F_{2\frac{1}{2}}$
3	421.990	236972	$s^2p^2\ ^2D_{2\frac{1}{2}}$	$-s^2p^2(^1D)4d\ ^2F_{3\frac{1}{2}}$
1	422.713	236567	$s^2p^2\ ^2D_{1\frac{1}{2}}$, $2\frac{1}{2}$	$-s^2p^2(^1D)4d\ ^2D_{1\frac{1}{2}}$, $2\frac{1}{2}$
0	433.664	230593	$s^2p^2\ ^2D_{1\frac{1}{2}}$	$-s^2p^2(^3P)4d\ ^2D_{2\frac{1}{2}}$
0	433.774	230535	$s^2p^2\ ^2D_{2\frac{1}{2}}$	$-s^2p^2(^3P)4d\ ^2D_{2\frac{1}{2}}$
3	441.398	226553	$s^2p^2\ ^2D_{2\frac{1}{2}}$	$-s^2p^2(^3P)4d\ ^2F_{3\frac{1}{2}}$
2	442.947	225761	$s^2p^2\ ^2D_{1\frac{1}{2}}$	$-s^2p^2(^3P)4d\ ^2F_{2\frac{1}{2}}$
3	457.169	218737	$s^2p^2\ ^2P_{1\frac{1}{2}}$	$-s^2p^2(^3P)4d\ ^2D_{2\frac{1}{2}}$
2	457.245	218701	$s^2p^2\ ^2P_{\frac{1}{2}}$	$-s^2p^2(^3P)4d\ ^2D_{1\frac{1}{2}}$
0	457.444	218606	$s^2p^2\ ^2P_{1\frac{1}{2}}$	$-s^2p^2(^3P)4d\ ^2D_{1\frac{1}{2}}$
2B	552.908	180862	$s^2p^2\ ^2D_{2\frac{1}{2}}$	$-s^2p^2(^1D)3d\ ^2P_{1\frac{1}{2}}$
6	556.232	179781	$s^2p^2\ ^4S$	$-s^2p^2(^3P)3d\ ^4P_{\frac{1}{2}}$
7	556.605	179661	$s^2p^2\ ^4S$	$-s^2p^2(^3P)3d\ ^4P_{1\frac{1}{2}}$
7	557.118	179495	$s^2p^2\ ^4S$	$-s^2p^2(^3P)3d\ ^4P_{2\frac{1}{2}}$
1	558.385	179088	$s^2p^2\ ^4S$	$-s^2p^2(^3P)4s\ ^4P_{1\frac{1}{2}}$
1	560.636	178369	$s^2p^2\ ^4S$	$-s^2p^2(^3P)4s\ ^2P_{\frac{1}{2}}$
7	561.530	178085	$s^2p^2\ ^2D_{1\frac{1}{2}}$	$-s^2p^2(^1D)3d\ ^2F_{2\frac{1}{2}}$
7	561.680	178037	$s^2p^2\ ^2D_{2\frac{1}{2}}$	$-s^2p^2(^1D)3d\ ^2F_{3\frac{1}{2}}$
7	561.738	178019	$s^2p^2\ ^2D_{2\frac{1}{2}}$	$-s^2p^2(^1D)3d\ ^2F_{2\frac{1}{2}}$
4	564.287	177215	$s^2p^2\ ^2D_{1\frac{1}{2}}$	$-s^2p^2(^1D)3d\ ^2D_{1\frac{1}{2}}$
2	564.514	177144	$s^2p^2\ ^2D_{2\frac{1}{2}}$	$-s^2p^2(^1D)3d\ ^2D_{1\frac{1}{2}}$
3	565.272	176906	$s^2p^2\ ^2D_{1\frac{1}{2}}$	$-s^2p^2(^1D)3d\ ^2D_{2\frac{1}{2}}$
4	565.480	176841	$s^2p^2\ ^2D_{2\frac{1}{2}}$	$-s^2p^2(^1D)3d\ ^2D_{2\frac{1}{2}}$
4	586.874	170394	$s^2p^2\ ^2D_{2\frac{1}{2}}$	$-s^2p^2(^1D)4s\ ^2D_{1\frac{1}{2}}$
3	587.078	170335	$s^2p^2\ ^2D_{1\frac{1}{2}}$, $2\frac{1}{2}$	$-s^2p^2(^1D)4s\ ^2D_{2\frac{1}{2}}$, $1\frac{1}{2}$
4	587.295	170272	$s^2p^2\ ^2D_{2\frac{1}{2}}$	$-s^2p^2(^1D)4s\ ^2D_{2\frac{1}{2}}$
3	591.118	169171	$s^2p^2\ ^2P_{\frac{1}{2}}$	$-s^2p^2(^1D)3d\ ^2P_{1\frac{1}{2}}$
4	591.428	169082	$s^2p^2\ ^2P_{1\frac{1}{2}}$	$-s^2p^2(^1D)3d\ ^2P_{1\frac{1}{2}}$
4	591.646	169020	$s^2p^2\ ^2P_{\frac{1}{2}}$	$-s^2p^2(^1D)3d\ ^2P_{\frac{1}{2}}$
2	591.962	168930	$s^2p^2\ ^2P_{1\frac{1}{2}}$	$-s^2p^2(^1D)3d\ ^2P_{\frac{1}{2}}$
4	594.636	168170	$s^2p^2\ ^2D_{1\frac{1}{2}}$	$-s^2p^2(^3P)3d\ ^2P_{\frac{1}{2}}$
3	595.990	167788	$s^2p^2\ ^2D_{1\frac{1}{2}}$	$-s^2p^2(^3P)3d\ ^2P_{1\frac{1}{2}}$
4	596.240	167718	$s^2p^2\ ^2D_{2\frac{1}{2}}$	$-s^2p^2(^3P)3d\ ^2P_{1\frac{1}{2}}$
1	605.855	165056	$s^2p^2\ ^2P_{1\frac{1}{2}}$	$-s^2p^2(^1D)3d\ ^2D_{2\frac{1}{2}}$
2	606.100	164989	$s^2p^2\ ^2D_{1\frac{1}{2}}$	$-s^2p^2(^3P)3d\ ^2D_{2\frac{1}{2}}$
5	606.345	164923	$s^2p^2\ ^2D_{2\frac{1}{2}}$	$-s^2p^2(^3P)3d\ ^2D_{2\frac{1}{2}}$
4	609.673	164022	$s^2p^2\ ^2D_{1\frac{1}{2}}$	$-s^2p^2(^3P)3d\ ^2D_{1\frac{1}{2}}$
0	609.901	163961	$s^2p^2\ ^2D_{2\frac{1}{2}}$	$-s^2p^2(^3P)3d\ ^2D_{1\frac{1}{2}}$
1	619.025	161544	$s^2p^2\ ^2D_{2\frac{1}{2}}$	$-s^2p^2(^3P)3d\ ^4P_{1\frac{1}{2}}$
3	621.027	161024	$s^2p^2\ ^2D_{1\frac{1}{2}}$	$-s^2p^2(^3P)4s\ ^2P_{1\frac{1}{2}}$
4	621.280	160958	$s^2p^2\ ^2D_{2\frac{1}{2}}$	$-s^2p^2(^3P)4s\ ^2P_{1\frac{1}{2}}$
3	623.768	160316	$s^2p^2\ ^2D_{1\frac{1}{2}}$	$-s^2p^2(^3P)4s\ ^2P_{\frac{1}{2}}$
1	630.380	158634	$s^2p^2\ ^2P_{\frac{1}{2}}$	$-s^2p^2(^1D)4s\ ^2D_{1\frac{1}{2}}$
1	630.746	158542	$s^2p^2\ ^2P_{1\frac{1}{2}}$	$-s^2p^2(^1D)4s\ ^2D_{1\frac{1}{2}}$
1	631.006	158477	$s^2p^2\ ^2P_{1\frac{1}{2}}$	$-s^2p^2(^1D)4s\ ^2D_{2\frac{1}{2}}$
1	639.757	156309	$s^2p^2\ ^2P_{1\frac{1}{2}}$	$-s^2p^2(^3P)3d\ ^2P_{\frac{1}{2}}$
1	640.928	156024	$s^2p^2\ ^2P_{\frac{1}{2}}$	$-s^2p^2(^3P)3d\ ^2P_{1\frac{1}{2}}$
1	641.304	155932	$s^2p^2\ ^2P_{1\frac{1}{2}}$	$-s^2p^2(^3P)3d\ ^2P_{1\frac{1}{2}}$
2	653.013	153136	$s^2p^2\ ^2P_{1\frac{1}{2}}$	$-s^2p^2(^3P)3d\ ^2D_{2\frac{1}{2}}$
2	656.772	152260	$s^2p^2\ ^2P_{\frac{1}{2}}$	$-s^2p^2(^3P)3d\ ^2D_{1\frac{1}{2}}$
2	657.320	152133	$s^2p^2\ ^2P_{1\frac{1}{2}}$	$-s^2p^2(^3P)3d\ ^2D_{1\frac{1}{2}}$
2	669.949	149265	$s^2p^2\ ^2P_{\frac{1}{2}}$	$-s^2p^2(^3P)4s\ ^2P_{1\frac{1}{2}}$
3	670.383	149169	$s^2p^2\ ^2P_{1\frac{1}{2}}$	$-s^2p^2(^3P)4s\ ^2P_{1\frac{1}{2}}$
3	673.127	148560	$s^2p^2\ ^2P_{\frac{1}{2}}$	$-s^2p^2(^3P)4s\ ^2P_{\frac{1}{2}}$
1	673.598	148457	$s^2p^2\ ^2P_{1\frac{1}{2}}$	$-s^2p^2(^3P)4s\ ^2P_{\frac{1}{2}}$
1	746.864	133893	$s^2p^2\ ^2D_{1\frac{1}{2}}$	$-s^2p^2(^3P)3d\ ^4D_{\frac{1}{2}}$
1	747.415	133795	$s^2p^2\ ^2D_{1\frac{1}{2}}$	$-s^2p^2(^3P)3d\ ^4D_{2\frac{1}{2}}$
1	747.553	133770	$s^2p^2\ ^2D_{2\frac{1}{2}}$	$-s^2p^2(^3P)3d\ ^4D_{1\frac{1}{2}}$
0	1683.18	59411.4	$s^2p^2(^3P)3d\ ^4F_{1\frac{1}{2}}$	$-s^2p^2(^3P)4p\ ^4S$
1	1689.50	59189.1	$s^2p^2(^3P)3d\ ^4F_{2\frac{1}{2}}$	$-s^2p^2(^3P)4p\ ^4S$
2	1797.98	55618.0	$s^2p^2(^3P)3d\ ^4F_{3\frac{1}{2}}$	$-s^2p^2(^3P)4p\ ^4D_{3\frac{1}{2}}$
4	1808.51	55294.1	$s^2p^2(^3P)3d\ ^4F_{4\frac{1}{2}}$	$-s^2p^2(^3P)4p\ ^4D_{3\frac{1}{2}}$
1	1810.26	55240.7	$s^2p^2(^3P)3d\ ^4F_{1\frac{1}{2}}$	$-s^2p^2(^3P)4p\ ^4D_{2\frac{1}{2}}$
4	1817.73	55013.7	$s^2p^2(^3P)3d\ ^4F_{2\frac{1}{2}}$	$-s^2p^2(^3P)4p\ ^4D_{2\frac{1}{2}}$
6	1822.50	54869.7	$s^2p^2(^3P)3d\ ^4F_{4\frac{1}{2}}$	$-s^2p^2(^3P)4p\ ^4D_{3\frac{1}{2}}$
3	1824.59	54806.8	$s^2p^2(^3P)3d\ ^4F_{1\frac{1}{2}}$	$-s^2p^2(^3P)4p\ ^4D_{1\frac{1}{2}}$
5	1828.40	54692.6	$s^2p^2(^3P)3d\ ^4F_{3\frac{1}{2}}$	$-s^2p^2(^3P)4p\ ^4D_{2\frac{1}{2}}$
4	1832.08	54582.8	$s^2p^2(^3P)3d\ ^4F_{3\frac{1}{2}}$	$-s^2p^2(^3P)4p\ ^4D_{1\frac{1}{2}}$
4	1833.31	54546.1	$s^2p^2(^3P)3d\ ^4F_{1\frac{1}{2}}$	$-s^2p^2(^3P)4p\ ^4D_{\frac{1}{2}}$
0	1848.74	54090.9	$s^2p^2(^3P)3d\ ^4D_{\frac{1}{2}}$	$-s^2p^2(^3P)4p\ ^4S$
0	1849.64	54064.6	$s^2p^2(^3P)3d\ ^4D_{1\frac{1}{2}}$	$-s^2p^2(^3P)4p\ ^4S$
2	1852.11	53992.5	$s^2p^2(^3P)3d\ ^4D_{\frac{1}{2}}$	$-s^2p^2(^3P)4p\ ^4S$
3	1880.10	53188.7	$s^2p^2(^3P)3d\ ^4D_{2\frac{1}{2}}$	$-s^2p^2(^3P)4p\ ^2D_{1\frac{1}{2}}$
0	1889.06	52936.4	$s^2p^2(^3P)4p\ ^2D_{2\frac{1}{2}}$	$-s^2p^2(^1D)5s\ ^2D_{2\frac{1}{2}}$
3	1897.85	52691.2	$s^2p^2(^3P)3d\ ^4D_{2\frac{1}{2}}$	$-s^2p^2(^3P)4p\ ^4P_{2\frac{1}{2}}$
5	1901.61	52587.0	$s^2p^2(^3P)3d\ ^4D_{3\frac{1}{2}}$	$-s^2p^2(^3P)4p\ ^4P_{2\frac{1}{2}}$
4	1912.90	52276.6	$s^2p^2(^3P)3d\ ^4D_{2\frac{1}{2}}$	$-s^2p^2(^3P)4p\ ^4P_{1\frac{1}{2}}$
3	1914.09	52244.1	$s^2p^2(^3P)3d\ ^4D_{1\frac{1}{2}}$	$-s^2p^2(^3P)4p\ ^4P_{1\frac{1}{2}}$
4	1916.53	52177.6	$s^2p^2(^3P)3d\ ^4D_{\frac{1}{2}}$	$-s^2p^2(^3P)4p\ ^4P_{1\frac{1}{2}}$
4	1917.87	52141.2	$s^2p^2(^3P)3d\ ^4D_{1\frac{1}{2}}$	$-s^2p^2(^3P)4p\ ^4P_{\frac{1}{2}}$
4	1920.32	52074.7	$s^2p^2(^3P)3d\ ^4D_{\frac{1}{2}}$	$-s^2p^2(^3P)4p\ ^4P_{\frac{1}{2}}$
3	1979.46	50518.8	$s^2p^2(^3P)3d\ ^4D_{2\frac{1}{2}}$	$-s^2p^2(^3P)4p\ ^4D_{2\frac{1}{2}}$
5	1983.61	50413.1	$s^2p^2(^3P)3d\ ^4D_{3\frac{1}{2}}$	$-s^2p^2(^3P)4p\ ^4D_{3\frac{1}{2}}$
3	2003.37	49915.9	$s^2p^2(^3P)3d\ ^4D_{2\frac{1}{2}}$	$-s^2p^2(^3P)4p\ ^4D_{2\frac{1}{2}}$
0	2004.62	49884.8	$s^2p^2(^3P)3d\ ^4D_{1\frac{1}{2}}$	$-s^2p^2(^3P)4p\ ^4D_{2\frac{1}{2}}$
4	2007.49	49813.4	$s^2p^2(^3P)3d\ ^4D_{3\frac{1}{2}}$	$-s^2p^2(^3P)4p\ ^4D_{3\frac{1}{2}}$
1	2011.99	49702.0	$s^2p^2(^3P)4p\ ^2P_{1\frac{1}{2}}$	$-s^2p^2(^1D)5s\ ^2D_{2\frac{1}{2}}$
3	2020.84	49484.4	$s^2p^2(^3P)3d\ ^4D_{2\frac{1}{2}}$	$-s^2p^2(^3P)4p\ ^4D_{1\frac{1}{2}}$
3	2022.11	49453.3	$s^2p^2(^3P)3d\ ^4D_{1\frac{1}{2}}$	$-s^2p^2(^3P)4p\ ^4D_{1\frac{1}{2}}$
3	2024.87	49385.9	$s^2p^2(^3P)3d\ ^4D_{\frac{1}{2}}$	$-s^2p^2(^3P)4p\ ^4D_{1\frac{1}{2}}$
3	2032.80	49193.2	$s^2p^2(^3P)3d\ ^4D_{1\frac{1}{2}}$	$-s^2p^2(^3P)4p\ ^4D_{\frac{1}{2}}$
3	2035.54	49127.0	$s^2p^2(^3P)3d\ ^4D_{\frac{1}{2}}$	$-s^2p^2(^3P)4p\ ^4D_{\frac{1}{2}}$
	λ Air			
2	2266.08	44115.4	$s^2p^2(^2P)4p\ ^4P_{2\frac{1}{2}}$	$-s^2p^2(^2P)4d\ ^2D_{2\frac{1}{2}}$
1	2272.8	43986.0	$s^2p^2(^3P)4p\ ^4P_{2\frac{1}{2}}$	$-s^2p^2(^3P)4d\ ^2D_{1\frac{1}{2}}$
3	2286.0	43731.0	$s^2p^2(^3P)4s\ ^2P_{\frac{1}{2}}$	$-s^2p^2(^1D)4p\ ^2P_{1\frac{1}{2}}$
4B	2291.83	43619.8	$s^2p^2(^3P)4p\ ^4D_{1\frac{1}{2}}$	$-s^2p^2(^3P)4d\ ^2D_{2\frac{1}{2}}$
5B	2298.51	43493.0	$s^2p^2(^3P)4p\ ^4D_{1\frac{1}{2}}$	$-s^2p^2(^3P)4d\ ^2D_{1\frac{1}{2}}$
			$s^2p^2(^3P)4s\ ^2P_{\frac{1}{2}}$	$-s^2p^2(^1D)4p\ ^2P_{\frac{1}{2}}$
6	2323.50	43025.3	$s^2p^2(^3P)4s\ ^2P_{1\frac{1}{2}}$	$-s^2p^2(^1D)4p\ ^2P_{1\frac{1}{2}}$
5	2336.45	42786.8	$s^2p^2(^3P)4s\ ^2P_{1\frac{1}{2}}$	$-s^2p^2(^1D)4p\ ^2P_{\frac{1}{2}}$
6	2340.64	42710.3	$s^2p^2(^3P)4p\ ^2D_{2\frac{1}{2}}$	$-s^2p^2(^3P)4d\ ^2D_{2\frac{1}{2}}$
2	2347.7	42581.4	$s^2p^2(^3P)4p\ ^2D_{2\frac{1}{2}}$	$-s^2p^2(^3P)4d\ ^2D_{1\frac{1}{2}}$
6	2359.67	42367.6	$s^2p^2(^1D)4p\ ^2F_{3\frac{1}{2}}$	$-s^2p^2(^1D)5s\ ^2D_{2\frac{1}{2}}$
6	2370.37	42174.6	$s^2p^2(^1D)4p\ ^2F_{2\frac{1}{2}}$	$-s^2p^2(^1D)5s\ ^2D_{1\frac{1}{2}}$
0	2372.7	42133.7	$s^2p^2(^3P)4p\ ^4D_{\frac{1}{2}}$	$-s^2p^2(^3P)4d\ ^4P_{\frac{1}{2}}$
3	2387.3	41875.3	$s^2p^2(^3P)4p\ ^4D_{1\frac{1}{2}}$	$-s^2p^2(^3P)4d\ ^4P_{\frac{1}{2}}$
5	2394.73	41745.6	$s^2p^2(^3P)4p\ ^4D_{1\frac{1}{2}}$	$-s^2p^2(^3P)4d\ ^4P_{1\frac{1}{2}}$
5	2419.5	41317.7	$s^2p^2(^3P)4p\ ^4D_{2\frac{1}{2}}$	$-s^2p^2(^3P)4d\ ^4P_{1\frac{1}{2}}$
2	2435.1	41054.0	$s^2p^2(^3P)4p\ ^4D_{2\frac{1}{2}}$	$-s^2p^2(^3P)4d\ ^4P_{2\frac{1}{2}}$
5	2436.1	41036.9	$s^2p^2(^1D)4p\ ^2D_{2\frac{1}{2}}$	$-s^2p^2(^1D)5s\ ^2D_{2\frac{1}{2}}$
5	2439.69	40976.4	$s^2p^2(^1D)4p\ ^2D_{1\frac{1}{2}}$	$-s^2p^2(^1D)5s\ ^2D_{1\frac{1}{2}}$
5	2469.20	40486.7	$s^2p^2(^3P)4p\ ^4D_{\frac{1}{2}}$	$-s^2p^2(^3P)4d\ ^4D_{\frac{1}{2}}$
5	2471.07	40456.1	$s^2p^2(^3P)4p\ ^4D_{2\frac{1}{2}}$	$-s^2p^2(^3P)4d\ ^4F_{2\frac{1}{2}}$
3	2485.1	40227.1	$s^2p^2(^3P)4p\ ^4D_{1\frac{1}{2}}$	$-s^2p^2(^3P)4d\ ^4D_{\frac{1}{2}}$
5	2490.3	40143.8	$s^2p^2(^3P)4p\ ^4P_{1\frac{1}{2}}$	$-s^2p^2(^3P)4d\ ^4F_{3\frac{1}{2}}$
5	2528.08	39543.9	$s^2p^2(^3P)4s\ ^2P_{\frac{1}{2}}$	$-s^2p^2(^1D)4p\ ^2D_{1\frac{1}{2}}$
5	2531.76	39486.4	$s^2p^2(^3P)4p\ ^2P_{\frac{1}{2}}$	$-s^2p^2(^3P)4d\ ^2D_{1\frac{1}{2}}$
5	2532.48	39475.2	$s^2p^2(^3P)4p\ ^2P_{1\frac{1}{2}}$	$-s^2p^2(^3P)4d\ ^2D_{2\frac{1}{2}}$
3	2540.84	39345.2	$s^2p^2(^3P)4p\ ^2P_{1\frac{1}{2}}$	$-s^2p^2(^3P)4d\ ^2D_{1\frac{1}{2}}$
3	2557.9	39082.5	$s^2p^2(^3P)4p\ ^4P_{1\frac{1}{2}}$	$-s^2p^2(^3P)4d\ ^4P_{\frac{1}{2}}$
3	2559.50	39058.4	$s^2p^2(^3P)4p\ ^4P_{\frac{1}{2}}$	$-s^2p^2(^3P)4d\ ^4P_{1\frac{1}{2}}$
1	2566.23	38956.0	$s^2p^2(^3P)4p\ ^4P_{1\frac{1}{2}}$	$-s^2p^2(^3P)4d\ ^4P_{1\frac{1}{2}}$
0	2574.13	38836.4	$s^2p^2(^3P)4s\ ^2P_{1\frac{1}{2}}$	$-s^2p^2(^1D)4p\ ^2D_{1\frac{1}{2}}$
5	2577.13	38791.3	$s^2p^2(^3P)4p\ ^2D_{1\frac{1}{2}}$	$-s^2p^2(^3P)4d\ ^2F_{3\frac{1}{2}}$
5	2578.26	38774.3	$s^2p^2(^3P)4s\ ^2P_{1\frac{1}{2}}$	$-s^2p^2(^1D)4p\ ^2D_{2\frac{1}{2}}$
6	2580.67	38738.1	$s^2p^2(^3P)4p\ ^2D_{2\frac{1}{2}}$	$-s^2p^2(^3P)4d\ ^2F_{3\frac{1}{2}}$
3	2588.80	38616.4	$s^2p^2(^1D)4p\ ^2F_{3\frac{1}{2}}$	$-s^2p^2(^1D)4d\ ^2F_{3\frac{1}{2}}$
2	2592.45	38562.0	$s^2p^2(^1D)4p\ ^2F_{2\frac{1}{2}}$	$-s^2p^2(^1D)4d\ ^2F_{3\frac{1}{2}}$
2	2593.97	38539.5	$s^2p^2(^3P)4p\ ^4P_{2\frac{1}{2}}$	$-s^2p^2(^3P)4d\ ^4P_{1\frac{1}{2}}$
4	2601.16	38432.9	$s^2p^2(^3P)4p\ ^4D_{\frac{1}{2}}$	$-s^2p^2(^3P)4d\ ^4F_{1\frac{1}{2}}$
5	2603.59	38397.0	$s^2p^2(^3P)4p\ ^4D_{1\frac{1}{2}}$	$-s^2p^2(^3P)4d\ ^4F_{2\frac{1}{2}}$
2	2605.04	38375.7	$s^2p^2(^1D)4p\ ^2F_{2\frac{1}{2}}$	$-s^2p^2(^1D)4d\ ^2F_{2\frac{1}{2}}$
4	2609.50	38310.1	$s^2p^2(^3P)4p\ ^4D_{2\frac{1}{2}}$	$-s^2p^2(^3P)4d\ ^4F_{2\frac{1}{2}}$
2	2611.45	38281.5	$s^2p^2(^3P)4p\ ^4P_{2\frac{1}{2}}$	$-s^2p^2(^3P)4d\ ^4P_{2\frac{1}{2}}$
4	2616.97	38200.8	$s^2p^2(^3P)4p\ ^4D_{2\frac{1}{2}}$	$-s^2p^2(^3P)4d\ ^4F_{1\frac{1}{2}}$
4	2618.78	38174.4	$s^2p^2(^3P)4p\ ^4D_{1\frac{1}{2}}$	$-s^2p^2(^3P)4d\ ^4F_{1\frac{1}{2}}$
4	2620.05	38155.8	$s^2p^2(^1D)4p\ ^2F_{2\frac{1}{2}}$	$-s^2p^2(^1D)4d\ ^2D_{2\frac{1}{2}}$
3	2624.71	38088.2	$s^2p^2(^1D)4p\ ^2F_{3\frac{1}{2}}$	$-s^2p^2(^1D)4d\ ^2D_{1\frac{1}{2}}$
5	2632.67	37973.0	$s^2p^2(^1D)4p\ ^2F_{3\frac{1}{2}}$	$-s^2p^2(^1D)4d\ ^2D_{2\frac{1}{2}}$
5	2633.18	37965.6	$s^2p^2(^3P)4p\ ^4D_{2\frac{1}{2}}$	$-s^2p^2(^3P)4d\ ^4F_{3\frac{1}{2}}$
3	2651.19	37707.7	$s^2p^2(^3P)4p\ ^4D_{1\frac{1}{2}}$	$-s^2p^2(^3P)4d\ ^4F_{2\frac{1}{2}}$
3	2663.20	37537.6	$s^2p^2(^3P)4p\ ^4P_{\frac{1}{2}}$	$-s^2p^2(^3P)4d\ ^4D_{\frac{1}{2}}$
2	2675.4	37366.2	$s^2p^2(^3P)4p\ ^4D_{3\frac{1}{2}}$	$-s^2p^2(^3P)4d\ ^4F_{2\frac{1}{2}}$
2	2680.88	37290.1	$s^2p^2(^1D)4p\ ^2D_{2\frac{1}{2}}$	$-s^2p^2(^1D)4d\ ^2F_{2\frac{1}{2}}$
3	2682.40	37269.0	$s^2p^2(^3P)4p\ ^4S$	$-s^2p^2(^3P)4d\ ^4P_{\frac{1}{2}}$
5	2684.76	37236.2	$s^2p^2(^1D)4p\ ^2D_{2\frac{1}{2}}$	$-s^2p^2(^1D)4d\ ^2F_{3\frac{1}{2}}$
4	2685.40	37227.3	$s^2p^2(^1D)4p\ ^2D_{1\frac{1}{2}}$	$-s^2p^2(^1D)4d\ ^2F_{2\frac{1}{2}}$
5B	2691.52	37142.8	$s^2p^2(^3P)4p\ ^4S$	$-s^2p^2(^3P)4d\ ^4P_{1\frac{1}{2}}$
1B	2699.8	37029.0	$s^2p^2(^1D)4p\ ^2P_{\frac{1}{2}}$	$-s^2p^2(^1D)5s\ ^2D_{1\frac{1}{2}}$
7	2710.37	36884.5	$s^2p^2(^3P)4p\ ^4S$	$-s^2p^2(^3P)4d\ ^4P_{2\frac{1}{2}}$
2	2714.37	36830.1	$s^2p^2(^1D)4p\ ^2D_{2\frac{1}{2}}$	$-s^2p^2(^1D)4d\ ^2D_{2\frac{1}{2}}$
2	2717.62	36786.0	$s^2p^2(^1D)4p\ ^2P_{1\frac{1}{2}}$	$-s^2p^2(^1D)5s\ ^2D_{2\frac{1}{2}}$
5B	2724.03	36699.5	$s^2p^2(^1D)4p\ ^2D_{1\frac{1}{2}}$	$-s^2p^2(^1D)4d\ ^2D_{1\frac{1}{2}}$
2	2727.7	36650.7	$s^2p^2(^3P)4p\ ^2D_{1\frac{1}{2}}$	$-s^2p^2(^3P)4d\ ^4D_{\frac{1}{2}}$
3	2769.3	36100.0	$s^2p^2(^3P)4p\ ^2D_{2\frac{1}{2}}$	$-s^2p^2(^3P)4d\ ^4D_{1\frac{1}{2}}$
1	2949.1	33898.4	$s^2p^2(^3P)4p\ ^2P_{1\frac{1}{2}}$	$-s^2p^2(^3P)4d\ ^4P_{1\frac{1}{2}}$
6	2965.56	33710.6	$s^2p^2(^1D)4s\ ^2D_{2\frac{1}{2}}$	$-s^2p^2(^1D)4p\ ^2P_{1\frac{1}{2}}$
4	2970.67	33652.6	$s^2p^2(^1D)4s\ ^2D_{1\frac{1}{2}}$	$-s^2p^2(^1D)4p\ ^2P_{1\frac{1}{2}}$
5	2991.82	33414.8	$s^2p^2(^1D)4s\ ^2D_{1\frac{1}{2}}$	$-s^2p^2(^1D)4p\ ^2P_{\frac{1}{2}}$
1	3123.74	32003.7	$s^2p^2(^1D)4p\ ^2F_{2\frac{1}{2}}$	$-s^2p^2(^3P)4d\ ^2D_{1\frac{1}{2}}$
4	3190.58	31333.3	$s^2p^2(^3P)4s\ ^4P_{2\frac{1}{2}}$	$-s^2p^2(^3P)4p\ ^4D_{2\frac{1}{2}}$
0	3193.84	31301.3	$s^2p^2(^3P)4s\ ^4P_{\frac{1}{2}}$	$-s^2p^2(^3P)4p\ ^4D_{1\frac{1}{2}}$
1	3230.78	30943.4	$s^2p^2(^3P)4s\ ^4P_{1\frac{1}{2}}$	$-s^2p^2(^3P)4p\ ^4D_{1\frac{1}{2}}$
5	3244.44	30813.1	$s^2p^2(^3P)4s\ ^2P_{\frac{1}{2}}$	$-s^2p^2(^3P)4p\ ^2P_{1\frac{1}{2}}$
2	3245.05	30807.3	$s^2p^2(^1D)4p\ ^2D_{2\frac{1}{2}}$	$-s^2p^2(^3P)4d\ ^2D_{2\frac{1}{2}}$
6	3259.32	30672.5	$s^2p^2(^3P)4s\ ^2P_{1\frac{1}{2}}$	$-s^2p^2(^3P)4p\ ^2P_{\frac{1}{2}}$
0	3265.45	30614.8	$s^2p^2(^1D)4p\ ^2D_{1\frac{1}{2}}$	$-s^2p^2(^3P)4d\ ^2D_{1\frac{1}{2}}$
7	3320.57	30106.7	$s^2p^2(^3P)4s\ ^2P_{1\frac{1}{2}}$	$-s^2p^2(^3P)4p\ ^2P_{1\frac{1}{2}}$
5	3336.16	29966.0	$s^2p^2(^3P)4s\ ^2P_{1\frac{1}{2}}$	$-s^2p^2(^3P)4p\ ^2P_{\frac{1}{2}}$
5	3386.22	29523.0	$s^2p^2(^1D)4s\ ^2D_{2\frac{1}{2}}$	$-s^2p^2(^1D)4p\ ^2D_{1\frac{1}{2}}$
8	3392.89	29465.0	$s^2p^2(^1D)4s\ ^2D_{1\frac{1}{2}}$	$-s^2p^2(^1D)\ 4p^2D_{1\frac{1}{2}}$
8	3393.45	29460.1	$s^2p^2(^1D)4s\ ^2D_{2\frac{1}{2}}$	$-s^2p^2(^1D)4p\ ^2D_{2\frac{1}{2}}$
2	3400.15	29402.1	$s^2p^2(^1D)4s\ ^2D_{1\frac{1}{2}}$	$-s^2p^2(^1D)4p\ ^2D_{2\frac{1}{2}}$

TABLE I. *(Continued.)*

Int.	λ Vac.	ν	Classification		Int.	λ Vac.	ν	Classification	
9	3530.03	28320.3	$s^2p^2(^1D)4s\ ^2D_{2\frac{1}{2}}$	$-s^2p^2(^1D)4p\ ^2F_{3\frac{1}{2}}$	1	4124.00	24241.5	$s^2p^2(^3P)3d\ ^4P_{\frac{1}{2}}$	$-s^2p^2(^3P)4p\ ^4P_{\frac{1}{2}}$
1	3553.35	28134.5	$s^2p^2(^1D)4s\ ^2D_{2\frac{1}{2}}$	$-s^2p^2(^1D)4p\ ^2F_{2\frac{1}{2}}$	4	4282.46	23344.5	$s^2p^2(^3P)3d\ ^4P_{1\frac{1}{2}}$	$-s^2p^2(^3P)4p\ ^4P_{1\frac{1}{2}}$
8	3560.68	28076.6	$s^2p^2(^1D)4s\ ^2D_{1\frac{1}{2}}$	$-s^2p^2(^1D)4p\ ^2F_{2\frac{1}{2}}$	0	4297.04	23265.3	$s^2p^2(^1D)3d\ ^2P_{\frac{1}{2}}$	$-s^2p^2(^1D)4p\ ^2P_{1\frac{1}{2}}$
2	3573.69	27974.4	$s^2p^2(^1D)4p\ ^2F_{3\frac{1}{2}}$	$-s^2p^2(^3P)4d\ ^2F_{3\frac{1}{2}}$	1	4308.42	23203.9	$s^2p^2(^3P)3d\ ^2P_{1\frac{1}{2}}$	$-s^2p^2(^3P)4p\ ^2P_{\frac{1}{2}}$
1	3661.48	27303.6	$s^2p^2(^1D)4p\ ^2F_{2\frac{1}{2}}$	$-s^2p^2(^3P)4d\ ^2F_{2\frac{1}{2}}$	2	4324.66	23116.7	$s^2p^2(^1D)3d\ ^2P_{1\frac{1}{2}}$	$-s^2p^2(^1D)4p\ ^2P_{1\frac{1}{2}}$
5	3683.39	27141.2	$s^2p^2(^1D)3d\ ^2D_{2\frac{1}{2}}$	$-s^2p^2(^1D)4p\ ^2P_{1\frac{1}{2}}$	2	4341.47	23027.2	$s^2p^2(^1D)3d\ ^2P_{\frac{1}{2}}$	$-s^2p^2(^1D)4p\ ^2P_{\frac{1}{2}}$
2	3688.10	27106.5	$s^2p^2(^3P)3d\ ^2D_{2\frac{1}{2}}$	$-s^2p^2(^3P)4p\ ^2P_{1\frac{1}{2}}$	2	4353.73	22962.4	$s^2p^2(^3P)3d\ ^2P_{\frac{1}{2}}$	$-s^2p^2(^3P)4p\ ^2P_{1\frac{1}{2}}$
6	3707.34	26965.9	$s^2p^2(^3P)3d\ ^2D_{1\frac{1}{2}}$	$-s^2p^2(^3P)4p\ ^2P_{\frac{1}{2}}$	2	4354.03	22960.8	$s^2p^2(^3P)3d\ ^2D_{1\frac{1}{2}}$	$-s^2p^2(^3P)4p\ ^2D_{1\frac{1}{2}}$
8	3720.45	26870.8	$s^2p^2(^3P)4s\ ^2P_{1\frac{1}{2}}$	$-s^2p^2(^3P)4p\ ^2D_{2\frac{1}{2}}$	3	4364.79	22904.2	$s^2p^2(^3P)3d\ ^2D_{2\frac{1}{2}}$	$-s^2p^2(^3P)4p\ ^2D_{2\frac{1}{2}}$
1	3725.46	26834.7	$s^2p^2(^1D)4p\ ^2D_{2\frac{1}{2}}$	$-s^2p^2(^1D)4d\ ^2F_{3\frac{1}{2}}$	2	4369.60	22879.0	$s^2p^2(^1D)3d\ ^2P_{1\frac{1}{2}}$	$-s^2p^2(^1D)4p\ ^2P_{\frac{1}{2}}$
3	3725.74	26832.7	$s^2p^2(^1D)3d\ ^2D_{1\frac{1}{2}}$	$-s^2p^2(^1D)4p\ ^2P_{1\frac{1}{2}}$	4	4370.91	22872.1	$s^2p^2(^3P)3d\ ^4P_{2\frac{1}{2}}$	$-s^2p^2(^3P)4p\ ^4D_{3\frac{1}{2}}$
8	3748.81	26667.6	$s^2p^2(^3P)4s\ ^2P_{\frac{1}{2}}$	$-s^2p^2(^3P)4p\ ^2D_{1\frac{1}{2}}$	2	4380.57	22821.7	$s^2p^2(^3P)3d\ ^2P_{\frac{1}{2}}$	$-s^2p^2(^3P)4p\ ^2P_{\frac{1}{2}}$
3	3759.10	26594.6	$s^2p^2(^1D)3d\ ^2D_{1\frac{1}{2}}$	$-s^2p^2(^1D)4p\ ^2P_{\frac{1}{2}}$	2B	4414.90	22644.2	$s^2p^2(^1D)3d\ ^2D_{1\frac{1}{2}}$	$-s^2p^2(^1D)4p\ ^2D_{1\frac{1}{2}}$
2	3764.42	26557.0	$s^2p^2(^1D)4p\ ^2P_{1\frac{1}{2}}$	$-s^2p^2(^3P)4d\ ^2D_{2\frac{1}{2}}$	1	4489.17	22269.6	$s^2p^2(^3P)3d\ ^4P_{2\frac{1}{2}}$	$-s^2p^2(^3P)4p\ ^4D_{2\frac{1}{2}}$
5	3779.35	26452.1	$s^2p^2(^3P)3d\ ^4P_{2\frac{1}{2}}$	$-s^2p^2(^3P)4p\ ^2D_{2\frac{1}{2}}$	4	4523.33	22101.4	$s^2p^2(^3P)3d\ ^4P_{1\frac{1}{2}}$	$-s^2p^2(^3P)4p\ ^4D_{2\frac{1}{2}}$
3	3803.57	26283.7	$s^2p^2(^3P)3d\ ^4P_{1\frac{1}{2}}$	$-s^2p^2(^3P)4p\ ^2D_{2\frac{1}{2}}$	4	4591.10	21775.2	$s^2p^2(^1D)3d\ ^2F_{3\frac{1}{2}}$	$-s^2p^2(^1D)4p\ ^2D_{1\frac{1}{2}}$
3	3804.83	26275.0	$s^2p^2(^3P)3d\ ^4P_{1\frac{1}{2}}$	$-s^2p^2(^1P)4p\ ^4S$	4	4596.22	21750.9	$s^2p^2(^1D)3d\ ^2D_{2\frac{1}{2}}$	$-s^2p^2(^1D)4p\ ^2F_{3\frac{1}{2}}$
4	3822.02	26156.8	$s^2p^2(^3P)3d\ ^4P_{\frac{1}{2}}$	$-s^2p^2(^3P)4p\ ^4S$	0	4604.43	21712.2	$s^2p^2(^1D)3d\ ^2F_{2\frac{1}{2}}$	$-s^2p^2(^1D)4p\ ^2D_{2\frac{1}{2}}$
4	3824.47	26140.1	$s^2p^2(^3P)3d\ ^2D_{2\frac{1}{2}}$	$-s^2p^2(^3P)4p\ ^2P_{1\frac{1}{2}}$	5	4608.21	21694.4	$s^2p^2(^1D)3d\ ^2F_{3\frac{1}{2}}$	$-s^2p^2(^1D)4p\ ^2D_{3\frac{1}{2}}$
4	3850.81	25961.2	$s^2p^2(^3P)4s\ ^2P_{1\frac{1}{2}}$	$-s^2p^2(^3P)4p\ ^2D_{1\frac{1}{2}}$	2	4613.78	21668.2	$s^2p^2(^3P)3d\ ^4P_{1\frac{1}{2}}$	$-s^2p^2(^3P)4p\ ^4D_{1\frac{1}{2}}$
3	3881.73	25754.5	$s^2p^2(^3P)4s\ ^2P_{\frac{1}{2}}$	$-s^2p^2(^3P)4p\ ^4P_{1\frac{1}{2}}$	0	4635.83	21565.1	$s^2p^2(^1D)3d\ ^2D_{2\frac{1}{2}}$	$-s^2p^2(^1D)4p\ ^2F_{2\frac{1}{2}}$
5	3925.87	25464.9	$s^2p^2(^3P)4s\ ^2P_{1\frac{1}{2}}$	$-s^2p^2(^3P)4p\ ^4P_{2\frac{1}{2}}$	2	4638.96	21550.5	$s^2p^2(^3P)3d\ ^4P_{\frac{1}{2}}$	$-s^2p^2(^3P)4p\ ^4D_{1\frac{1}{2}}$
0	3958.39	25255.7	$s^2p^2(^3P)3d\ ^4P_{\frac{1}{2}}$	$-s^2p^2(^3P)4p\ ^2D_{1\frac{1}{2}}$	0	4669.50	21409.6	$s^2p^2(^3P)3d\ ^4P_{1\frac{1}{2}}$	$-s^2p^2(^3P)4p\ ^4D_{\frac{1}{2}}$
7	3991.50	25046.2	$s^2p^2(^3P)3d\ ^4P_{2\frac{1}{2}}$	$-s^2p^2(^3P)4p\ ^4P_{2\frac{1}{2}}$	1	4695.07	21293.0	$s^2p^2(^3P)3d\ ^4P_{\frac{1}{2}}$	$-s^2p^2(^3P)4p\ ^4D_{\frac{1}{2}}$
6	4018.50	24877.9	$s^2p^2(^3P)3d\ ^4P_{1\frac{1}{2}}$	$-s^2p^2(^3P)4p\ ^4P_{2\frac{1}{2}}$	3	4703.14	21256.5	$s^2p^2(^1D)3d\ ^2D_{1\frac{1}{2}}$	$-s^2p^2(^1D)4p\ ^2F_{2\frac{1}{2}}$
6	4059.07	24629.3	$s^2p^2(^3P)3d\ ^4P_{2\frac{1}{2}}$	$-s^2p^2(^3P)4p\ ^4P_{1\frac{1}{2}}$	1	4808.00	20792.9	$s^2p^2(^1D)4s\ ^2D_{2\frac{1}{2}}$	$-s^2p^2(^3P)4p\ ^2P_{1\frac{1}{2}}$
4	4087.00	24461.0	$s^2p^2(^3P)3d\ ^4P_{1\frac{1}{2}}$	$-s^2p^2(^3P)4p\ ^4P_{1\frac{1}{2}}$	0	4854.37	20594.3	$s^2p^2(^1D)4s\ ^2D_{1\frac{1}{2}}$	$-s^2p^2(^3P)4p\ ^2P_{\frac{1}{2}}$
5	4104.23	24358.3	$s^2p^2(^3P)3d\ ^4P_{1\frac{1}{2}}$	$-s^2p^2(^3P)4p\ ^4P_{\frac{1}{2}}$	1	4863.75	20554.6	$s^2p^2(^1D)3d\ ^2F_{3\frac{1}{2}}$	$-s^2p^2(^1D)4p\ ^2F_{3\frac{1}{2}}$
5	4106.83	24342.8	$s^2p^2(^3P)3d\ ^4P_{\frac{1}{2}}$	$-s^2p^2(^3P)4p\ ^4P_{1\frac{1}{2}}$	0	4971.64	20108.5	$s^2p^2(^3P)3d\ ^2P_{1\frac{1}{2}}$	$-s^2p^2(^3P)4p\ ^2D_{2\frac{1}{2}}$

B, blend

TABLE II. *Term values of Cl III.*

$\Sigma l=2$		3		4			
		$s^2p^3\ ^4S$	321936.	$sp^4\ ^4P_{2\frac{1}{2}}$	223416.	$s^2p^2(^3P)4d\ ^4F_{1\frac{1}{2}}$	82429.7
		$s^2p^3\ ^2D_{1\frac{1}{2}}$	303883.	$sp^4\ ^4P_{1\frac{1}{2}}$	222806.	$s^2p^2(^3P)4d\ ^4F_{2\frac{1}{2}}$	82206.1
		$s^2p^3\ ^2D_{2\frac{1}{2}}$	303816.	$sp^4\ ^4P_{\frac{1}{2}}$	222461.	$s^2p^2(^3P)4d\ ^4F_{3\frac{1}{2}}$	81860.8
		$s^2p^3\ ^2P_{\frac{1}{2}}$	292124.	$s^2p^2(^3P)3d\ ^4F_{1\frac{1}{2}}$	175410.4	$s^2p^2(^3P)4d\ ^4F_{4\frac{1}{2}}$	81367.6
		$s^2p^3\ ^2P_{1\frac{1}{2}}$	292029.	$s^2p^2(^3P)3d\ ^4F_{2\frac{1}{2}}$	175186.1	$s^2p^2(^3P)4d\ ^4D_{\frac{1}{2}}$	80376.6
				$s^2p^2(^3P)3d\ ^4F_{3\frac{1}{2}}$	174863.0	$s^2p^2(^3P)4d\ ^4D_{1\frac{1}{2}}$	80363.6
$s^2p^2(^3P)4s\ ^4P_{\frac{1}{2}}$	148200.0	$s^2p^2(^2P)4p\ ^4D_{\frac{1}{2}}$	120862.6	$s^2p^2(^3P)3d\ ^4F_{4\frac{1}{2}}$	174438.1	$s^2p^2(^3P)4d\ ^4D_{2\frac{1}{2}}$	80250.9
$s^2p^2(^3P)4s\ ^4P_{1\frac{1}{2}}$	147842.2	$s^2p^2(^2P)4p\ ^4D_{1\frac{1}{2}}$	120604.0	$s^2p^2(^3P)3d\ ^4D_{\frac{1}{2}}$	170087.4	$s^2p^2(^3P)4d\ ^4D_{3\frac{1}{2}}$	79889.8
$s^2p^2(^3P)4s\ ^4P_{2\frac{1}{2}}$	147322.1	$s^2p^2(^2P)4p\ ^4D_{2\frac{1}{2}}$	120170.9	$s^2p^2(^3P)3d\ ^4D_{1\frac{1}{2}}$	170056.1	$s^2p^2(^3P)4d\ ^4P_{2\frac{1}{2}}$	79113.2
$s^2p^2(^3P)4s\ ^2P_{\frac{1}{2}}$	143566.3	$s^2p^2(^2P)4p\ ^4D_{3\frac{1}{2}}$	119568.4	$s^2p^2(^3P)3d\ ^4D_{\frac{1}{2}}$	169989.6	$s^2p^2(^3P)4d\ ^4P_{1\frac{1}{2}}$	78855.3
$s^2p^2(^3P)4s\ ^2P_{1\frac{1}{2}}$	142859.9	$s^2p^2(^2P)4p\ ^4P_{\frac{1}{2}}$	117914.4	$s^2p^2(^3P)3d\ ^4D_{2\frac{1}{2}}$	169982.5	$s^2p^2(^3P)4d\ ^4P_{\frac{1}{2}}$	78728.8
$s^2p^2(^1D)4s\ ^2D_{2\frac{1}{2}}$	133545.9	$s^2p^2(^2P)4p\ ^4P_{1\frac{1}{2}}$	117812.0	$s^2p^2(^3P)3d\ ^4P_{2\frac{1}{2}}$	142440.8	$s^2p^2(^3P)4d\ ^2F_{3\frac{1}{2}}$	78107.6
$s^2p^2(^1D)4s\ ^2D_{1\frac{1}{2}}$	133487.9	$s^2p^2(^2P)4p\ ^4P_{2\frac{1}{2}}$	117394.8	$s^2p^2(^3P)3d\ ^4P_{1\frac{1}{2}}$	142272.5	$s^2p^2(^3P)4d\ ^2F_{2\frac{1}{2}}$	77251.1
		$s^2p^2(^3P)4p\ ^2D_{1\frac{1}{2}}$	116898.7	$s^2p^2(^3P)3d\ ^4P_{\frac{1}{2}}$	142155.0	$s^2p^2(^3P)4d\ ^2D_{1\frac{1}{2}}$	73407.8
		$s^2p^2(^3P)4p\ ^4S$	115997.5	$s^2p^2(^3P)3d\ ^2D_{1\frac{1}{2}}$	139859.7	$s^2p^2(^3P)4d\ ^2D_{2\frac{1}{2}}$	73278.3
		$s^2p^2(^3P)4p\ ^2D_{2\frac{1}{2}}$	115989.1	$s^2p^2(^3P)3d\ ^2D_{2\frac{1}{2}}$	138893.3	$s^2p^2(^1D)4d\ ^2D_{1\frac{1}{2}}$	67323.3?
		$s^2p^2(^3P)4p\ ^2P_{\frac{1}{2}}$	112893.9	$s^2p^2(^3P)3d\ ^2P_{1\frac{1}{2}}$	136097.7	$s^2p^2(^1D)4d\ ^2D_{2\frac{1}{2}}$	67252.6?
		$s^2p^2(^3P)4p\ ^2P_{1\frac{1}{2}}$	112753.2	$s^2p^2(^3P)3d\ ^2P_{\frac{1}{2}}$	135715.6	$s^2p^2(^1D)4d\ ^2F_{3\frac{1}{2}}$	66849.7
		$s^2p^2(^1D)4p\ ^2F_{3\frac{1}{2}}$	105411.4	$s^2p^2(^1D)3d\ ^2D_{2\frac{1}{2}}$	126976.5	$s^2p^2(^1D)4d\ ^2F_{3\frac{1}{2}}$	66795.6
$s^2p^2(^3P)5s\ ^4P_{\frac{1}{2}}$	76984.5	$s^2p^2(^1D)4p\ ^2F_{2\frac{1}{2}}$	105225.6	$s^2p^2(^1D)3d\ ^2D_{1\frac{1}{2}}$	126667.8		
$s^2p^2(^3P)5s\ ^4P_{1\frac{1}{2}}$	76543.6	$s^2p^2(^1D)4p\ ^2D_{2\frac{1}{2}}$	104085.8	$s^2p^2(^1D)3d\ ^2F_{2\frac{1}{2}}$	125798.1		
$s^2p^2(^3P)5s\ ^4P_{2\frac{1}{2}}$	75798.8	$s^2p^2(^1D)4p\ ^2D_{1\frac{1}{2}}$	104022.9	$s^2p^2(^1D)3d\ ^2F_{3\frac{1}{2}}$	125780.2		
$s^2p^2(^1D)5s\ ^2D_{2\frac{1}{2}}$	63050.2	$s^2p^2(^1D)4p\ ^2P_{\frac{1}{2}}$	100073.1	$s^2p^2(^1D)3d\ ^2P_{\frac{1}{2}}$	123100.5		
$s^2p^2(^1D)5s\ ^2D_{1\frac{1}{2}}$	63045.2	$s^2p^2(^1D)4p\ ^2P_{1\frac{1}{2}}$	99835.3	$s^2p^2(^1D)3d\ ^2P_{1\frac{1}{2}}$	122952.1		

TABLE III. *Classified lines of Cl IV.*

Int.	λ Vac.	ν	Classification	Int.	λ Vac.	ν	Classification
1	318.750	313725.	$s^2p^2\ ^3P_1-s^2p5s\ ^3P_2$	0	1440.95	69398.7	$s^2p3d\ ^3P_1-s^2p4p\ ^3P_0$
1	319.513	312976.	$s^2p^2\ ^3P_0-s^2p5s\ ^3P_1$	0	1529.28	65390.2	$s^2p3d\ ^3D_1-s^2p4p\ ^3P_2$
3	319.616	312875.	$s^2p^2\ ^3P_2-s^2p5s\ ^3P_2$	1	1532.19	65266.1	$s^2p4p\ ^3D_2-s^2p5s\ ^3P_2$
0	319.993	312507.	$s^2p^2\ ^3P_1-s^2p5s\ ^3P_1$	1	1533.25	65220.9	$s^2p3d\ ^3D_2-s^2p4p\ ^3P_2$
1	320.250	312256.	$s^2p^2\ ^3P_1-s^2p5s\ ^3P_0$	3	1537.21	65052.9	$s^2p3d\ ^3D_3-s^2p4p\ ^3P_2$
1	320.881	311642.	$s^2p^2\ ^3P_2-s^2p5s\ ^3P_1$	2	1539.30	64964.6	$s^2p4p\ ^3D_2-s^2p5s\ ^3P_1$
4	437.825	228402.	$sp^3\ ^5S\ -sp^24s\ ^5P_3$	2	1545.19	64717.0	$s^2p3d\ ^3D_1-s^2p4p\ ^3P_1$
3	439.255	227658.	$sp^3\ ^5S\ -sp^24s\ ^5P_2$	2	1549.15	64551.5	$s^2p3d\ ^3D_2-s^2p4p\ ^3P_1$
2	440.245	227146.	$sp^3\ ^5S\ -sp^24s\ ^5P_1$	1	1551.27	64463.3	$s^2p3d\ ^3D_1-s^2p4p\ ^3P_0$
8	534.727	187011.	$s^2p^2\ ^3P_0-s^2p3d\ ^3D_1$	1	1617.43	61826.5	$s^2p4p\ ^3P_2-s^2p5s\ ^3P_2$
7	535.666	186683.	$s^2p^2\ ^3P_1-s^2p3d\ ^3D_2$	2	1622.86	61619.6	$s^2p3d\ ^3D_3-s^2p4p\ ^3D_3$
6	536.150	186515.	$s^2p^2\ ^3P_1-s^2p3d\ ^3D_1$	0	1638.95	61014.7	$s^2p3d\ ^3D_1-s^2p4p\ ^3D_2$
9	537.606	186010.	$s^2p^2\ ^3P_2-s^2p3d\ ^3D_3$	1	1643.40	60849.5	$s^2p3d\ ^3D_2-s^2p4p\ ^3D_2$
6	538.119	185833.	$s^2p^2\ ^3P_2-s^2p3d\ ^3D_2$	0	1648.04	60678.1	$s^2p3d\ ^3D_3-s^2p4p\ ^3D_2$
4	538.595	185668.	$s^2p^2\ ^3P_2-s^2p3d\ ^3D_1$	1	1651.21	60561.6	$s^2p3d\ ^3D_1-s^2p4p\ ^3D_1$
5	549.219	182077.	$s^2p^2\ ^3P_0-s^2p3d\ ^3P_1$		λ Air		
4	550.020	181812.	$s^2p^2\ ^3P_1-s^2p3d\ ^3P_0$	4	2701.36	37007.4	$s^2p4s\ ^3P_1-s^2p4p\ ^3P_2$
3	550.706	181585.	$s^2p^2\ ^3P_1-s^2p3d\ ^3P_1$	5B	2724.03	36699.5	$s^2p4s\ ^3P_0-s^2p4p\ ^3P_1$
7	552.017	181154.	$s^2p^2\ ^3P_1-s^2p3d\ ^3P_2$	5	2751.23	36336.7	$s^2p4s\ ^3P_1-s^2p4p\ ^3P_1$
6	553.297	180735.	$s^2p^2\ ^3P_2-s^2p3d\ ^3P_1$	4	2770.64	36082.1	$s^2p4s\ ^3P_1-s^2p4p\ ^3P_0$
7	554.619	180304.	$s^2p^2\ ^3P_2-s^2p3d\ ^3P_2$	7	2782.47	35928.7	$s^2p4s\ ^3P_2-s^2p4p\ ^3P_2$
2	668.770	149528.	$sp^3\ ^3D_3-s^2p4p\ ^3P_2$	4	2835.4	35258.0	$s^2p4s\ ^3P_2-s^2p4p\ ^3P_1$
0	672.428	148715.	$sp^3\ ^3D_1-s^2p4p\ ^3P_0$	5	3063.13	32636.9	$s^2p4s\ ^3P_1-s^2p4p\ ^3D_2$
0	684.490	146094.	$sp^3\ ^3D_2-s^2p4p\ ^3D_3$	3	3071.36	32549.4	$s^2p4s\ ^3P_0-s^2p4p\ ^3D_1$
0	776.91	128715.	$sp^3\ ^3P_2-s^2p4p\ ^3D_3$	6	3076.68	32493.1	$s^2p4s\ ^3P_2-s^2p4p\ ^3D_3$
1	1413.39	70751.9	$s^2p3d\ ^3P_2-s^2p4p\ ^3P_2$	1	3106.09	32185.5	$s^2p4s\ ^3P_1-s^2p4p\ ^3D_1$
1	1421.97	70325.0	$s^2p3d\ ^3P_1-s^2p4p\ ^3P_2$	2	3167.87	31557.9	$s^2p4s\ ^3P_2-s^2p4p\ ^3D_2$
1	1426.89	70082.5	$s^2p3d\ ^3P_2-s^2p4p\ ^3P_1$				

TABLE IV. *Term values of Cl IV.*

$\Sigma l=1$		2		3	
		$s^2p^2\ ^3P_0$	431226.	$sp^3\ ^3D_1$	328474.
		$s^2p^2\ ^3P_1$	430735.	$sp^3\ ^3D_2$	328439.
		$s^2p^2\ ^3P_2$	429885.	$sp^3\ ^3D_3$	328357.
				$sp^3\ ^3P_2$	310970.
				$sp^3\ ^3P_1$	310952.
				$sp^3\ ^3P_0$	310926.
$s^2p4s\ ^3P_0$	216200.0	$s^2p4p\ ^3D_1$	183650.9?	$sp^3\ ^3S$	266505.
$s^2p4s\ ^3P_1$	215836.7	$s^2p4p\ ^3D_2$	183199.9	$s^2p3d\ ^3P_2$	249583.
$s^2p4s\ ^3P_2$	214757.9	$s^2p4p\ ^3D_3$	182264.8	$s^2p3d\ ^3P_1$	249153.
		$s^2p4p\ ^3P_0$	179754.6	$s^2p3d\ ^3P_0$	248926.
$s^2p5s\ ^3P_0$	118479.	$s^2p4p\ ^3P_1$	179500.2	$s^2p3d\ ^3D_1$	244218.
$s^2p5s\ ^3P_1$	118235.	$s^2p4p\ ^3P_2$	178829.3	$s^2p3d\ ^3D_2$	244052.
$s^2p5s\ ^3P_2$	117001.			$s^2p3d\ ^3D_3$	243880.

TABLE V. *Classified lines of Cl V.*

Int.	λ Vac.	ν	Classification
2	286.127	349495.	$s^23p\ ^2P_{\frac{1}{2}}$ — $s^24d\ ^2D$
3	287.327	348036.	$s^23p\ ^2P_{1\frac{1}{2}}$ — $s^24d\ ^2D$
2	372.589	268392.	$sp^2\ ^4P_{1\frac{1}{2}}$ — $sp4s\ ^4P_{2\frac{1}{2}}$
2	373.165	267978.	$sp^2\ ^4P_{\frac{1}{2}}$ — $sp4s\ ^4P_{1\frac{1}{2}}$
3	373.776	267540.	$sp^2\ ^4P_{2\frac{1}{2}}$ — $sp4s\ ^4P_{2\frac{1}{2}}$
0	373.911	267443.	$sp^2\ ^4P_{\frac{1}{2}}$, $1\frac{1}{2}$ — $sp4s\ ^4P_{\frac{1}{2}}$, $1\frac{1}{2}$
1	374.662	266907.	$sp^2\ ^4P_{1\frac{1}{2}}$ — $sp4s\ ^4P_{\frac{1}{2}}$
2	375.103	266593.	$sp^2\ ^4P_{2\frac{1}{2}}$ — $sp4s\ ^4P_{1\frac{1}{2}}$
4	390.148	256313.	$s^23p\ ^2P_{\frac{1}{2}}$ — $s^24s\ ^2S$
5	392.433	254821.	$s^23p\ ^2P_{1\frac{1}{2}}$ — $s^24s\ ^2S$
2	535.455	186757.	$sp^2\ ^4P_{\frac{1}{2}}$ — $sp3d\ ^4D_{1\frac{1}{2}}$
2	535.916	186596.	$sp^2\ ^4P_{\frac{1}{2}}$ — $sp3d\ ^4D_{\frac{1}{2}}$
3	536.532	186382.	$sp^2\ ^4P_{1\frac{1}{2}}$ — $sp3d\ ^4D_{\frac{1}{2}}$
4	537.006	186218.	$sp^2\ ^4P_{1\frac{1}{2}}$ — $sp3d\ ^4D_{1\frac{1}{2}}$
4	538.681	185639.	$sp^2\ ^4P_{2\frac{1}{2}}$ — $sp3d\ ^4D_{2\frac{1}{2}}$
3	538.977	185537.	$sp^2\ ^4P_{2\frac{1}{2}}$ — $sp3d\ ^4D_{2\frac{1}{2}}$
0	539.441	185377.	$sp^2\ ^4P_{2\frac{1}{2}}$ — $sp3d\ ^4D_{1\frac{1}{2}}$
2	551.117	181450.	$sp^2\ ^4P_{1\frac{1}{2}}$ — $sp3d\ ^4P_{\frac{1}{2}}$
1	551.643	181277.	$sp^2\ ^4P_{1\frac{1}{2}}$ — $sp3d\ ^4P_{1\frac{1}{2}}$
2B	552.908	180862.	$sp^2\ ^4P_{1\frac{1}{2}}$ — $sp3d\ ^4P_{2\frac{1}{2}}$
1	554.210	180437.	$sp^2\ ^4P_{2\frac{1}{2}}$ — $sp3d\ ^4P_{1\frac{1}{2}}$
1	555.484	180023.	$sp^2\ ^4P_{2\frac{1}{2}}$ — $sp3d\ ^4P_{2\frac{1}{2}}$

B, blend.

TABLE VI. *Term values of Cl V.*

$\Sigma l=0$		1		2		3	
		$s^23p\ ^2P_{\frac{1}{2}}$	547000.	$sp^2\ ^4P_{\frac{1}{2}}$	461000.	$p^2\ ^4S$	313243.
		$s^23p\ ^2P_{1\frac{1}{2}}$	545508.	$sp^2\ ^4P_{1\frac{1}{2}}$	460462.	$sp3d\ ^4P_{2\frac{1}{2}}$	279598.
				$sp^2\ ^4P_{2\frac{1}{2}}$	459619.	$sp3d\ ^4P_{1\frac{1}{2}}$	279184.
				$sp^2\ ^2D_{1\frac{1}{2}}$	433766.	$sp3d\ ^4P_{\frac{1}{2}}$	279012.
				$sp^2\ ^2D_{2\frac{1}{2}}$	433694.	$sp3d\ ^4D_{\frac{1}{2}}$	274404.
				$sp^2\ ^2S$	400356.	$sp3d\ ^4D_{1\frac{1}{2}}$	274243.
				$sp^2\ ^2P_{\frac{1}{2}}$	389069.	$sp3d\ ^4D_{2\frac{1}{2}}$	274081.
				$sp^2\ ^2P_{1\frac{1}{2}}$	388108.	$sp3d\ ^4D_{3\frac{1}{2}}$	273980.
				$s^23d\ ^2D_{1\frac{1}{2}}$	361139.		
		$sp4s\ ^4P_{\frac{1}{2}}$	193555.	$s^23d\ ^2D_{2\frac{1}{2}}$	361107.		
s^24s^2S	290687.	$sp4s\ ^4P_{1\frac{1}{2}}$	193022.				
		$sp4s\ ^4P_{2\frac{1}{2}}$	192075.	$s^24d\ ^2D$	197489.		

The Dirac Vector Model in Complex Spectra

J. H. VAN VLECK, *University of Wisconsin*

(Received January 23, 1934)

Dirac has shown that the secular problem presented by the permutation degeneracy is formally equivalent to a problem in vector coupling for which the Hamiltonian function is $-\frac{1}{2}\Sigma K_{ij}(1+4\mathbf{s}_i\cdot\mathbf{s}_j)$ where $\mathbf{s}_i$, $\mathbf{s}_j$ are respectively the spin vectors of orbits i, j and K_{ij} is the exchange integral which connects i and j. The vector model can be used in place of Slater's determinantal wave functions to calculate atomic spectral terms, provided one still retains much of Slater's powerful method of diagonal sums. The configuration d^3 is treated as an example. Configurations of the form sa^k ($a=p,\ d,\ f\cdots$; $0<k<4l_a+2$) are particularly amenable to the vector model, as it enables us immediately to write down the energy of sa^k if that of a^k is known. One thus finds that the two states $S=S_k\pm\frac{1}{2}$ built upon a given configuration S_k, L_k of the core a^k should have a separation proportional to $S_k+\frac{1}{2}$ and independent of L_k. Experimentally, this prediction is confirmed only roughly, like the interval relations found by Slater, because perturbations by other configurations are neglected. Various applications to molecular spectra are given. The Heitler-Rumer theory of valence, which neglects directional effects, has a particularly simple interpretation in terms of the vector model.

In configurations of the form p^n both spin-orbit and electrostatic energy can be calculated by the vector model without use of the invariance of diagonal sums. For this particular configuration the Pauli principle is equivalent to a constraint $2\mathbf{s}_i\cdot\mathbf{s}_j=-(\mathbf{l}_i\cdot\mathbf{l}_j)^2-(\mathbf{l}_i\cdot\mathbf{l}_j)+\frac{1}{2}$ connecting the relative orientations of spin and of angular momentum vectors.

1. INTRODUCTION

THE method commonly used for calculating energy levels in problems involving permutation degeneracy is that due to Slater.[1] It appears to have been rather generally overlooked that Dirac's[2] vector model is, as we shall show, likewise often very convenient for many computations in complex and molecular spectra. The beauty of the vector method is that it gives a simple kinematical picture for the results and does not require the explicit determination of proper final wave functions.[3] Yet we must grant that many physicists find wave methods easier than matrix ones and to a large extent it is a matter of taste and training whether the Dirac or Slater method is the more tractable. Both of these procedures are simpler than full-fledged group methods and are alike in that they owe their strength essentially to recognition at the outset that the allowable "characters" for the permutation group are very severely limited by the Pauli principle, so that the group technique is more general and complicated than needed.

Before removal of the permutation degeneracy, a typical orbital wave function of the system may be taken to be the product

$$\Psi=\psi_1(x_1, y_1, z_1)\psi_2(x_2, y_2, z_2)\cdots\psi_n(x_n, y_n, z_n) \tag{1}$$

of the wave functions of the n individual electrons, which we shall suppose separately normalized to unity. We shall throughout use the term "orbit" to designate the quantum numbers, etc., of one electron, considered individually, and the term "state" to specify the condition of the entire system of all n electrons. We shall always assume that the only permutation effects which need to be con-

[1] J. C. Slater, Phys. Rev. **34**, 1293 (1929).

[2] P. A. M. Dirac, Proc. Roy. Soc. **A123**, 714 (1929), or *The Principles of Quantum Mechanics*, chapter XI. A brief resumé of Dirac's method is also given in chapter XII of the writer's *Theory of Electric and Magnetic Susceptibilities*.

[3] At first sight it seems as if we would need to find the wave functions if we desire intensities rather than simply energy levels. However, Condon and Ufford find that oftentimes the intensities can be found from the principle of spectroscopic stability without determining the final wave functions; Phys. Rev. **44**, 740 (1933).

sidered are simple exchanges. The higher order permutations will be treated by R. Serber in a paper to appear in the *Physical Review* shortly.[4] They do not enter if the wave functions of the various orbits are orthogonal and are usually neglected even if they are not. Orthogonality of the ψ's will be assumed unless otherwise stated.

We shall, like Slater, use the notation K_{ij} for the exchange integral

$$K_{ij}=\int\cdots\int\psi_i^*(x_1, y_1, z_1)\psi_j^*(x_2, y_2, z_2)H\psi_j(x_1, y_1, z_1)\psi_i(x_2, y_2, z_2)d\tau_1 d\tau_2, \tag{2}$$

and J_{ij} for the Coulomb one

$$J_{ij}=\int\cdots\int\psi_i^*(x_1, y_1, z_1)\psi_j^*(x_2, y_2, z_2)(e^2/r_{12})\psi_i(x_1, y_1, z_1)\psi_j(x_2, y_2, z_2)d\tau_1 d\tau_2. \tag{3}$$

Clearly the Hamiltonian operator H has the structure

$$H=\Sigma_i f(x_i, y_i, z_i, \partial\cdots/\partial x_i, \partial\cdots/\partial y_i, \partial\cdots/\partial z_i)+\Sigma_{j>i}e^2/r_{ij}.$$

We shall throughout omit the Coulomb terms arising from $\Sigma_i f(x_i, \cdots, \partial\cdots/\partial z_i)$, as they enter merely as additive constants in the problems which we shall consider. We shall use Mulliken's Greek notation for the spatial quantum number; thus $2p\pi_+$ means $n=2$, $l=1$, $m_l=+1$ (or $\lambda=+1$ if the axial quantum number is denoted by λ, as in molecular problems). We use the term "configuration" for the totality of states which arise when the orbital quantum numbers of all the orbits are specified, apart from permutations of electrons among the orbits. This agrees with the use of the word configuration in molecular spectroscopy, where three quantum numbers are used to specify an orbit, but atomic spectroscopists do not distinguish between different values of the spatial quantum number. When there is danger of confusion, we shall speak of atomic and spatial configurations. Thus $2p\pi 2p\sigma$, $2p\pi^2$ are two different spatial configurations but represent the same atomic configuration $2p^2$. A single configuration may have several possible values for its resultant spin S and a given value of S for the configuration may yield more than one energy level. The frequency of occurrence ν of any S is obtained by the "branching rule" which is illustrated in Fig. 1 and which is constructed by building up the configuration electron by electron. Electrons in equivalent orbits are not to be counted in constructing the branching patterns, as their resultant spin can only be zero because of the Pauli principle. The analytical formula for ν is

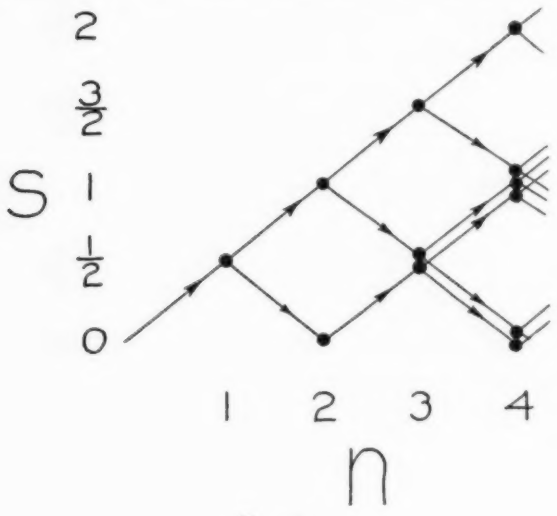

FIG. 1.

$$\nu=\binom{n}{k}-\binom{n}{k-1}$$

where $k=\frac{1}{2}n-S$, and n is the number of free orbits.[5]

For the present we shall consider only the secular problem connected with a single configuration. The problem of treating simultaneously the permutation degeneracy and the interaction of two or more configurations is naturally more complicated (unless this interaction vanishes, as often happens) and will be examined in Serber's article.[4]

[4] R. Serber, Phys. Rev. to be published, April 1, 1934.

[5] Cf., for instance, J. H. Van Vleck, *The Theory of Electric and Magnetic Susceptibilities*, p. 324, Eq. (14).

Slater's way of solving the permutation problem is to superpose on (1) the Pauli spin functions, permute the arguments, take antisymmetric linear combinations and then construct the secular determinant. Dirac has shown that, instead, we can utilize the theorem that the energy levels are the same as those of a Hamiltonian function

$$\mathfrak{H}=\Sigma_{j>i}J_{ij}+\Sigma_{j>i}K_{ij}\mathcal{P}_{ij}=\Sigma_{j>i}J_{ij}-\tfrac{1}{2}\Sigma_{j>i}K_{ij}(1+4\mathbf{s}_i\cdot\mathbf{s}_j) \tag{4}$$

provided we confine our attention to one configuration. Here $\mathbf{s}_i$ (half Dirac's σ_i) is the spin vector associated with the orbit i, measured in multiples of $h/2\pi$, and $\mathcal{P}_{ij}$ is the permutation matrix associated with interchange of orbits i and j. *All expressions printed in bold-face type are vector matrices.* The proof of (4) we can omit, as it is given by Dirac.[2] The result (4) is, however, fairly obvious from the following considerations. First we remember that the characteristic values of $\mathcal{P}_{ij}$ are ±1 and that the resultant spin quantum number of i, j has respectively the values 0, 1 when $\mathcal{P}_{ij}=+1$, -1. We shall have frequent occasion to use the relation

$$2\Sigma_{j>i}\mathbf{s}_i\cdot\mathbf{s}_j=(\Sigma\mathbf{s}_i)^2-\Sigma\mathbf{s}_i^2=S(S+1)-\tfrac{3}{4}n, \tag{5}$$

where S is the total-spin quantum number for a system of n non-equivalent orbits. When bold-face type appears on the left and ordinary italic type on the right of an equality, it means that the left side is a matrix and the right side is a typical characteristic value of the matrix. Thus $\mathbf{s}_i^2=s_i(s_i+1)$. This convention obviates the necessity of inserting indices on the left side. The factor $\frac{3}{4}$ is involved in (5) since for a single electron $s_i(s_i+1)=\frac{3}{4}$. When we specialize (5) to $n=2$, the only possible values of S are 0, 1. Hence the characteristic values of the bracketed factor in (4) are ±1 and this factor is the same as $\mathcal{P}_{ij}$ since these two matrices are simultaneously diagonal with the same characteristic values.

As Dirac also briefly mentions, the procedure must be modified when a pair of orbits α, α' belonging to a configuration are identical. Here one must drop from the summation in (4) the term involving $K_{\alpha\alpha'}$, for there is no distinction between exchange and direct Coulomb energy between two identical orbits and the proper mutual energy is already included in $J_{\alpha\alpha'}$. Let q be any third orbit not belonging to the pair. Then since $K_{q\alpha}=K_{q\alpha'}$ and since $\mathbf{s}_\alpha+\mathbf{s}_{\alpha'}=0$ because of the Pauli principle, we have

$$-\tfrac{1}{2}K_{q\alpha}[1+4\mathbf{s}_\alpha\cdot\mathbf{s}_q]-\tfrac{1}{2}K_{q\alpha'}[1+4\mathbf{s}_{\alpha'}\cdot\mathbf{s}_q]=-K_{q\alpha}[1+2(\mathbf{s}_\alpha+\mathbf{s}_{\alpha'})\cdot\mathbf{s}_q]=-K_{q\alpha}. \tag{6}$$

Let Roman and Greek subscripts be used for orbits which occur once and twice in the configuration. Such orbits we shall call respectively "free" and "filled" (or "paired") orbits. In place of (4) the proper formula is now

$$\mathfrak{H}=\Sigma_{j>i}[J_{ij}-\tfrac{1}{2}(1+4\mathbf{s}_i\cdot\mathbf{s}_j)K_{ij}]+\Sigma_{j,\,\mu}[2J_{j\mu}-K_{j\mu}]+\Sigma_{\mu>\eta}[4J_{\mu\eta}-2K_{\mu\eta}]+\Sigma_\mu J_{\mu\mu}. \tag{7}$$

In this connection it is to be understood that each pair of identical orbits gives rise to only one term in the Greek summations.

Eq. (4) or (7) shows that, except for additive terms, *there is a formal mathematical similarity between the permutation problem associated with a configuration of n free orbits and the problem of n angular momentum vectors, each of quantum number* $\frac{1}{2}$, *whose coupling energies vary as their scalar products.* The configuration can also involve any number of filled orbits, since by (7) such orbits contribute only an additive constant to the energy. Formulas for the coupling energy of 3 and of 4 angular momentum vectors have been given, respectively, by Güttinger and Pauli[6] and by Johnson.[7] Their results can immediately be adapted to our problem but are more general than we need since they did not specialize the quantum numbers of the component vectors to the value $\frac{1}{2}$. This specialization simplifies the formulas materially and enables them to be obtained often by Goudsmit's inspection method.[8]

[6] W. Güttinger and W. Pauli, Zeits. f. Physik **67**, 762 (1931).

[7] M. H. Johnson, Jr., Phys. Rev. **38**, 1628 (1931).

[8] S. Goudsmit, Phys. Rev. **35**, 1325 (1930). The inspection method consists in noting that the constants involved in a quadratic secular equation can often be uniquely evaluated if its behavior is known for extreme cases of the coupling parameters. This method will be used to formulate the secular equations for the states of minimum spin in the three and four electron problems, in an article by A. Sherman to appear in *Reviews of Modern Physics.*

The secular equations appropriate to the cases $n=5, 6, 7, 8$ will be considered in a later paper by Serber and Sherman and have, as a matter of fact, already been formulated by Eyring and colleagues[9] for the important states of minimum spin. The latter, however, did not use the vector model but, instead, a Slater procedure based on electron pair bonds. Heisenberg's theory of ferromagnetism involves unfortunately the case $n=N$, where N is the enormous number of atoms composing the microcrystal. Here accurate solution of the secular equation is clearly impossible. The mean energy and mean square energy belonging to a given spin S of the microcrystal can, however, easily be computed by the vector model. This has been done by the writer.[10] The results are the same as obtained by more complicated group theory. Knowing these means one can, of course, determine the constants of Heisenberg's assumed Gaussian spread of energy levels. Quite irrespective of ferromagnetic applications, the formula for the mean energy $\overline{W}$ of those states of a configuration which have a total spin S is often very useful. It is

$$\overline{W}=C-\tfrac{1}{2}[1+(4S^2+4S-3n)/n(n-1)]\Sigma_{j>i}K_{ij}, \tag{8}$$

where C is an additive constant representing the effect of all Coulomb terms and of exchange terms which involve filled orbits (types $j, \mu; \mu, \eta$; and μ, μ in Eq. (7)). As Dirac has also shown, formula (8) is proved by using (4) or (7) and noting that, on the average, each $\mathbf{s}_i\cdot\mathbf{s}_j$ absorbs $1/(n^2-n)$ of the sum (5) inasmuch as there are $\frac{1}{2}n(n-1)$ pairs of structure $j>i$.

2. Atomic Spectra

In the calculation of atomic spectral terms there is the degeneracy connected with spatial orientation as well as that connected with the permutation problem. Hence the secular problem usually involves more than one configuration. Nevertheless as Slater[1] has ingeniously shown, this complication can very often be circumvented by utilization of the invariance of the spur and the fact that with given L, S the energy is independent of the quantum numbers M_L, M_S. Here M_L, M_S denote, respectively, the projections of the orbital and spin angular momenta $\mathbf{L}$, $\mathbf{S}$ along some arbitrary spatial direction. We shall not consider spin-orbit coupling, so that introduction of the quantum number J is unnecessary and the Hamiltonian function is diagonal in M_L, M_S. Slater always starts with what we shall call an m_l, m_s system of representation, in which the electrons are individually space quantized, so that $M_L=\Sigma m_{l_i}$, $M_S=\Sigma m_{s_i}$. Ordinarily, two or more spatial configurations will lead to the same values of M_L, M_S. Nevertheless, development of an elaborate inter-configurational theory is unnecessary as far as the sum of the roots of the secular equation is concerned. Indeed it is a well-known theorem that this sum equals the invariant spur or diagonal sum of the matrix elements of the Hamiltonian function regardless of what transformations are made and the spur in question clearly is by definition independent of the troublesome off-diagonal elements which represent the interaction of the various spatial configurations. Furthermore, a certain number of individual roots in the sum for a given M_L, M_S are known if we have already solved the secular equations for larger values of M_L, M_S. This is true since a state of given L, S appears once in the secular equation for each pair of values of M_L, M_S consistent with the inequalities

$$M_L=-L, -(L-1), \cdots, L; \qquad M_S=-S, -(S-1), \cdots, S. \tag{9}$$

Let us begin with the state of maximum M_L, M_S consistent with the given atomic configuration and progress to states of lower and lower M_L, M_S. If at each step the degree of the secular determinant never advances by more than one unit and if it is of degree unity for $M_{L\max}$, $M_{S\max}$ as is usually true, all the roots can be calculated without an inter-configurational theory. As Slater shows,[1] these

[9] A. Sherman and H. Eyring, J. Am. Chem. Soc. **54**, 2661 (1932); H. Eyring and G. E. Kimball, J. Chem. Phys. **1**, 239 (1933).

[10] J. H. Van Vleck, *The Theory of Electric and Magnetic Susceptibilities*, p. 340.

conditions are always met if we confine our attention to a single atomic configuration and if, in addition, this configuration contains no more than one multiplet of any one type. For an example consider the atomic configuration d^3. Here, by well-known principles, the multiplets are

$$^2H,\ ^2G,\ ^2F,\ ^4F,\ ^2D_+,\ ^2D_-,\ ^4P,\ ^2P. \tag{10}$$

One can easily calculate, as we shall show, the energies of all the states (10) except that one obtains in this fashion only the mean energy of the two ^2D multiplets which, following Ufford,[11] we shall denote by $^2D_+$ and $^2D_-$. To isolate the energies of $^2D_+$, $^2D_-$ or to include perturbations by other configurations, it is necessary to have recourse to a more comprehensive theory, such as has been developed by Ufford and Shortley[12] with the Slater method and which will be examined by Serber[4] in the light of the vector model.

Slater[1] develops the following theorem: *the exchange part of the diagonal sum for the energy can be calculated by using an m_l, m_s system of representation and giving an exchange integral K_{ij} the coefficient -1 if the spins of the corresponding orbits are parallel (i.e., if $m_{s_i}=m_{l_i}=\pm\frac{1}{2}$) and the coefficient zero if they are anti-parallel.* This result is readily deducible from our vector model as follows. The diagonal elements such as are involved in the spur have the physical interpretation of being mean values. If the z axis is that of quantization, the angular momentum vectors precess about the z axis so that only the z component is constant and has a mean value different from zero. The precession rates for the various vectors are different, so that the average product equals the product of the averages. Thus

$$-\tfrac{1}{2}[1+4\overline{\mathbf{s}_i\cdot\mathbf{s}_j}]=-\tfrac{1}{2}[1+4\mathbf{s}_{z_i}\mathbf{s}_{z_j}]=-\tfrac{1}{2}[1+4m_{s_i}m_{s_j}]. \tag{11}$$

Eq. (11) embodies the same kinematical principle as in Landé's or Goudsmit's well-known use of the permanence of Γ-sums in strong fields; instead of appealing to our kinematical intuition via the correspondence principle one could, of course, also derive (11) by simple matrix algebra.[13] Clearly, in agreement with Slater, the expression (11) equals -1 if $m_{s_i}=m_{s_j}=\pm\frac{1}{2}$ and vanishes if $|m_{s_i}|=\frac{1}{2}$, $m_{s_i}=-m_{s_j}$.

Once (11) has been established, the calculation of the levels proceeds in a well-known fashion based on the spur theorem and first described by Slater. Hence details or examples need not be repeated here. Thus, in applying the Dirac model to atomic spectra, one draws very heavily on the powerful Slater technique of diagonal sums and the main difference is that the theorem stated in the preceding paragraph can be proved by the vector model instead of by using determinantal wave functions.

In Slater's original procedure, in order to determine the energies of the states of a given multiplicity, it was necessary first to find the energies of the states of higher multiplicity belonging to the atomic configuration under consideration. This is true since the results for a particular multiplicity are usually obtained by "subtracting out" from the diagonal sums for given M_L, M_S all the roots belonging to states with $S>M_S$. With the aid of the formula (8) based on the vector model (but which could doubtless also be established by other means) it is possible to determine the energy levels for any one multiplicity without the knowledge of those for the higher multiplicities. Another way of saying the same thing is that with (8) one can avoid using the intermediary of individual space quantization for the spin, though such quantization is still needed for the orbit, so that one can begin with the energy values for an m_l, S rather than m_l, m_s system of representation. The former is, of course, nearer the final L, S system. This is only a nominal advantage since the amount of labor saved is not great and since usually one desires the energies of all multiplets belonging to a given configuration. Nevertheless, the m_l, S procedure is an interesting variant from the m_l, m_s one and can also serve as a useful arithmetical check on the latter.

To illustrate and so make more lucid the statements of the preceding paragraph, we shall calculate

[11] C. W. Ufford, Phys. Rev. **44**, 732 (1934).

[12] C. W. Ufford and G. H. Shortley, Phys. Rev. **42**, 167 (1932).

[13] A. Landé, Zeits. f. Physik **19**, 121 (1923); S. Goudsmit, Phys. Rev. **31**, 946 (1928); W. Heisenberg and P. Jordan, Zeits. f. Physik **37**, 263 (1926) (matrix proof).

the energies of the doublet levels belonging to the configuration d^3 without determining those of the quartets. Out of all the multiplets listed in (10) for d^3, the only one yielded by the spatial configuration $M_L=5$ is ^2H, since all the others demand $M_L<5$. In this configuration there is one free orbit and one closed pair, so that the situation is that covered by (7) when we restrict the i, μ summations to one term each, with no j or η at all, and identify i, μ with $d\pi$, $d\delta^2$, respectively.[14] Hence by (7)

$$W(^2H)=2J(d\delta;\,d\pi)+J(d\delta;\,d\delta)-K(d\delta;\,d\pi). \tag{12}$$

There are two spatial configurations $d\delta d\pi^2$, $d\delta^2 d\sigma$ compatible with $M_L=4$. Both are of the type just discussed, *viz.*, one free orbit and one pair. Hence by (7) and the invariance of the diagonal sum

$$W(^2H)+W(^2G)=2J(d\delta;\,d\pi)+J(d\pi;\,d\pi)-K(d\delta;\,d\pi)+2J(d\delta;\,d\sigma)+J(d\delta;\,d\delta)-K(d\delta;\,d\sigma). \tag{13}$$

When one comes to $M_L=3$, the state of affairs is somewhat different. Here by (10) there are both quartets and doublets, *viz.*, ^2H, ^2G, ^2F, ^4F. From the branching rule given in Fig. 1, one sees that the spatial configuration $d\delta d\pi d\sigma$ admits one quartet and two doublets. The energy spur x for the two doublets is

$$x=2\overline{W}=2[J(d\delta;\,d\pi)+J(d\pi;\,d\sigma)+J(d\delta;\,d\sigma)]. \tag{14}$$

This result is obtained by taking $n=3$, $S=\frac{1}{2}$ in (8) and evaluating the constant C which in the present case consists entirely of Coulombic energy, inasmuch as all three orbits are free. To form the complete spur for $M_L=3$ one must add the part contributed by the other configuration $d\delta^2 d\pi_-$ belonging to $M_L=3$. Hence

$$W(^2H)+W(^2G)+W(^2F)=x+2J(d\delta;\,d\pi_-)+J(d\delta;\,d\delta)-K(d\delta;\,d\pi_-) \tag{15}$$

since $d\delta^2 d\pi_-$ involves one closed pair and so is treated by the same principle as involved in (12).

When $M_L=2$, there is one spatial configuration $d\delta d\pi d\pi_-$ which involves only free orbits and which hence contributes two doublets. Also there are three configurations $d\delta d\sigma^2$, $d\delta^2 d\delta_-$, $d\pi^2 d\sigma$ which involve a pair in each case. Hence applying three times the procedure contained in (12) and once that in (14), we find

$$\begin{aligned}W(^2H)+W(^2G)+W(^2F)+W(^2D_+)+W(^2D_-)&=[2J(d\delta;\,d\sigma)+J(d\sigma;\,d\sigma)-K(d\delta;\,d\sigma)]\\&+[2J(d\delta;\,d\delta_-)+J(d\delta;\,d\delta)-K(d\delta;\,d\delta_-)]+[2J(d\pi;\,d\sigma)+J(d\pi;\,d\pi)-K(d\pi;\,d\sigma)]\\&+2[J(d\delta;\,d\pi)+J(d\delta;\,d\pi_-)+J(d\pi;\,d\pi_-)].\end{aligned} \tag{16}$$

It is, of course, only a trivial matter to solve (12), (13), (15), (16) for $W(^2H)$, $W(^2G)$, $W(^2F)$, $W(^2D_+)+W(^2D_-)$. If one also desires $W(^2P)$ one must also compute the diagonal sums for $M_L=1$ but we shall not do this explicitly as no new principles are involved. By means of Slater's tables[15] or Brinkman's[16] evaluation of the product of three spherical harmonics by the symbolic method, the J's and K's may be expressed in terms of the Slater-Condon F's and G's. One thus finally finds the same formulas for the energy levels of d^3 as those given by Condon and Shortley.[17] The isolation of $^2D_+$, $^2D_-$ with the extended Dirac method will be given by Serber.[4]

Almost closed shells. Shortley's[18] results on shells which are more than half completed can be nicely and succinctly formulated in terms of the vector model. Suppose that one has an atomic configuration of the form $a^x b^{\tau-y}$, where a, b symbolize s, p, d, f etc., and where $\tau=4l_b+2$, $y\leqq\frac{1}{2}\tau$. Clearly τ has the significance of being the maximum number of electrons allowed in the b shell by the Pauli principle. One has the following rule: *A part from an additive constant common to all the multiplets, the energy levels belonging to $a^x b^{\tau-y}$ are given by the same formulas as those of $a^x b^y$ if in the latter one replaces J_{ij} by $-J_{ij}$*

[14] We henceforth write $d\pi$, $d\delta$ for $d\pi_+$, $d\delta_+$. It is thus to be understood that $m_l>0$ unless a negative sign is appended, as in, e.g., $d\pi_-$.

[15] J. C. Slater, Phys. Rev. **34**, 1312 (1929).

[16] H. C. Brinkman, Zeits. f. Physik **79**, 762 (1932).

[17] E. U. Condon and G. H. Shortley, Phys. Rev. **37**, 1025 (1931).

[18] G. H. Shortley, Phys. Rev. **40**, 185 (1932).

and if one takes the exchange potential to be $+\frac{1}{2}[1-4\mathbf{s}_i\cdot\mathbf{s}_j]K_{ij}\dagger$, *rather than* $-\frac{1}{2}[1+4\mathbf{s}_i\cdot\mathbf{s}_j]K_{ij}$ *as in* (4), *whenever* i *refers to an electron in the group* a^x *and* j *to one in* b^y, *or vice versa.* Here the expression $K\dagger$ is defined by $K\dagger(n_il_im_{l_i};\, n_jl_jm_{l_j})=K(n_il_im_{l_i};\, n_jl_j-m_{l_j})$. No sign reversals (or substitutions of $K\dagger$ for K) in either the Coulomb or exchange terms are, however, to be made when they connect orbits which both belong to a^x or both to b^y.

A corollary of the above rule, obtained by taking $x=0$, is that the levels of the configuration b^{r-y} are, apart from a constant, the same as those of b^y. If $\mu=4l_a+2$ and if one applies the rule twice in succession, first reducing $a^{\mu-x}b^{r-y}$ to a^xb^{r-y} and then a^xb^{r-y} to a^xb^y, there are two successive sign changes which cancel and so one sees that the energy levels of $a^{\mu-x}b^{r-y}$ are the same as those of a^xb^y, except for a constant.

The proof of the rule we shall omit, as it has already been given by Shortley[18] except for formulation in terms of the vector model. The demonstration is substantially the same with either the Slater or Dirac method, centering about Eq. (11) appropriate to the m_s, m_l system of representation, and applies only to problems amenable to the method of diagonal sums.

3. Molecular Spectra

In molecules, there is no longer the degeneracy with respect to M_L and so this degeneracy cannot be used to depress the degree of the secular equations. The energy is still independent of M_S (neglecting, as always, spin-orbit coupling). As in the preceding section, use of individual space quantization for the spin in evaluating the diagonal sums can be avoided by using Eq. (8). Because the M_L degeneracy is lost, the information derivable from the diagonal sum of the energy is naturally much less than in the atomic case.

In the molecular case the orbital wave functions are in general no longer orthogonal. Nevertheless the corrections for non-orthogonality are easily made if we consider only the terms arising from simple permutations. This is not rigorous, since triple permutations, for instance, do not yield wave functions always orthogonal to the original wave function but this "higher order non-orthogonality" is not usually of paramount importance and is often neglected in the literature. (It will, however, be considered by Serber.[4]) Let

$$W=f(J_{12},\, J_{13},\, \cdots J_{1N},\, J_{23},\, \cdots J_{N-1N},\, K_{12},\, \cdots,\, K_{N-1N}) \tag{17}$$

be the solution obtained by disregarding all corrections for non-orthogonality, of whatsoever kind. Here N denotes the total number of orbits, both free and filled. Let Δ_{ij} be the value of the integral (2) when H is stricken out. To include accurately the effect of non-orthogonality as involved in simple permutations, one may use the following rule: substitute $K_{ij}-\Delta_{ij}W$ for each K_{ij} in (17),[19] solve this modified form of (17) for W and take only the root which agrees with (17) when every Δ_{ij} vanishes. That this is the proper answer is readily demonstrated from the fact that the secular determinant involves the matrix elements of $H-W$, with W appearing off the principal diagonal when the wave functions are not orthogonal.

4. Case that Certain Component Spins are Good Quantum Numbers

The total spin vector $\mathbf{S}$ commutes with the Hamiltonian function and its magnitude is a constant of the motion which can immediately be quantized. This means that in Mulliken's terminology, the total spin S is a "good quantum number." Sometimes the resultant spins of certain groups of orbits which constitute only a portion of the complete system[20] may also be good quantum numbers. If

[19] Here the subscripts i, j relate to both free and filled orbits rather than free orbits only as in (7).

[20] We do not mean the trivial case that the "certain groups" consist entirely of filled orbits. Filled groups have rigorously zero resultant spin by the Pauli principle. On the other hand, it is not necessary that the orbits involved in Eq. (18), etc., be all free. For instance, in the application to sa^k, some of the k electrons belonging to a^k may have identical spatial quantum numbers and so occur in filled pairs. Since, by (7), filled orbits introduce only an additive constant in the Hamiltonian function, they never introduce any complication.

$$K_{ij} \text{ is independent of } i \text{ for } i \leqq k \text{ and } j > k, \tag{18}$$

then the magnitude of the resultant spin $\mathbf{S}_k = \mathbf{s}_1 + \cdots + \mathbf{s}_k$ of the first k orbits may be quantized simultaneously with that of the total spin $\mathbf{S}$, so that

$$\mathbf{S}_k^2 = S_k(S_k+1), \qquad \mathbf{S}^2 = S(S+1).$$

To prove this, we note that when (18) is satisfied, Eq. (7) becomes

$$\mathcal{H} = C - \tfrac{1}{2}\Sigma_{i,j=1\cdots k(j>i)}(1+4\mathbf{s}_i\cdot\mathbf{s}_j)K_{ij} - \tfrac{1}{2}\Sigma_{i,j=k+1\cdots n(j>i)}(1+4\mathbf{s}_i\cdot\mathbf{s}_j)K_{ij} + D, \tag{19}$$

with C as in (8) and also with the abbreviation

$$D = -\tfrac{1}{2}\Sigma_{j=k+1\cdots n}[k + 4\mathbf{S}_k\cdot\mathbf{s}_j]K_{ij}. \tag{20}$$

The important thing is that D is a function of $\mathbf{S}_k$ rather than of $\mathbf{s}_1\cdots\mathbf{s}_k$ separately. Now it is easily verified that $\mathbf{S}_k^2$ commutes with $\mathbf{s}_i\cdot\mathbf{s}_j$ if i, j are both in the group $1\cdots k$ or both in the group $k+1\cdots n$. Also $\mathbf{S}_k^2$ obviously commutes with $\mathbf{S}_k$ and with $\mathbf{s}_j$ for $j>k$. Hence $\mathbf{S}_k^2$ commutes with the complete Hamiltonian function (19) and with $\mathbf{S}$, and so can be quantized. (In the general case where (18) is not satisfied, $\mathbf{S}_k^2$ cannot be quantized since it does not commute with $\mathbf{s}_i\cdot\mathbf{s}_j$ if i, j relate to different groups.)

In case K_{ij} is independent of j as well as of i in (18), the magnitude of spin $\mathbf{S}_{>k} = \mathbf{s}_{k+1} + \cdots + \mathbf{s}_i$ can also be quantized so that $\mathbf{S}_{>k}^2 = S_{>k}(S_{>k}+1)$. Then Eq. (20) reduces to

$$D = -\tfrac{1}{2}K_{1n}[k(n-k) + 4\mathbf{S}_k\cdot\mathbf{S}_{>k}] = -\tfrac{1}{2}K_{1n}\{k(n-k) + 2[S(S+1) - S_k(S_k+1) - S_{>k}(S_{>k}+1)]\}, \tag{21}$$

and, except for an additive term (21) which can be evaluated immediately,[21] our n-electron problem factors into the k and $n-k$ electron problems. Formula (21) can always be used to simplify (20) when $k = n-1$, as then there is only one possible value for j in (18).

Some important cases in which the preceding theorem can be used to good advantage are the following:

I. Atomic configurations of the form sa^k ($a = p$, d, etc; $0 < k < 4l_a+2$). One of the nicest applications is to an s electron outside an incomplete shell of equivalent electrons.[22] Because of the spherical symmetry of the s wave function, the Coulomb and exchange integrals, $J(s;a)$, $K(s;a)$ connecting the s electron with any given electron of the a group are independent of the spatial quantum number of the latter and so do not involve any of the Greek indices. (These statements do not apply to interatomic integrals involving s electrons in molecular problems, since the wave functions of s and a are not concentric if they relate to different atoms.) Hence we can apply (19) and (21), taking $S_{>k} = \frac{1}{2}$ and $n = k+1$. So we find

$$W = W(a^k) - \tfrac{1}{2}K_{as}\{k + 2[S(S+1) - S_k(S_k+1) - \tfrac{3}{4}]\} + kJ_{as} \tag{22}$$

where S_k and $W(a^k)$ are, respectively, the spin and the energy of the configuration a^k without addition of the s electron. It is particularly to be noted that *in configurations of the form* sa^k, *the spin of the "core" is rigorously a good quantum number* (when we neglect, as we do throughout, spin-orbit distortion and perturbations by other atomic configurations). This point does not appear to have been generally realized by spectroscopists.

One can use (22), for example, to calculate the levels of the configuration sp^3 in terms of the Slater-Condon F's and G's if the corresponding formulas for p^3 are already known. This application was used in a previous discussion of the carbon spectrum by the writer.[23] The formulas thus obtained for sp^3 agree with those calculated by Johnson[24] with Slater's method.

[21] When, on the other hand, K_{ij} is not independent of j in (18), one cannot use (21) and D ceases to be an additive constant or even a diagonal matrix.

[22] The writer is indebted to Dr. R. Schlapp for mentioning to him that configurations of the form sa^k are more easily treated by the vector model than by other methods.

[23] J. H. Van Vleck, J. Chem. Phys. **2**, 20 (1934).

[24] M. H. Johnson, Jr., Phys. Rev. **39**, 209 (1932).

According to (22), the interval $h\Delta\nu$ between the two states $S=S_k\pm\frac{1}{2}$ of the atom which can be built upon a given spin configuration S_k of the core should have a value

$$h\Delta\nu=2|K_{as}|(S+\tfrac{1}{2}) \tag{23}$$

independent of the azimuthal quantum number L_k of the core. To test this prediction the following data are available[25, 26]

Ti I: $3d^34s$: $^1P-{}^3P=1970$, $^1D-{}^3D=2740$, $^1G-{}^3G=3120$, $^1H-{}^3H=2670$,
$\frac{1}{2}[{}^3P-{}^5P]=2410$, $\frac{1}{2}[{}^3F-{}^5F]=2480$ cm^{-1}

Co I: $3d^84s$: $^2P-{}^4P=4500$, $^2F-{}^4F=3710$	Fe I: $3d^74s$: $^3P-{}^5P=5210$, $^3F-{}^5F=4940$ cm^{-1}
Ni II: $3d^84s$: $^2P-{}^4P=4300$, $^2F-{}^4F=4820$	Ti II: $3d^24s$: $^2P-{}^4P=6620$, $^2F-{}^4F=4560$ cm^{-1}

If (23) were strictly valid, the various intervals quoted for a given ion should be equal. The very appreciable deviations from equality are doubtless due mainly to perturbations by other configurations and, to a lesser extent, to the influence of spin-orbit forces. It is well known that such perturbations often cause the intervals between the different levels of a configuration to have ratios which differ widely from those calculated by means of the Slater-Condon F's and G's, and (22) or (23) represents the same order of approximation as involved in F, G relations.

Ia. Configurations of the type $a^kmsns(m\neq n)$ can be treated by means of (19), (20), but one can no longer use (21). Such configurations will be considered more fully by R. W. Merrill.

II. Body-centered arrangements. Consider a molecular or crystalline structure in which k identical atoms are equidistant from the remaining atom $k+1$ and suppose that in each atom the only electron not in a closed shell is in an s-state. Then one may use (22) with S_k symbolizing the collective spin of the k atoms and $W(a^k)$ their energy in the absence of atom $k+1$. This type of application of the vector model has been discussed by Eyring and colleagues[27] and need not be elaborated here. It shows that the secular problem for the body-centered cube is no more difficult than for the pure cube, if directional valence be disregarded.

III. For checking purposes it is sometimes useful to see if (19) is satisfied when the simplification (18) is artificially imposed in problems in which actually (18) is not satisfied. It is well to make K_{ij} also independent of j in (18), as then one can use (21). Thus errors in arithmetic might be detected in complicated formulas by seeing that they reduce properly when artificial simplifications are imposed. This principle has been used by Seitz and Sherman[28] in molecular problems.

IV. Heitler-Rumer theory. In the chemistry of the light elements the valence electrons (other than those of H atoms) are all in incomplete 2-quantum orbits and are in four kinds of states: *viz.*, $2s$, $2p\sigma_x$, $2p\sigma_y$, $2p\sigma_z$. Here $2p\sigma_x$ means a $2p\sigma$ orbit when the spatial quantization is relative to the x axis, etc. To simplify calculations, it has often been assumed in the literature, notably in the work of Heitler and Rumer,[29] that the inter-atomic Coulomb and exchange integrals connecting the two quantum orbits of one atom and an orbit q of a second atom are the same for all four kinds, so that

[25] I wish to thank Mr. R. Serber for perusal of Bacher and Goudsmit's book to obtain the separations listed in this table. The numerical figures are often only reliable to 50 cm^{-1} or so since the various terms have a multiplet structure whereas we are interested only in electrostatic energy. In each case an attempt has been made to subtract out the spin-orbit energy but this correction can only be made approximately when the Landé interval rule is not obeyed.

[26] When singlet-triplet separations are quoted in the table, it is to be understood that the two terms whose difference is taken are both built on doublet states of the core a^k. Similarly triplet and quartet core states are implied in connection with the doublet-quartet and triplet-quintet separations, respectively. Note that in Ti I, the ^3P terms involved in $^1P-{}^3P$ and $^3P-{}^5P$ are unlike, *viz.*, $3d^3(^2P)4s^3P$ and $3d^3(^4P)4s^3P$, respectively. In comparing the singlet-triplet and triplet-quintet separations in Ti I, the latter have been multiplied by $\frac{1}{3}$ in the table since (23) has twice as large a value for $S=\frac{3}{2}$ as for $S=\frac{1}{2}$.

[27] A. E. Stearn, C. Lindsley and H. Eyring, to appear in J. Chem. Phys.

[28] F. Seitz and A. Sherman, J. Chem. Phys. **2**, 11 (1934).

[29] W. Heitler and G. Rumer, Zeits. f. Physik **68**, 12 (1931).

$$A(2p\sigma_x;\, q) = A(2p\sigma_y;\, q) = A(2p\sigma_z;\, q) = A(2s;\, q). \qquad (A = J \text{ or } K). \tag{24}$$

Actually this is not true (except that $A(2p\sigma_x;\, q) = A(2p\sigma_y;\, q)$ if q is a $p\sigma_z$ or s orbit and z is the inter-atomic axis). The assumption (24) is in a certain sense equivalent to saying that all valence electrons are effectively in s states. In reality two electrons at most could be in a common s state and even then their resultant spin would be zero, precluding free valence. We have shown elsewhere[23] that it is usually a poor approximation thus to ignore directional valence but our point is now that if this is done, one has a mathematical problem which has a particularly simple interpretation in terms of the vector model. When all the 2-quantum exchange integrals can thus be considered identical, the spin of each atom becomes a "good quantum number" since the exchange integrals can be taken outside the summation over the electrons of an atom. With the Heitler-Rumer theory one can easily convince oneself that the valence attraction is maximized by making the spin of each atom assume its maximum possible value. To illustrate these ideas consider the molecule CNOH. Because of the Pauli principle, the number of free valence electrons for the C, N, and O atoms are respectively 4, 3, 2, so that we may take $S_C = 2$, $S_N = 3/2$, $S_O = 1$. Apart from intra-atomic terms, Coulomb terms and exchange terms involving closed shells, the Hamiltonian function (7) is thus

$$\mathcal{H} = -\tfrac{1}{2}K_{CN}[4\times 3 + 4\mathbf{S}_C\cdot\mathbf{S}_N] - \tfrac{1}{2}K_{CO}[4\times 2 + 4\mathbf{S}_C\cdot\mathbf{S}_O] - \tfrac{1}{2}K_{NO}[3\times 2 + 4\mathbf{S}_N\cdot\mathbf{S}_O]. \tag{25}$$

Except for an additive constant, this is a four-vector problem of precisely the general type considered by Johnson[7] and his results are immediately available. Usually one is interested only in the secular equation for the two states of zero spin. Since this equation is a quadratic, it may be evaluated by Goudsmit's[8] inspection method without even resorting to Johnson's work. In other molecules treated by Heitler and Rumer there is often only one state of minimum spin and then the results may be obtained particularly simply. In CNH, for example, the exchange energy is thus $3K_{CN} + K_{CH} - 3K_{HN}$ since the spins of N and H must be parallel to each other and anti-parallel to that of C in order to neutralize the spin of the latter.[30] If the molecule is composed of only two atoms, we have the elementary two-vector problem and the inter-atomic exchange energy is given by (21), with S_k, $S_{>k}$ denoting the spins of the two atoms and K_{1n} the inter-atomic exchange integral. This result has been mentioned by Dirac himself,[31] who notes that this diatomic formula is the same as that previously obtained by Heitler[32] with rather abstruse group theory. Born[33] re-derives the same formula with Slater's method, without noting that the vector model is still simpler when one has only s electrons.

The model of the benzene molecule without directional valence which has recently been considered by M. Markov[34] is clearly simply the six-vector problem with the value $3/2$ for each constituent spin, since Markov assumes three equivalent valence electrons for each CH group. The geometrical symmetry of the benzene ring makes the problem much more tractable than if the groups were unevenly spaced.

V. Distant atoms. Even if the inter-atomic exchange integrals are not regarded as the same for all types of two quantum orbits, it may still be a valid approximation to regard the spin of the atom as a good quantum number. This will be true if the atom is so remote from other atoms that the intra-atomic exchange integrals are large compared to inter-atomic ones. In (4) or (7) we can then, in accordance with the well-known theory of vector coupling,[35] replace $\mathbf{s}_i\cdot\mathbf{s}_j$ by

[30] The coefficient of K_{CN} is 3 because $-\tfrac{1}{2}[3\times 4 + 4\mathbf{S}_N\cdot\mathbf{S}_C] = 3$ when $S_N = \tfrac{3}{2}, S_C = 2, S_{N+C} = \tfrac{1}{2}$. Similarly $-2[1 + \mathbf{S}_H\cdot\mathbf{S}_C] = 1$ when $S_H = \tfrac{1}{2}$, $S_{C+H} = \tfrac{3}{2}$; and $-\tfrac{1}{2}[3 + 4\mathbf{S}_H\cdot\mathbf{S}_N] = -3$ when $S_{H+N} = 2$. Note that in the three vector problem presented by $\mathbf{S}_C$, $\mathbf{S}_N$, $\mathbf{S}_H$ it is usually impossible to diagonalize simultaneously $\mathbf{S}^2_{N+C}$, $\mathbf{S}^2_{C+H}$, $\mathbf{S}^2_{H+N}$ and in consequence S_{N+C}, S_{C+H}, S_{H+N} do not usually represent good quantum numbers. However, the particular case $S = 0$ in which we are interested is an exception and is achieved only when $\mathbf{S}^2_{N+C}$, $\mathbf{S}^2_{C+H}$, $\mathbf{S}^2_{H+N}$ are simultaneously diagonal and correspond, respectively, to quantum numbers $S_{N+C} = \tfrac{1}{2}$, $S_{C+H} = \tfrac{3}{2}$, $S_{H+N} = 2$.

[31] P. A. M. Dirac, Proc. Roy. Soc. **A123**, 733 (1929).

[32] W. Heitler, Zeits. f. Physik **47**, 855 (1928); Phys. Zeits. **31**, 197 (1930).

[33] M. Born, Zeits. f. Physik **64**, 729 (1930), Eq. (55).

[34] M. Markov, J. Chem. Phys. **1**, 784 (1933).

[35] Cf., for instance, Hund, *Linienspektren*, p. 123. It must be cautioned that (26) cannot be applied to a system composed of two *identical* atoms or radicals a, b when $S_a \neq S_b$. The reason is that there is then a degeneracy difficulty arising from the fact that the energy is the same for $S_a = x$, $S_b = y$ as for $S_a = y$, $S_b = x$, making it necessary to consider off-diagonal elements in S_a, S_b.

$$\overline{\mathbf{s}_i\cdot\mathbf{s}_j}=\frac{\overline{(\mathbf{s}_i\cdot\mathbf{S}_a)}(\mathbf{S}_a\cdot\mathbf{S}_b)\overline{(\mathbf{S}_b\cdot\mathbf{s}_j)}}{\mathbf{S}_a^2\mathbf{S}_b^2}=\overline{(\mathbf{s}_i\cdot\mathbf{S}_a)}\,\overline{(\mathbf{S}_b\cdot\mathbf{s}_j)}\left[\frac{S(S+1)-S_a(S_a+1)-S_b(S_b+1)}{2S_a(S_a+1)S_b(S_b+1)}\right] \tag{26}$$

in cases where i and j relate to electrons of different atoms a, b, respectively. The kinematical principle involved in (26) is that only the components of $\mathbf{s}_i$, $\mathbf{s}_j$ parallel to $\mathbf{S}_a$, $\mathbf{S}_b$, respectively, are effective when we discard off-diagonal matrix elements and so take average values. Eq. (26) may be further simplified by using the relation

$$2\mathbf{s}_i\cdot\mathbf{S}_a=S_a(S_a+1)-S_{a-i}(S_{a-i}+1)+s_i(s_i+1) \tag{27}$$

if the spin S_{a-i} of atom a exclusive of electron i is a good quantum number: this will be the case if (a) atom a has only two valence electrons, in which case $S_{a-i}=\frac{1}{2}$, $S_a=0, 1$; (b) if a has only equivalent valence electrons except for i and if in addition a is an s electron; or (c) if a has its maximum multiplicity $S_a=\frac{1}{2}n$ where n is the number of free electrons. The expression $\mathbf{S}_b\cdot\mathbf{s}_j$ may be similarly simplified if conditions analogous to (a), (b), (c) are met in atom b.

In case the exchange integrals within radicals are large in absolute magnitude compared to those connecting electrons of different radicals, the remarks of the preceding paragraph (except item (b)) all apply with the word "radical" everywhere substituted for "atom."

As an illustration, consider the interaction of an H atom with a C atom so distant as not to destroy the Russell-Saunders coupling of the carbon atom, though close enough so that the inter-atomic forces overpower the spin-orbit coupling, which can hence be disregarded. These conditions are equivalent to saying that the atomic L, S, but not J, remain good quantum numbers. Apart from the contributions of the closed $1s$ and $2s$ shells, the inter-atomic energy for the states built on the ^3P state of C is given by the following formulas:

$$W(^3P1s^{3\pm1}\Pi)=a+b-\tfrac{1}{2}(c+d)[1+(1\pm\tfrac{1}{2})(2\pm\tfrac{1}{2})-\tfrac{3}{4}-2], \tag{28}$$

$$W(^3P1s\,^4\Sigma)=2b-2d, \qquad W(^3P1s\,^2\Sigma)=2b+d \tag{29}$$

inasmuch as here $S_a=1$, $S_b=\frac{1}{2}$, $S=1\pm\frac{1}{2}$, $S_{a-i}=\frac{1}{2}$ in (26), (27). We have used the abbreviations

$$a=J(2p\sigma;\,1s), \qquad b=J(2p\pi;\,1s), \qquad c=K(2p\sigma;\,1s), \qquad d=K(2p\pi;\,1s).$$

The index $1s$, of course, relates to the H atom. The formulas for the states built upon ^1D or ^1S are

$$W(^1D1s\,^2\Delta)=2b-d, \qquad W(^1D1s\,^2\Pi)=a+b-\tfrac{1}{2}(c+d), \tag{30}$$

$$W(^1D1s\,^2\Sigma)=2(\tfrac{2}{3}a+\tfrac{1}{3}b)-\tfrac{2}{3}c-\tfrac{1}{3}d, \qquad W(^1S1s\,^2\Sigma)=2(\tfrac{1}{3}a+\tfrac{2}{3}b)-\tfrac{1}{3}c-\tfrac{2}{3}d. \tag{31}$$

In obtaining these results we have utilized the fact that the orbital wave functions for Σ states of the C atom are of the form

$$\Psi=\alpha\psi_{2p\sigma}(1)\psi_{2p\sigma}(2)+\beta\psi_{2p\pi+}(1)\psi_{2p\pi-}(2)+\gamma\psi_{2p\pi-}(1)\psi_{2p\pi+}(2)$$

with $\alpha, \beta, \gamma=(\frac{2}{3})^{\frac{1}{2}}, (\frac{1}{6})^{\frac{1}{2}}, (\frac{1}{6})^{\frac{1}{2}}$ for ^1D; $(\frac{1}{3})^{\frac{1}{2}}, -(\frac{1}{3})^{\frac{1}{2}}, -(\frac{1}{3})^{\frac{1}{2}}$ for ^1S; $0, (\frac{1}{2})^{\frac{1}{2}}, -(\frac{1}{2})^{\frac{1}{2}}$ for ^3P. This is proved by the Wigner[36] formulas or otherwise.

VI. Atoms with strongly coupled cores. The same principles as involved in V can also be utilized in atomic problems where the electrons outside the core are not all of the s type, so that the spin of the core is not rigorously a good quantum number, but where the core is so firmly bound that its spin can nevertheless be quantized with good approximation.

VII. Electron pairs. Very often, because of directional valence, the exchange forces between two electrons i and j of different atoms are large compared to all other exchange forces acting on i and j which depend on the alignment of $\mathbf{s}_i$ and $\mathbf{s}_j$. Then the resultant spin $\mathbf{s}_i+\mathbf{s}_j$ will represent a good

[36] E. Wigner, *Gruppentheorie*, p. 206; J. H. Bartlett, Jr., Phys. Rev. **38**, 1623 (1931).

quantum number, which will have the value 0 for the state of deepest energy in the usual molecular case $K_{ij}<0$. Then if q is any electron other than i, j

$$\overline{\mathbf{s}_i\cdot\mathbf{s}_q}=\overline{\mathbf{s}_j\cdot\mathbf{s}_q}=\tfrac{1}{2}(\mathbf{s}_i+\mathbf{s}_j)\cdot\mathbf{s}_q=0 \quad \text{so that} \quad -\tfrac{1}{2}[\overline{1+4\mathbf{s}_i\cdot\mathbf{s}_q}]=-\tfrac{1}{2} \quad \text{whereas} \quad -\tfrac{1}{2}[1+4\mathbf{s}_i\cdot\mathbf{s}_j]=+1.$$

Under such circumstances we say that i, j form an electron pair (not to be confused with the pairs involved in filled orbits) and we have the theorem that the exchange coefficient is $+1$ between two members of a pair and is $-\frac{1}{2}$ between a member of a pair and any electron outside the pair. This principle is constantly used in any molecular calculation for which electron pairing is a good approximation.[37] It has already been employed in (30), (31) since the two electrons of C form a pair in the singlet cases.

As an illustration, consider a CH molecule at a C–H distance so small that the inter-atomic forces disrupt the L, S structure of the C atom. This is the case at the actual inter-nuclear distance. Then we can no longer neglect the matrix elements connecting $^1D1s\,^2\Pi$ and $^3P1s\,^2\Pi$ or $^1D1s\,^2\Sigma$ and $^1S\,^2\Sigma$, which was done to obtain (28)–(31). Quite approximately the H electron is paired with a $2p\sigma$ electron in the deepest state $2p\pi 2p\sigma 1s\,^2\Pi$, replacing the intra-atomic pairing involved in Eq. (30) and so the formula for this state is $a+b+c-\frac{1}{2}d$ rather than (28) or (30). Formulas for the other states of CH at close distances will be given by J. R. Stehn in a paper in the *Journal of Chemical Physics*.

VIII. Combination of (IV) and (V). One can obtain, for example, Heitler and Rumer's results on NH_2-NH_2 (hydrazine), by applying simultaneously the principles involved in *IV* and *V*. The spin of each NH_2 radical can be treated as a good quantum number because the binding forces internal to the NH_2 radicals are larger than those between two such radicals. Inside NH_2, the spin of the N atom and the collective spin of the two H atoms are good quantum numbers in virtue of the hypothesis (24) and the equidistance of the two H atoms from N. We can use (26), (27) if we substitute S_i, S_j for s_i, s_j. (This modification is necessary because the spin of the N atom is not a one-electron unit.) The state of deepest energy is obtained by taking $S_i=S_j=S_N=\frac{3}{2}$, $S_a=S_b=S_{NH_2}=\frac{1}{2}$, $S_{a-i}=S_{b-j}=S_{H_2}=1$. If we neglect the forces between H atoms of different radicals, the exchange energy connecting the two radicals is thus[38] $-\frac{1}{2}(3\times 3+4\overline{S_i\cdot S_j})K_{NN}=-\frac{1}{3}K_{NN}$.

Other examples of the vector model in molecular structure will be given by A. Sherman in an article on valence to appear in *Reviews of Modern Physics*.

5. The Interaction of a Group of Equivalent p Electrons

The vector model has a very striking application to a group of equivalent p electrons. Here, once the energy levels have been determined for p^2, it is possible to derive expressions for the energies of the configurations $p^3\cdots p^6$ without appealing to the method of diagonal sums at all. We might characterize our treatment of d^3 in Section 2 as based on the intermediary of an S, m_l system of quantization, whereas we shall show that for $p^3\cdots p^6$ not even this intermediary is necessary and one can write down formulas for the energy directly in the S, L system. The trick is to note that when we are restricting ourselves to one particular configuration, the matrices are of finite, low degree, so that certain matrix identities are readily established.

First consider the interaction of two equivalent p electrons. Here the terms allowed by the Pauli principle are ^1D, ^3P, ^1S. Now since

$$2\mathbf{s}_i\cdot\mathbf{s}_j+\tfrac{3}{2}=S(S+1), \qquad 2\mathbf{l}_i\cdot\mathbf{l}_j+4=L(L+1) \tag{32}$$

we see that $\mathbf{s}_i\cdot\mathbf{s}_j$, $\mathbf{l}_i\cdot\mathbf{l}_j$ are both diagonal for these terms. Furthermore the characteristic values of

[37] For other examples and references see J. H. Van Vleck, J. Chem. Phys. **1**, 177, 219 (1933).

[38] This result agrees with that obtained p. 39 of the H–R paper[29] by the Slater method. Since presumably $K_{NN}<0$, the interaction energy of the two NH_2 radicals is positive and hence repulsive with the present type of calculation, whereas actually hydrazine is a stable compound.

$\mathbf{s}_i\cdot\mathbf{s}_j+\frac{1}{2}(\mathbf{l}_i\cdot\mathbf{l}_j+\frac{1}{2})^2-\frac{3}{8}$ are all zero by (32) inasmuch as the allowed pairs of values for L, S are 2, 0; 1, 1; 0, 0. Hence we have the matrix identity

$$2\mathbf{s}_i\cdot\mathbf{s}_j=-(\mathbf{l}_i\cdot\mathbf{l}_j)^2-(\mathbf{l}_i\cdot\mathbf{l}_j)+\tfrac{1}{2}, \tag{33}$$

which, of course is valid in any system of representation, since a null matrix remains a null matrix under any canonical transformation. Eq. (33) has an interesting kinematical interpretation. It shows that *the Pauli principle uniquely determines the angle between the two* **s** *vectors once the angle between the two* **l** *vectors is given.* Now consider the energy of interaction between our two equivalent p electrons. In terms of the Slater-Condon F's and G's, it is known that[39]

$$W(^3P)=F_0-5F_2, \qquad W(^1D)=W_0+F_2, \qquad W(^1S)=F_0+10F_2. \tag{34}$$

Hence we have the identity

$$W=F_0+[-5-3\mathbf{l}_i\cdot\mathbf{l}_j-12\mathbf{s}_i\cdot\mathbf{s}_j]F_2, \quad \text{or} \quad W=F_0+[-8+3\mathbf{l}_i\cdot\mathbf{l}_j+6(\mathbf{l}_i\cdot\mathbf{l}_j)^2]. \tag{35}$$

We have written the identity in two forms which are equivalent in view of (33). To prove (35), we have only to note that (35) reduces to (34) when one uses (32) and substitutes the proper values of L and S. It may be remarked that the most general function of the relative orientation of two equivalent p electrons is a polynomial of degree 2 in $\mathbf{l}_i\cdot\mathbf{l}_j$, for any polynomial of higher degree can immediately be depressed to a quadratic by means of the identity

$$(\mathbf{l}_i\cdot\mathbf{l}_j)^3=-2(\mathbf{l}_i\cdot\mathbf{l}_j)^2+(\mathbf{l}_i\cdot\mathbf{l}_j)+2. \tag{36}$$

(36) is a consequence of the fact that the characteristic values of $q=\mathbf{l}_i\cdot\mathbf{l}_j$ are 1, -1, -2 by (32), so that $(q^2-1)(q+2)=0$.

Configurations $p^3\cdots p^6$. We are now in a position to calculate immediately the energies of $p^n(n=3,\cdots 6)$. We have only to note that here by (35) the matrix of the interaction is

$$W=\tfrac{1}{2}n(n-1)(F_0-5F_2)+\Sigma_{j>i}(-3\mathbf{l}_i\cdot\mathbf{l}_j-12\mathbf{s}_i\cdot\mathbf{s}_j)F_2. \tag{37}$$

This is brought to diagonal form by diagonalizing $\Sigma\mathbf{s}_i\cdot\mathbf{s}_j$ and $\Sigma\mathbf{l}_i\cdot\mathbf{l}_j$, for then (37) reduces to

$$W=\tfrac{1}{2}n(n-1)F_0+\tfrac{1}{2}[-5n^2+20n-3L(L+1)-12S(S+1)]F_2, \tag{38}$$

in virtue of (5) and the analogous relation

$$2\Sigma_{j>i}\mathbf{l}_i\cdot\mathbf{l}_j+2n=L(L+1) \tag{39}$$

obeyed by the l vectors.[40]

If we substitute the proper values of n, L, and S, one finds that (38) gives exactly the same energy levels as those deduced by Slater and by Condon and Shortley.[39] For instance, for the configuration p^3, the only terms allowed by the Pauli principle are ^2P, ^2D, ^4S so that in (38) we must use $n=3$ and the following pairs of values of L, S: 1, $\frac{1}{2}$; 2, $\frac{1}{2}$; or 0, $\frac{3}{2}$. Eq. (38) shows immediately that the energy levels of p^{6-n} are the same as those of p^n except for an additive constant, since both configurations involve the same L, S pairs. This, of course, agrees with the general theorem on almost closed shells given near the end of section 2.

Spin-orbit Energy. It is well known that in the expression $A\mathbf{L}\cdot\mathbf{S}$ for the spin-orbit energy of a group of equivalent electrons in Russell-Saunders coupling, the constant of proportionality A is not the

[39] J. C. Slater, Phys. Rev. **34**, 1316 (1929); E. U. Condon and G. H. Shortley, Phys. Rev. **37**, 1025 (1931). To avoid fractions we use the Condon-Shortley rather than Slater convention in the definition of the F's.

[40] It is clearly to be understood that in the coupling problems which we consider, individual terms in the summation in (5) or (39) are not diagonal except when $n=2$. Instead only the complete sums are diagonal. The identities (33), (36) are nevertheless valid for any value of n.

same as the value a appropriate to a one-electron system. The standard method of determining A in terms of a and the number of electrons n is that due to Goudsmit.[41] It is based on the invariance of the diagonal sum or spur in the passage from m_l, m_s to S, L quantization, as applied to the matrix $a\Sigma\mathbf{l}_i\cdot\mathbf{s}_i$. In the m_l, m_s this sum is simply $a\Sigma m_{l_i}m_{s_i}$. With our vector model, one can write down the spin-orbit energy in the L, S system without using the spur theorem or the intermediary of m_l, m_s quantization, by the following procedure which furnishes a rather interesting alternative to Goudsmit's method.

In Russell-Saunders coupling, spin-orbit energy has the value

$$a\Sigma\mathbf{l}_i\cdot\mathbf{s}_i=[a\Sigma_i\overline{(\mathbf{l}_i\cdot\mathbf{L})(\mathbf{s}_i\cdot\mathbf{S})}/L(L+1)S(S+1)]\mathbf{L}\cdot\mathbf{S}=A\mathbf{L}\cdot\mathbf{S}, \tag{40}$$

since there is no correlation between the rate of precession of $\mathbf{l}_i$ about $\mathbf{L}$ and that of $\mathbf{s}_i$ about $\mathbf{S}$,[42] so that we may project $\mathbf{l}_i$ along $\mathbf{L}$ and $\mathbf{s}_i$ along $\mathbf{S}$ in taking mean values. The final form of (40) is simply the definition of A. We have been very careful in (40) to write the average energy as proportional to the average of the product $(\mathbf{l}_i\cdot\mathbf{L})(\mathbf{s}_i\cdot\mathbf{S})$ rather than to the product of the averages of $(\mathbf{l}_i\cdot\mathbf{L})$ and $(\mathbf{s}_i\cdot\mathbf{S})$. It is tempting at first to try the latter, for then the calculation is particularly simple inasmuch as all equivalent electrons are on a par, making $n\overline{(\mathbf{l}_i\cdot\mathbf{L})}=\mathbf{L}^2$, $n\overline{(\mathbf{l}_i\cdot\mathbf{L})}=\mathbf{S}^2$. Then we would have $A=a/n$, which is an incorrect formula for the A constant since by trying a few simple examples one finds that it does not agree with the results of Goudsmit's method of diagonal sums. It does not, for instance, give a zero A for $p^3\,{}^2D$. Our vector model immediately removes this paradox by making it clear that it is not at all correct to replace the average of the product by the product of separate averages.[43] Eq. (33) shows that there is a constraint between $\mathbf{l}_i\cdot\mathbf{l}_j$ and $\mathbf{s}_i\cdot\mathbf{s}_j$, so that the motions of $\mathbf{l}_i$ and $\mathbf{s}_i$ are not independent and consequently

$$\overline{(\mathbf{l}_i\cdot\mathbf{L})(\mathbf{s}_i\cdot\mathbf{S})}\neq\overline{(\mathbf{l}_i\cdot\mathbf{L})}\,\overline{(\mathbf{s}_i\cdot\mathbf{S})}. \tag{41}$$

For instance, it might be that the times when $\mathbf{l}_i$ is parallel to $\mathbf{L}$ are those when $\mathbf{s}_i\cdot\mathbf{S}$ is near its maximum, and then the left side of (41) is greater than the right side. Thus we cannot in general divide the bar in Eq. (41). (In the particular case of only two electrons this is allowable, as then each factor in (41) is constant, and $A=a/2$.)

Since $\mathbf{L}=\Sigma\mathbf{l}_i$, $\mathbf{S}=\Sigma\mathbf{s}_i$ we see from (40) that the correct formula for A may be written

$$A=a\Sigma_i\{\Sigma_j(\mathbf{l}_i\cdot\mathbf{l}_j)\Sigma_k(\mathbf{s}_i\cdot\mathbf{s}_k)\}/[L(L+1)S(S+1)]. \tag{42}$$

First let us consider the configuration p^3. Here, $\mathbf{s}_i^2=\frac{3}{4}$, $\mathbf{l}_i^2=2$,

$$\Sigma_i\{\Sigma_j(\mathbf{l}_i\cdot\mathbf{l}_j)\Sigma_k(\mathbf{s}_i\cdot\mathbf{s}_k)\}=3\times2\times\tfrac{3}{4}+2\Sigma_{j>i}[2\mathbf{s}_i\cdot\mathbf{s}_j+\tfrac{3}{4}\mathbf{l}_i\cdot\mathbf{l}_j+(\mathbf{l}_i\cdot\mathbf{l}_j)(\mathbf{s}_i\cdot\mathbf{s}_j)]+\Sigma_i'{}_{,j,k}(\mathbf{l}_i\cdot\mathbf{l}_j)(\mathbf{s}_i\cdot\mathbf{s}_k). \tag{43}$$

The prime attached to the summation means that no terms are to be included in which any two of the indices i, j, k are equal. The relation

$$(2\Sigma_{j>i}\mathbf{l}_i\cdot\mathbf{l}_j)(2\Sigma_{j>i}\mathbf{s}_i\cdot\mathbf{s}_j)=[L(L+1)-2n][S(S+1)-\tfrac{3}{4}n]$$

when applied to a three electron system gives us

$$4\Sigma'_{i,j,k}(\mathbf{l}_i\cdot\mathbf{l}_j)(\mathbf{s}_i\cdot\mathbf{s}_k)+4\Sigma_{j>i}(\mathbf{l}_i\cdot\mathbf{l}_j)(\mathbf{s}_i\cdot\mathbf{s}_j)=[L(L+1)-6][S(S+1)-\tfrac{n}{4}], \tag{44}$$

inasmuch as no terms of the form i, j, k, l (i, j, k, l all unequal) are encountered until there are four electrons or more. The triple sum on the right of (43) can now be eliminated by means of (44). Furthermore certain terms in (43) and (44) can be simplified by the relation

---

[41] S. Goudsmit, Phys. Rev. **31**, 946 (1928).

[42] Use of (40) is equivalent to rejection of off-diagonal elements in L, S and so amounts to assuming that Russell-Saunders coupling is a good approximation, as is always true in light atoms.

[43] We could, however, divide the bar in (26), as in electrostatic problems there is nothing analogous to the constraint (33). The bar is incorrectly divided in Goudsmit's[41] spin-orbit Eq. (3), but fortunately he does not use his Eq. (3) in cases where this matters.

$$(\mathbf{l}_i\cdot\mathbf{l}_j)(\mathbf{s}_i\cdot\mathbf{s}_j)=\tfrac{1}{2}(\mathbf{l}_i\cdot\mathbf{l}_j)^2-\tfrac{1}{4}(\mathbf{l}_i\cdot\mathbf{l}_j)-1=-\mathbf{s}_i\cdot\mathbf{s}_j-\tfrac{3}{4}(\mathbf{l}_i\cdot\mathbf{l}_j)-\tfrac{3}{4}, \tag{45}$$

which is a consequence of (33) and (36). By (44), (45), (5) and (39), the right side of (43) may be written

$$\tfrac{9}{4}+\tfrac{3}{8}[L(L+1)-6]+\tfrac{3}{2}[S(S+1)-\tfrac{9}{4}]+\tfrac{1}{4}[L(L+1)-6][S(S+1)-\tfrac{9}{4}] \tag{46}$$

when $n=3$. The only pairs of values of L, S which occur for p^3 are $1,\frac{1}{2}$; $2,\frac{1}{2}$; $0,\frac{3}{2}$ and so the expression (46) vanishes. This is, of course, in accord with the fact that the configuration p^3 represents half completion of the shell p^6 and so is devoid of multiplet structure (in our degree of approximation) by one of Goudsmit's theorems. Because (46) and hence (43) vanish for $n=3$, we have the matrix relation

$$(\mathbf{l}_i^2+\mathbf{l}_i\cdot\mathbf{l}_j+\mathbf{l}_i\cdot\mathbf{l}_k)(\mathbf{s}_i^2+\mathbf{s}_i\cdot\mathbf{s}_j+\mathbf{s}_i\cdot\mathbf{s}_k)=0. \tag{47}$$

Since (47) is a matrix identity, it is valid for any group of three electrons i, j, k even though occurring in p^4, p^5, etc.

To calculate the values of A appropriate to p^4, p^5, we note that when there are more than three electrons

$$\Sigma_i\{\Sigma_j(\mathbf{l}_i\cdot\mathbf{l}_j)\Sigma_k(\mathbf{s}_i\cdot\mathbf{s}_k)\}=\Sigma'(\mathbf{l}_i^2+\mathbf{l}_i\cdot\mathbf{l}_j+\mathbf{l}_i\cdot\mathbf{l}_k)(\mathbf{s}_i^2+\mathbf{s}_i\cdot\mathbf{s}_j+\mathbf{s}_i\cdot\mathbf{s}_k)-\tfrac{1}{2}n[(n-1)(n-2)-2]\tfrac{3}{4}\times 2$$
$$-2(n-3)\Sigma_{j>i}\{\tfrac{3}{4}\mathbf{l}_i\cdot\mathbf{l}_j+2\mathbf{s}_i\cdot\mathbf{s}_j+(\mathbf{l}_i\cdot\mathbf{l}_j)(\mathbf{s}_i\cdot\mathbf{s}_j)\},$$

or using (42), (45), (47), (5), (39), we finally have

$$A=-(n-3)a/L(L+1). \tag{48}$$

This gives the proper result, *viz.*, that the A's for p^4, p^5 are the negative of those for p^2, p. For instance $A=-\frac{1}{2}a$ for $p^4\ {}^3P$. It is interesting to note that (48) is a correct formula for the A constants for the entire range of the p group, checking with Goudsmit's results in every case.[44]

The preceding methods cannot be extended, at least in a simple way, to other configurations, such as, for example, equivalent d electrons or non-equivalent p electrons. The reason in the equivalent case is that the algebraic equations which are identically fulfilled are of too high a degree to reduce the problem sufficiently. For instance, with d^n the scalar product $\mathbf{s}_i\cdot\mathbf{s}_j$ is uniquely determined by $\mathbf{l}_i\cdot\mathbf{l}_j$ but is now a polynomial of degree 4 in $\mathbf{l}_i\cdot\mathbf{l}_j$, whereas it was of degree 2 in the case of p^n. If i and j are non-equivalent electrons, the value of $\mathbf{s}_i\cdot\mathbf{s}_j$ ceases to be uniquely determined by $\mathbf{l}_i\cdot\mathbf{l}_j$. Thus except for p^n, one must fall back on spur methods, at least as applied to the **L** part of the problem. Our calculations for p^n by the full vector method applied to both **L** and **S** rather than by our usual Dirac vector scheme applicable only to **S** must be regarded as a special procedure which is available only for the configuration p^n and which is of interest primarily because of the kinematical insight furnished into the Pauli principle.

[44] For singlet or for S states, the values of A given by (48) have no meaning, as such states are devoid of multiplet structure. For this reason we need not worry over the fact that (40) reduces to the indeterminate form 0/0 when L or S vanishes, or that (48) becomes infinite when $L=0$.

Large Barkhausen Discontinuities and Their Propagation in Ni-Fe Alloys

RAYMOND E. REINHART, *University of Kansas, Department of Physics and Astronomy, Lawrence, Kansas*

(Received November 13, 1933)

The velocity of propagation of large Barkhausen discontinuities has been investigated as a function of circular field, longitudinal field, torsion and tension for a cold drawn 10 percent Ni-Fe alloy wire 0.0334 cm in diameter. Curves relating velocity of propagation and circular field were found to be similar to curves relating velocity of propagation and longitudinal field, thus suggesting that the functional relationship between velocity and circular field is identical with that between velocity and longitudinal field. These relationships were explained when it was found by two different experimental studies that only the component of the resultant field, impressed on the wire, in the direction of the principal strain axis of elongation is important in determining the velocity of propagation. The component perpendicular to this direction of maximum elongation produces no appreciable effect on the velocity. A method of heat treating 70 percent Ni-Fe alloy wire 0.0321 cm in diameter has been developed which made it possible to investigate the relationship between velocity of propagation and longitudinal field over much greater ranges of field and velocity than was possible for untreated wire. Over a range of field strengths of 2.23 oersteds the velocity was observed to vary from 1000 cm sec.$^{-1}$ to 140,750 cm sec.$^{-1}$. The relationship between velocity and field for this wire is definitely not linear. Discontinuities in which the change in induction was accurately equal to the total change in induction between saturation in the two directions were observed for these heat treated wires.

I. INTRODUCTION

THE propagation of large Barkhausen discontinuities in cold drawn Ni-Fe alloy wires has been investigated by Sixtus and Tonks.[1] For wires subjected to tensile stress they found a relationship between the velocity of propagation and longitudinal field given by $v=A(H-H_0)$ where the slope A is nearly the same for all values of tensile stress. For wires subjected to torsional stress they also found a linear relationship between velocity and field. In the latter case however A was found to vary with the degree of torsional stress. Other investigations reported by Sixtus and Tonks include the effects of temperature, heat treatment, and circular magnetic field upon propagation.

Previous to the appearance of the later papers of Sixtus and Tonks dealing with the effects of heat treatment and circular field upon propagation phenomena some investigations along these lines were started in this laboratory. Many observations similar to those reported by Sixtus and Tonks have been made and in addition the results described in the following pages have been obtained.

[1] K. J. Sixtus and L. Tonks, Phys. Rev. **37**, 930 (1931); **42**, 419 (1932); **43**, 70 (1933).

II. APPARATUS

The complete time measuring arrangement used was identical with that used by Sixtus and Tonks. The complete arrangement was calibrated by checking it against known time intervals obtained by having an arm on the shaft of a synchronous motor open two circuits in succession which were a known distance apart. The complete arrangement was found to be accurate even for time intervals as small as 2×10^{-4} seconds.

The solenoid used to obtain the uniform longitudinal field was wound on the outer wall of a Pyrex glass water jacket through which tap water was circulated to eliminate heating effects of the magnetizing current. The axis of this main field solenoid was made to coincide with the direction of the earth's field. The earth's field was then completely balanced out by sending a small direct current through an auxiliary winding.

III. RESULTS FOR A 10 PERCENT Ni-Fe ALLOY

Some cold drawn 10 percent Ni-Fe alloy wire 0.0332 cm in diameter was obtained from the General Electric Laboratories. The following

investigations into the relationships existing between circular field, longitudinal field, tensile stress, and torsional stress were carried out for this wire. The symbols denoting the various magnetic fields referred to in the following are: H, the main or longitudinal magnetic field produced by the magnetizing solenoid; H_c, the circular field (always specified at the surface of the wire) produced by sending a direct current through the wire; H_s, the starting field, the maximum value of H or of H_c that can be impressed upon the wire without the discontinuity occurring.

It is convenient to define the direction of the magnetic fields with respect to the principal strain axis of elongation. In the following a circular field in such a direction that its component along the direction of maximum elongation has the same sense as the component of longitudinal field along the same direction will be considered positive.

A length of the 10 percent Ni-Fe wire was subjected to a purely torsional stress of 12°/cm. Data were then taken for a series of velocity-circular field curves for various fixed values of H. The curves were distributed over the entire range of fields for which propagation could be obtained. A section of this series of curves is shown in Fig. 1. The velocity-circular field characteristics are all parallel throughout the entire range of fields.

Data for a series of velocity-longitudinal field characteristics were also taken for various fixed circular fields for the same wire and for the same torsional stress as for the series of velocity-circular field curves. The velocity-longitudinal field curves were also found to be parallel throughout the entire range of field strengths for which propagation could be obtained.

The interchangeableness of H and H_c in the two sets of curves mentioned above clearly indicates some simple relationship between the two fields and the velocity of propagation. To investigate this relationship the relation between H and H_c was found from the series of curves of which Fig. 1 is a section for a constant velocity of 5000 cm/sec. This relation is shown by curve A of Fig. 2. Since, the velocity circular field curves are all parallel obviously for any other fixed velocity another straight line parallel to

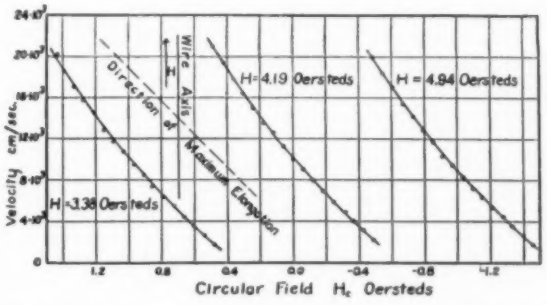

FIG. 1. A section of a series of velocity-circular field curves for different longitudinal fields. The series of curves is for a cold drawn 10 percent Ni-Fe wire for a torsion of 12°/cm.

curve A would result. Now theory demands that for a wire subjected to purely torsional stress the principal strain axes make angles of 45° with the wire axis. The direction of maximum elongation demanded by theory is shown by the broken line in Fig. 2. Since the velocity remains constant while the component of field in the direction of maximum elongation remains constant the conclusion can hardly be avoided that for a given strain only the component of field in the direction of maximum elongation effects the velocity. The component of the resultant field in the direction of the compression axis has little or no effect. The critical field relationship reported by Sixtus

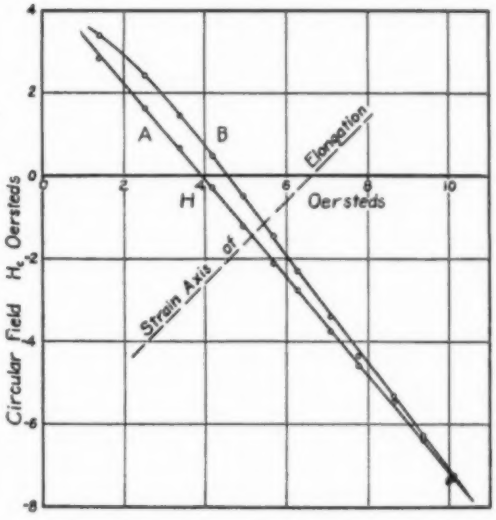

FIG. 2. Curve A is the relationship between the circular and longitudinal fields for a constant velocity of 5000 cm/sec. The relationship is for a 10 percent Ni-Fe wire under a torsion of 12°/cm. Curve B is the relationship between longitudinal and starting fields for the same wire under the same stress as for curve A.

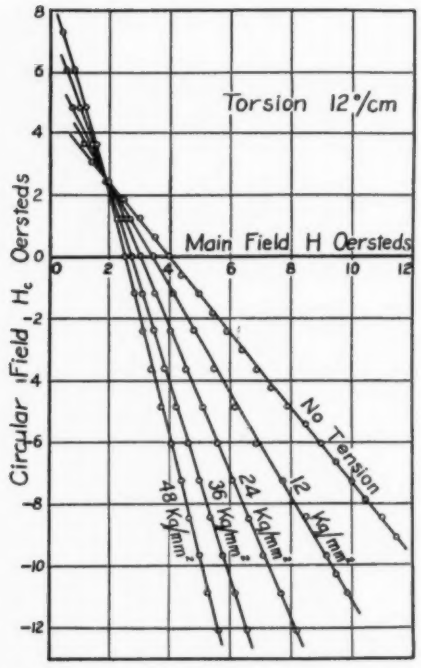

FIG. 3. A series of relationships between circular and longitudinal fields for a velocity of 5000 cm/sec., and for different tensions. The relationships are for 10 percent Ni-Fe alloy wire under a torsion of 12°/cm. The slope of the strain axis of maximum elongation is positive for these relationships.

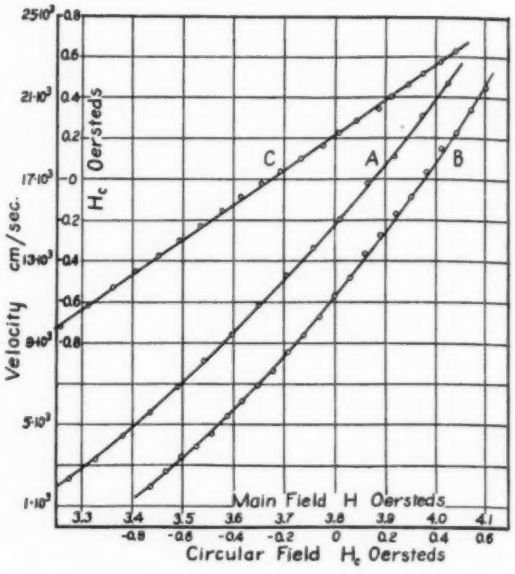

FIG. 4. Curve *A* gives the relationships between velocity and longitudinal field for a 10 percent Ni-Fe wire under a torsional stress of 12°/cm and a tensile stress of 12 kg/mm². Curve *B* gives the relationship between velocity and circular field for the same stresses as for curve *A*. The linear relationship *C* is the relation between the longitudinal and circular fields. It was obtained by eliminating velocity between the relationships given by curves *A* and *B*.

and Tonks[2] is a special case of this general relationship. The straight line relating H and H_c for zero velocity, parallel to curve *A* above, should correspond to their vector critical field relationship.

Curve *A* of Fig. 2 should not be expected to be exactly perpendicular to the theoretical strain axis of elongation since the circular field has in each case been calculated at the surface of the wire. In actual propagation some finite layer must be considered and the effective field for this layer must be considered rather than the field at the wire surface. If the circular field is considered at a distance from the center of the wire equal to 5/6 of the radius of the wire, instead of at the surface, curve *A* becomes accurately perpendicular to the direction of maximum elongation.

The range of field strengths for which propagation could be obtained in a series of velocity-circular field curves, such as that of which Fig. 1 is a section, was found to decrease as the circular field increased. Curve *B* in Fig. 2 shows the relationship between the circular starting fields and the longitudinal field. Differences between the ordinates of curves *A* and *B* at any point are thus a measure of the range of circular field strengths for which propagation could be obtained.

Investigations into the relationship between velocity of propagation, H and H_c were extended to the case where the wire was subjected to both tensile and torsional stresses. A torsional stress of 12°/cm was applied to a length of wire and held constant. Various fixed tensile stresses were then applied to the wire and the relation between H and H_c obtained in each case for a constant velocity of 5000 cm/sec. This series of straight lines is shown in Fig. 3. The change in slope of these straight lines with tension is qualitatively just as one should expect.

While under the same stresses as for the curves in Fig. 3 other data were taken. For each stress velocity-circular field and velocity-longitudinal field curves were obtained. These two curves for the case where the tensile stress was

[2] K. J. Sixtus and L. Tonks, Phys. Rev. **43**, 70 (1933).

12 kg/mm² are shown in Fig. 4. The straight line *C* of Fig. 4 is the relationship between H and H_c which was obtained from the curves *A* and *B* by eliminating velocity directly from the curves.

In Fig. 5 is a set of straight line relationships between H and H_c which were obtained as was curve *C* of Fig. 4. Upon comparing slopes of corresponding straight lines in Figs. 3 and 5 it will be seen that they are exactly the same in magnitude but opposite in sign. The significance of the linear relationships in Fig. 5 becomes apparent when their slopes are considered relative to the direction of the principal strain axis of elongation. The directions of maximum elongation are known since they are perpendicular to the straight lines of Fig. 3. In Fig. 5 the direction of maximum elongation, in the case of the relationship where the tensile stress was 12 kg/mm². is shown by the broken line. For this linear relationship the velocity can be changed from the value existing at 0 to that existing at *A* either by leaving H_c zero and increasing H by an amount *ON* or by leaving H unchanged and increasing H_c by an amount *OM*. The projections of these field changes *ON* and *OM* which give rise to the same change in velocity, upon the principal strain axis of elongation are exactly the same. For each of the linear relationships in Fig. 5 the same is true. The relationship between the velocity of propagation, H and H_c is then perfectly general. For any direction of maximum elongation it is only the field in that direction which influences the velocity.

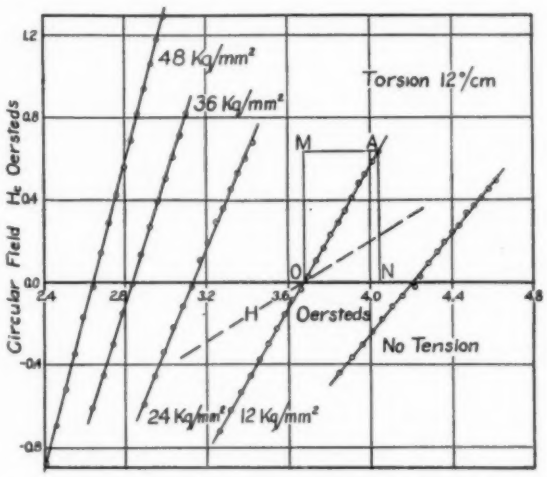

FIG. 5. A set of linear relationships between the circular and longitudinal fields for different tensions. These relationships were obtained as was the linear relationship *C* in Fig. 5 and are for the same wire as the relationships in Fig. 4.

Sets of data similar to those presented above have been obtained for different lengths of the 10 percent Ni-Fe alloy wire. In each case the results are essentially the same.

The above relation between velocity of propagation and field component in the direction of maximum elongation makes possible the interpretations of a number of phenomena. For one thing it explains why the slope of velocity longitudinal field curves changes with torsion. It is also easily seen why a circular field in one direction should increase the velocity and in the opposite direction decrease it. For a wire under a purely tensile stress no change in velocity with circular field should be expected and no appreciable change has been observed. Such curves as those obtained by Sixtus and Tonks[3] are also readily interpretable.

IV. Results for a 70 Percent Ni-Fe Alloy

A commercial alloy wire 0.0321 cm in diameter (B and S gauge No. 28) containing 70 percent nickel with the remainder iron was obtained from the Driver Harris Company. This wire had been annealed in hydrogen by the manufacturers.

Pieces of this wire, when taken directly from the spool on which it was wound and placed under tension, gave large discontinuities in which the total change in induction was approximately 97 percent of the total change in induction between saturation in the two directions. The maximum range of velocities observed for this wire was approximately from 1000 to 20,000 cm/sec. and the maximum range of field strengths 0.4 oersted. The velocity longitudinal field characteristics were not straight lines.

The effects of annealing and annealing under tensile stress were investigated for this wire. The wire was annealed in air by passing a 60 cycle alternating current through it. While investigating the effects of annealing under stress it was observed that if the heating circuit were abruptly broken and the wire allowed to cool rapidly the starting field was increased. The range of field strengths for which propagation

[3] Reference 2, p. 71, Fig. 2.

could be obtained was thus increased. A further study of the factors influencing this tempering effect (temperature, tensile stress) led to the following method of heat treatment. A tensile stress of 6 kg/mm² was applied to the wire by means of a hanger and weights. The heating circuit was then closed sending a current through the wire of such magnitude that it was quickly brought to a bright yellow heat and began to flow rapidly under the tensile stress. When the wire had increased in length some three or four percent the heating circuit was broken and the wire allowed to cool quickly. Upon cooling the wire would shrink to within one percent of its original length.

Hysteresis loops for a wire which had been subjected to the above heat treatment and then placed under tension were found to be perfectly rectangular. That is the maximum discontinuous change in magnetization observed was exactly the same as the double saturation value. Further the change in magnetization ΔI was the same for all fields for which propagation could be obtained. A set of velocity longitudinal field curves for such a wire is shown in Fig. 6. The velocity longitudinal field curves are definitely not linear.

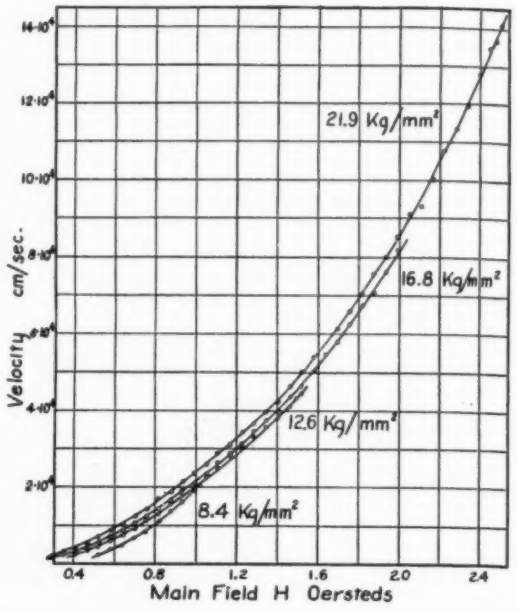

FIG. 6. Velocity field curves for a 70 percent Ni-Fe alloy wire (0.0321 cm in diameter) for different tensions. This wire had been heated to a bright yellow heat while under a tensile stress of 6 kg/mm² and allowed to cool quickly.

The author wishes to thank Dr. J. D. Stranathan for his interest in and many helpful suggestions in regard to the work of this paper. He also wishes to thank Dr. C. V. Kent for his interest and many helpful suggestions. He wishes also to thank Mr. K. J. Sixtus who supplied the 10 percent Ni-Fe wire for the above work.

LETTERS TO THE EDITOR

Prompt publication of brief reports of important discoveries in physics may be secured by addressing them to this department. Closing dates for this department are, for the first issue of the month, the twentieth of the preceding month; for the second issue, the fifth of the month. The Board of Editors does not hold itself responsible for the opinions expressed by the correspondents.

Emission of Neutrons from Fluorine and Beryllium

The purpose of this experiment was to investigate the emission of neutrons from fluorine and beryllium as a function of the velocity of the alpha-particles producing the disintegration. A diagram of apparatus is given in Fig. 1.

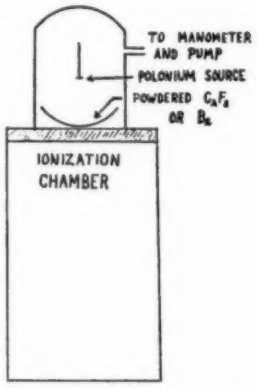

FIG. 1. Diagram of apparatus.

The source of alpha-particles was about 10 millicuries of polonium on a silver disk of 0.3 cm radius. Powdered calcium fluoride or beryllium was spread on a portion of a glass sphere of 3.8 cm radius. The residual range of the alpha-particles was varied by changing the pressure of the air inside the bell-jar. Since calcium has been found to give no appreciable emission of neutrons, the effects observed when calcium fluoride was used in this experiment are due to neutrons emitted from fluorine. An ionization chamber containing hydrogen at 20 atmospheres pressure was used to measure the ionization currents. Less than 5 percent of the current produced by the radiation from Po+F could have been due to γ-rays emitted along with the neutrons.

Fig. 2 shows the curves of the ionization produced by the neutrons from fluorine and beryllium as a function of the residual range of the alpha-particles. The beryllium-neutron curve is similar to that reported by Curie and Joliot.[1] The fluorine-neutron ionization current becomes zero when the residual range of the alpha-particles is less than 2.3 cm in air. Thus alpha-particles with ranges of more than 2.3 cm are necessary to produce neutrons from fluorine. An alpha-particle of this range has an energy of 3.7×10^6 e.v.

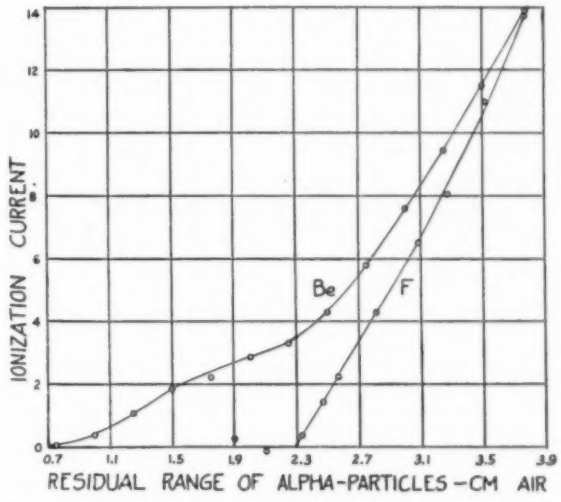

FIG. 2. Emission of neutrons from beryllium and fluorine. (Fluorine ordinates have been multiplied by 16.)

The maximum energy of the neutrons emitted by Po+Be is of the order of 12×10^6 e.v., which is greater than the energy of the exciting alpha-particles. Thus the nuclear reaction is possible for alpha-particles of any velocity, and so there is no alpha-particle velocity below which there is no emission of neutrons. The emission of neutrons from beryllium has been observed by Crane, Lauristen and Soltan[2] when the energy of the alpha-particles was as low as 500,000 volts. However with boron[1] and fluorine there is a definite threshold alpha-particle velocity for the emission of neutrons. The maximum energy of neutrons emitted from an element can be calculated from the threshold alpha-particle energy for neutron emission. For Po+F, the maximum energy of the neutrons is calculated to be $5.3\times10^6-3.7\times10^6=1.6\times10^6$ e.v.

T. W. BONNER

Rice Institute,
Houston, Texas,
February 19, 1934.

[1] I. Curie and F. Joliot, J. de Phys. et Radium **4**, 278 (1933).

[2] Crane, Lauristen and Soltan, Phys. Rev. **44**, 514 (1933).

Vibrational Isotope Effects in Polyatomic Molecules. III

In a previous paper on this subject[1] expressions have been derived for isotopic frequency shifts on the assumption that $\Delta m/m$, the relative mass difference between the two isotopes, was small so that $(\Delta m/m)^2 \ll 1$ could be neglected. While this assumption is applicable in a large number of cases it is necessary to derive exact expressions for the case of hydrogen isotopes.

Consider first the triatomic case. With the notation of I[2] we get as the exact expression for the vibration frequencies of $YX^{(m+\Delta_m)}X^{(m)}$

$$\{m\lambda^* - \tfrac{1}{2}B\mu^{-1}[1-\mu\kappa+\mu\cot^2\alpha(1-\kappa)]\}\{m^2\lambda^{*2} - m\lambda^*[2A(1-\kappa)+\tfrac{1}{2}C\mu^{-1}(1-\mu\kappa)] + \mu^{-1}(1-\mu\kappa-\kappa)(AC-D^2)\} - \kappa^2 m\lambda^*[AB + \tfrac{1}{4}BC\cot^2\alpha + BD\cot\alpha - (AC-D^2)] = 0, \quad (1)$$

where $\kappa = \frac{1}{2}\Delta m(m+\Delta m)^{-1}$. There is no analogue in this case to the sum relations previously given; the only expression independent of the intramolecular forces is $(\omega_1^*/\omega_1)(\omega_2^*/\omega_2)(\omega_3^*/\omega_3)$ which is of no help in assigning frequencies to definite modes of vibration.

For a collinear molecule where $D=0$ and $\cot\alpha = 0$, Eq. (1) reduces to:

$$m\lambda_1^* - \tfrac{1}{2}C\mu^{-1}(1-\mu\kappa) = 0,$$

$$[m\lambda^* - 2A(1-\kappa)][m\lambda^* - \tfrac{1}{2}B\mu^{-1}(1-\mu\kappa)] - AB\kappa^2 = 0; \quad (2)$$

so that in this case:

$$\omega_1^*/\omega_1 = (1-\mu\kappa)^{\frac{1}{2}}; \quad (\omega_2^*/\omega_2)(\omega_3^*/\omega_3) = (1-\mu\kappa-\kappa)^{\frac{1}{2}}. \quad (3)$$

The frequencies of the symmetrical molecule $YX_2^{(m+\Delta_m)}$ (denoted by ω^{**}) are immediately derivable from Eq. (8a) in I. We obtain for them:

$$\omega_3^{**}/\omega_3 = [1-2\kappa\mu(\sin^2\alpha+\mu\cos^2\alpha)^{-1}];$$
$$(\omega_1^{**}/\omega_1)(\omega_2^{**}/\omega_2) = (1-2\kappa\mu)^{\frac{1}{2}}(1-2\kappa)^{\frac{1}{2}}. \quad (4)$$

Eq. (1) contains five unknown molecular constants; and, in a case where not all frequencies or isotopic shifts have been observed experimentally, this large number of unknowns is a handicap in the explanation of results. The number of constants in the potential energy function may be reduced by means of suitable physical assumptions as has been done by Dennison,[3] Bjerrum[4] and others. We shall give here the connection between the general expression and some special cases. The potential energy function V' which includes central forces and a force perpendicular to the lines of bonds is:[5]

$$V' = \tfrac{1}{2}[k_1'(q_2^2+q_3^2) + k_2'q_1^2 + k_3'(r\delta\alpha)^2], \quad (5)$$

where r is the equilibrium distance between the Y and X atoms and $\delta\alpha$ the change in the apex half angle α. Then:

$$k_1' = \tfrac{1}{2}B\operatorname{cosec}^2\alpha;$$
$$k_2' = A - \tfrac{1}{4}B(1-\cot^2\alpha)\operatorname{cosec}^2\alpha - \tfrac{1}{4}C\cot^2\alpha;$$
$$k_3' = (C - B\cot^2\alpha)\operatorname{cosec}^2\alpha. \quad (6)$$

Also $D = \frac{1}{2}\cot\alpha(B\operatorname{cosec}^2\alpha - C)$, since there are only three independent constants. Obviously there are additional equations of linear dependence between A, B and C if either $k_2'=0$ or $k_3'=0$ corresponding respectively to a "valence" or a central force case.

The frequencies of the tetratomic molecule $YX_2^{(m)}X^{(m+\Delta_m)}$ are given by the following expressions:

$$m^2\lambda^{*2} - m\lambda^*[\tfrac{1}{2}A\mu^{-1}(b-\mu\kappa) + 3D(1-\kappa) + 2\kappa E] + [b\mu^{-1}(1-\kappa)-\kappa](AD-E^2) = 0,$$
$$m^4\lambda^{*4} - m^3\lambda^{*3}P_1 + m^2\lambda^{*2}P_2 - m\lambda^*P_3 + P_4 = 0, \quad (7)$$

where

$$\kappa = \tfrac{1}{2}\Delta m(m+\Delta m)^{-1}, \quad b' = b(1-2\kappa)+2\kappa-\mu\kappa, \quad C' = 2C-D;$$

$$P_1 = 3(1-\kappa)(C'+D) + \tfrac{1}{3}\mu^{-1}(1-\mu\kappa)B + \tfrac{1}{2}b'\mu^{-1}A - 2\kappa E,$$

$$P_2 = (1/9)AB\mu^{-2}[(1-\mu\kappa)b' - 2\mu\kappa^2(b-1)] + \mu^{-1}[(1-\kappa)b' - \mu\kappa^2](AC'+AD-E^2) - 4(3)^{-\frac{1}{2}}\kappa^2(c/a)AF - 4\kappa^2(3)^{\frac{1}{2}}(c/a)EF + \mu^{-1}(1-\kappa)(1-\mu\kappa)(BC'+BD-F^2) - \tfrac{2}{3}\kappa\mu^{-1}(1-\mu\kappa)BE + 9(1-2\kappa)C'E - 6\kappa C'E,$$

$$P_3 = (AD-E^2)\mu^{-2}\{\tfrac{1}{3}B[(1-\kappa-\mu\kappa)b' - \mu\kappa^2(b-1)] + 3\mu C'[(1-2\kappa)b' - 2\mu\kappa^2] - 4(3)^{\frac{1}{2}}\kappa^2\mu^2(c/a)F\} + (BC'-F^2)\mu^{-2}\{\tfrac{1}{3}A[(1-\kappa-\mu\kappa)b' - \mu\kappa^2(b-1)] + 3\mu(1-2\kappa)(1-\mu\kappa)D - 2\mu\kappa(1-\mu\kappa)E\},$$

$$P_4 = b'\mu^{-2}(1-2\kappa-\mu\kappa)(AD-E^2)(BC'-F^2).$$

The equations of linear dependence connecting A, B, C, D, E and F for the central force case may be obtained immediately from formulas given in I. The "valence" force case is now being studied.

JENNY E. ROSENTHAL

Physics Department,
New York University,
University Heights,
February 14, 1934.

---

[1] E. O. Salant and J. E. Rosenthal Phys. Rev. **42**, 812 (1932) denoted henceforth as I.

[2] The last term in Eqs. (7a) and (8a) in I should read $AC-D^2$ since the coefficient of vq_1 in the potential energy is defined as $2D$.

[3] D. M. Dennison, Phil. Mag. **1**, 195 (1926).

[4] N. Bjerrum, Verh. d. deutsch. phys. Ges. **16**, 737 (1914).

[5] We shall denote by a prime everything referring to this special case.

Calculation of Vibrational Isotope Effect in Polyatomic Molecules by a Perturbation Method

The perturbation theory devised by Lord Rayleigh for treating vibrating systems provides a convenient method of calculating the vibrational isotope effect in polyatomic molecules, especially those of high symmetry. Special cases of this problem have been treated by other investigators[1] but I believe the following method to be more convenient than any other of comparable accuracy so far proposed.

The difficulty in computing isotope shifts arises when the insertion of the isotope lowers the symmetry of the molecule so that the frequency formulas and normal coordinates for a molecule of lower symmetry would have to be used for a direct calculation. These formulas are always more complicated than those for the symmetric molecule and frequently are not available.

If the displacement of each atom is described by the use of a set of rectangular coordinates q_i with origin at the equilibrium position of the atom and if the change of scale $q_i=(m_i)^{\frac{1}{2}}q_i'$ is made, which introduces the masses into the potential energy, then the kinetic and potential energies are given by

$$2T=\Sigma_i\dot{q}_i^2; \quad 2V=\Sigma_{i,j}B_{ij}q_iq_j.$$

The solution of the normal coordinate problem is obtained when the characteristic values $\lambda_k=4\pi^2\nu_k^2$ (ν_k is the normal frequency) and the transformation

$$Q_k=\Sigma_i l_{ik}q_i$$

with matrix $L=(l_{ik})$ are known. The Q_k's are the normal coordinates.

If a perturbation $2V'=\Sigma_{i,j}C_{ij}q_iq_j$ with matrix $C=(C_{ij})$ is added to the potential energy, perturbation theory (which is analogous to that used in quantum mechanics) gives for the shift $\Delta\lambda_k$ of the kth characteristic value λ_k (λ_k non-degenerate) the expression

$$\Delta\lambda_k=(L^{-1}CL)_{kk}$$

or, on writing out the matrix product

$$\Delta\lambda_k=\Sigma_{i,j}l_{ik}C_{ij}l_{jk}.$$

If λ_k is degenerate, for example double, so that both Q_k and Q_r have the same frequency, it is necessary to solve the secular equation involving these two modes. Thus

$$\begin{vmatrix}(L^{-1}CL)_{kk}-\Delta\lambda & (L^{-1}CL)_{kr}\\ (L^{-1}CL)_{rk} & (L^{-1}CL)_{rr}-\Delta\lambda\end{vmatrix}=0$$

will give the two roots $\Delta\lambda$, which may be equal if the symmetry of the perturbation is high enough so as not to cause splitting of the degenerate frequency. In the above equation

$$(L^{-1}CL)_{kr}=\Sigma_{i,j}l_{ik}C_{ij}l_{jr}.$$

Detailed applications of this method will be reserved for a later paper but the calculation of the isotope effect for the symmetrical vibration (ν_1) of tetrahedral molecules AB_4 is so simple it is given below. Here $Q_1=\frac{1}{2}(r_1+r_2+r_3+r_4)$ if r_i is the radial displacement of the ith atom. If one isotopic B atom, say atom 1, is introduced, the part of the perturbation which is a function of the r's is

$$2V'=KSr_1^2+2K'R(r_1r_2+r_1r_3+r_1r_4),$$

in which K and K' are constants which appear in the potential energy of the unperturbed molecule while

$$S=(m+\Delta m)^{-1}-m^{-1}\cong-\Delta m/m^2,$$
$$R=[m(m+\Delta m)]^{-1}-m^{-1}\cong-\Delta m/2m^2,$$

for $\Delta m/m$ small. From the expression for Q_1, $l_{i1}=\frac{1}{2}$ for $q_i=r_1$, r_2, r_3 or r_4 and is zero otherwise. Therefore

$$\Delta\lambda_1=(L^{-1}CL)_{11}\cong-\tfrac{1}{4}(K+3K')\Delta m/m^2.$$

But

$$\lambda_1=(K+3K')/m \quad \text{so that} \quad \Delta\lambda_1/\lambda_1=-\Delta m/4m,$$

which for $\Delta m/m$ small agrees with Salant and Rosenthal's result. In a later paper complete details of the method together with applications to the isotope effect and other phenomena will be given.

E. Bright Wilson, Jr.

Gates Chemical Laboratory,
California Institute of Technology,
February 20, 1934.

[1] E. O. Salant and J. E. Rosenthal, Phys. Rev. **43**, 581 (1933); **42**, 812 (1932).
A. Langseth, Zeits. f. Physik **72**, 350 (1931).

Separable Systems in Euclidean 3-Space

In 1891 Stäckel[1] showed how to determine the quantities H_i in the Hamiltonian-Jacobi equation

$$\Sigma_i\frac{1}{H_i^2}\left(\frac{\partial\varphi}{\partial x_i}\right)^2+k^2(E-V)\varphi=0, \qquad (1)$$

so that the variables are separable, the solution being of the form $\Sigma_i X_i$ where X_i is a function of x_i alone. In 1927 Robertson[2] showed that for an equation of the form

$$\Sigma_i\frac{1}{H}\frac{\partial}{\partial x_i}\left(\frac{H}{H_i^2}\frac{\partial\varphi}{\partial x_i}\right)+k^2(E-V)\varphi=0, \quad H=H_1\cdots H_n, \qquad (2)$$

to admit by separation of the variables a solution of the form ΠX_i, where X_i is a function of x_i alone, the functions H_i must be of the Stäckel form, and $V=\Sigma[f(x_i)/H_i^2]$, where $f(x_i)$ is an arbitrary function of x_i alone, just as in the case of Eq. (1) as shown by Stäckel; also he showed that the determinant φ of the Stäckel functions φ_{ij} must satisfy the condition

$$\varphi=\Pi[H_i/\psi(x_i)], \qquad (3)$$

where ψ_i is a function of x_i alone.

[1] Stäckel, *Habilitationsschrift*, Halle.
[2] Robertson, *Bemerkung über separierbare Systeme in der Wellenmechanik*, Math. Annalen, Vol. 98, pp. 749–752.

In the *Annals of Mathematics* for April, 1934, I derive the conditions for the Stäckel result in such a form that I have been able to determine all the real type forms so that the space with the fundamental form

$$ds^2=H_1^2dx_1^2+H_2^2dx_2^2+H_3^2dx_3^2 \qquad (4)$$

is euclidean, and I have shown that they satisfy the condition (3). These forms and the relation between the coordinates x_i and cartesian coordinates are as follows:

$$H_i=1, \text{ cartesian;} \qquad (I)$$

$$H_1=H_2=1,\ H_3=x_1, \text{ cylindrical polar coordinates;} \qquad (II)$$

$$H_1=1,\ H_2=x_1,\ H_3=x_1\sin x_2, \text{ polar coordinates;} \qquad (III)$$

$$H_1^2=1,\ H_2^2=H_3^2=a^2(\cosh 2x_2-\cos 2x_3),$$
elliptic cylinder coordinates;

$$x=x_1;\ y=a\cosh x_2\cos x_3,\ z=a\sinh x_1\sin x_3; \qquad (IV)$$

$$H_1^2=1,\ H_2^2=H_3^2=x_1^2x_3^2,$$
parabolic cylinder coordinates;

$$x=x_1,\ y=x_2^2-x_3^2,\ z=x_2x_3; \qquad (V)$$

$$H_1^2=1,\ H_2^2=H_3^2=x_1^2[k^2cn^2(x_2,k)+k'^2cn^2(x_3,k')],$$
$$k^2+k'^2=1,\ x=x_1dn(x_2,k)sn(x_3,k'),$$
$$y=x_1sn(x_2,k)dn(x_3,k'),\ z=x_1cn(x_2,k)cn(x_3,k'); \qquad (VI)$$

$$H_1^2=H_3^2=x_1^2+x_3^2,\ H_2^2=x_1^2x_3^2,$$
parabolic coordinates,

$$x=x_1x_3\cos x_2,\ y=x_1x_3\sin x_2,\ z=\tfrac{1}{2}(x_1^2-x_3^2); \qquad (VII)$$

$$H_1^2=H_3^2=a^2(\sinh^2x_1+\sin^2x_3),$$
$$H_2^2=a^2\sinh^2x_1\sin^2x_3,$$
prolate spheroidal coordinates,

$$x=\sinh x_1\sin x_3\cos x_2,\ y=a\sinh x_1\sin x_3\sin x_2,$$
$$z=a\cosh x_1\cos x_2; \qquad (VIII)$$

$$H_1^2=H_3^2=a^2(\cosh^2x_1-\sin^2x_3),$$
$$H_2^2=a^2\cosh^2x_1\sin^2x_3,$$
oblate spheroidal coordinates,

$$x=a\cosh x_1\sin x_3\cos x_2,\ y=a\cosh x_1\sin x_3\sin x_2,$$
$$2=a\sinh x_1\cos x_3; \qquad (IX)$$

$$H_i^2=(x_i-x_j)(x_i-x_k)/f(x_i),$$
$$f(x_i)=4(\alpha-x_i)(\beta-x_i)(\gamma-x_i),\ (i,j,k\neq),$$
confocal ellipsoidal coordinates; (X)

$$H_i^2=(x_i-x_j)(x_i-x_k)/f(x_i),$$
$$f(x_i)=4(a-x_i)(b-x_i),\ (i,j,k\neq),$$
confocal parabolic coordinates,

$$x=(x_1+x_2+x_3-a-b)/2,$$
$$y^2=(a-x_1)(a-x_2)(a-x_3)/(b-a)$$
$$z^2=(b-x_1)(b-x_2)(b-x_3)/(a-b),\ x_1>b>x_2>a>x_3. \qquad (XI)$$

In each case the coordinate surfaces consist of confocal quadrics including the cases when one or more families consist of planes. All such systems yield solutions and only these. Consequently the only orthogonal systems of coordinates in which the three-dimensional Schrödinger equation can be solved by separation of the variables are the above types.

LUTHER PFAHLER EISENHART

Fine Hall,
Princeton, New Jersey,
February 24, 1934.

On the Inversion of Doublets in Alkali-Like Spectra

In a recent paper[1] we considered the effect of the polarization of the core on the doublet separations in alkali-like spectra. We are indebted to Professor Van Vleck for pointing out to us that such an effect may be formulated as a third order perturbation in a systematic application of perturbation theory. If H is the Hamiltonian the third order correction to the energy of the state i is

$$\delta E_i=-\Sigma_{jj'}\frac{H_{ij}H_{jj'}H_{j'i}}{(H_{ii}-H_{jj})(H_{ii}-H_{j'j'})}. \qquad (1)$$

A careful examination shows that, for our case, and for both the coupling schemes which we considered for the excited core states, the terms in (1) reduce to those calculated by us. But whereas (1) is clearly independent of the representation chosen for the excited core states, our results, based on two different assumptions for this representation, differed by a factor of two. We have found that in the table of doublet separations on p. 646 the values given for terms arising from triplet parents are incorrect: the coefficients of ξ_1 for these three doublets should all be reduced by a factor of three. When this is done, and the corresponding correction is made in Table III, the result, on the assumption of LS coupling, reduces to $\delta E=-(F_0G/E_0^2)\xi_1-2(fG+gF_0)/3E_0$, in complete agreement with that given on p. 648 for the other coupling scheme considered.

MELBA PHILLIPS

Department of Physics,
University of California,
February 22, 1934.

[1] Melba Phillips, Phys. Rev. **44**, 644 (1933).

Artificial Radioactivity Produced by Deuton Bombardment

Following the discovery by I. Curie and F. Joliot[1] that radionitrogen is formed when boron is bombarded with alpha-particles, it seemed probable, as they in fact suggest, that this new radioactive element might be formed by bombarding carbon with high speed protons and deutons. Indeed, in the light of our recent experiments in which

[1] Curie and Joliot, Nature **133**, 201 (1934).

neutrons and protons were found to be emitted from many elements when bombarded with deutons, the possibility presented itself that in these nuclear reactions new radioactive isotopes of many of the elements might be formed.

Using both deutons and protons we have bombarded all the elements, except neon and sulphur, from lithium through chlorine and also calcium. Except possibly in the case of carbon, we observed no radioactivity induced by bombardment with one and one-half million volt protons. But every substance was observed to emit both gamma-radiation and ionizing particles of approximately electronic mass for some time after bombardment with three million volt deutons. In the light of the Curie-Joliot experiments these particles are presumably positrons.

Preliminary measurements of the half-lives of the radioelements produced in the several targets are as follows: Calcium fluoride, forty seconds; calcium chloride, thirteen minutes; boric oxide, sodium phosphate, lithium carbonate and ammonium nitrate about two minutes; aluminum three minutes; magnesium nine minutes; beryllium nine minutes with some evidence of a shorter lived group of about three minutes; carbon twelve minutes. The possibility that some of the observed effects are ascribable to impurities remains to be investigated.

We are indebted to Professor J. R. Oppenheimer for many helpful discussions, to Professor Gilbert N. Lewis for furnishing the necessary deuterium, to the Research Corporation and The Chemical Foundation for their financial support and to Commander Telesio Lucci and Alexander Hildebrand for their assistance.

MALCOLM C. HENDERSON
M. STANLEY LIVINGSTON
ERNEST O. LAWRENCE

Radiation Laboratory,
Department of Physics,
University of California,
Berkeley, California,
February 27, 1934.

Invariants of Quadrics and Electrical Circuit Theory

It is the purpose of this letter to call attention to a paper upon a *Classification of Quadrics in Affine n-space by Means of Arithmetic Invariants* which I wrote in 1931 and subsequently published;[1] and which, when translated into electrical language, indicates the answers to a number of questions raised at the end of the recent paper by Nathan Howitt.[2]

Howitt showed, in his paper on *Group Theory and the Electric Circuit*, that two-terminal linear passive networks of a finite number of meshes consisting of inductances, capacitances and resistances, form a group under the real linear affine non-singular transformations of matrix B, on the charges and currents, with the driving-point impedance function as an absolute invariant; i.e., to a given impedance function there corresponds an infinite number of networks, any one of which can be obtained from the other by a special affine transformation of the instantaneous mesh currents and charges. This was done by applying the matrix B to the matrices of the three fundamental quadratic energy forms of the network, resulting in the formation of new quadratic forms congruent (equivalent) under the transformation used.

Consider the two-terminal linear network (with positive or negative circuit parameters) of total instantaneous magnetic energy T, power loss R, and electrostatic energy V. Let A denote the matrix of a real fundamental energy form F, (T, R or V), which is quadratic in the instantaneous currents (or charges). Suppose the currents (and charges) are subject to a transformation of matrix B, which leaves the driving-point current (and charge) in nth mesh invariant. Let R, S; r, s, denote the ranks and signatures, respectively, of A and a, where a is matrix A with last row and column deleted. Then, according to my paper, we have the answer to certain questions raised by Howitt.

If $(R-r)\neq 2$, A can be reduced by a transformation B to a diagonal form for which F is the sum of the squares of the (instantaneous) mesh currents, p being positive and q being negative, where $2p=R+S$ and $2q=R-S$; and, theoretically, all mutual parameters of type F can be eliminated, R being the minimal number of type F circuit parameters. If $(R-r)=2$, F may be reduced to the sum of the squares of the mesh currents, p positive and q negative, plus twice the product of the currents in $(n-1)$th and nth meshes, where $2p=r+s$ and $2q=r-s$; and, theoretically, all mutual parameters of type F can be eliminated, save one, $(R-1)$ being the minimal number of type F circuit parameters. If the circuit is passive, $R=S$, $r=s$ and we can dispense with the signatures altogether.

The reduction of F to normal form indicated in the proofs of the theorems of my paper should simplify computations considerably. It is hoped that these methods may prove of practical value. Though we may not need to know the value of the impedance function many times, and we may characterize it by other means, I hardly think that the concept of impedance can be scrapped, because any absolute invariant is of fundamental significance from the mathematical point of view.

If instead of imposing the invariance of the current in nth mesh, we impose the invariance of the current in jth mesh, the above results go through with n and j interchanged, the transfer impedance being an absolute invariant then.

The extension of these methods to pairs and triples of energy forms and the resulting network interpretation I hope to indicate later in an extended paper.

RICHARD S. BURINGTON

Case School of Applied Science,
Cleveland, Ohio,
February 26, 1934.

[1] R. S. Burington, Am. Math. Monthly **39**, No. 9, 528–532 (1932).

[2] N. Howitt, Phys. Rev. **37**, 1583–1595 (1931).

The Nuclear Energies of Aluminum and Beryllium

According to the theory recently suggested by the writer[1] the nuclei of the radioactive atoms have possible energies equal to multiples of 3.85×10^5 electron-volts. This idea was suggested by the fact that the gamma-ray, beta-ray and disintegration energies form many pairs with sums equal to multiples of 3.85×10^5 electron-volts.

When aluminum is bombarded by alpha-rays it emits protons and there are several alpha-ray energies for which the proton emission has maximum values. These alpha-ray energies probably correspond to energy levels of the aluminum nucleus. The values found for these resonance levels by Chadwick and Constable[2] are 52.5, 48.6, 44.9 and 40 with 10^5 electron-volts as unit. The differences between these energies are 3.9, 3.7 and 4.9 which do not differ from 3.85 by amounts greater than the possible errors.

In the same way when beryllium is bombarded by alpha-rays the emission of neutrons varies with the energy of the rays and has maximum and minimum values. The minimum values found by Kirsch and Slonek[3] occur at about 52.5, 48.5, 44, 40 and 37 and the differences between these values are equal to 4, 4.5, 4 and 3. These differences are not far from 3.85. The mean value is 3.88.

These results together with those for the radioactive atoms, suggest that the nuclei of the atoms of all the elements have possible energies equal to $3.85n$ or to $3.85n+c$ where $n=0, 1, 2, 3\cdots$ and c is a constant.

H. A. Wilson

Rice Institute,
Houston, Texas,
February 27, 1934.

[1] Wilson, Phys. Rev. **44**, 858 (1933).

[2] Chadwick and Constable, Proc. Roy. Soc. **A135**, 48 (1932).

[3] Kirsch and Slonek, Naturwiss. **4**, 62 (1933).

Radioactivity from Carbon and Boron Oxide Bombarded with Deutons and the Conversion of Positrons into Radiation

In a note to *Science* we announced that we had observed radioactivity from certain light elements after they had been bombarded with deutons of 0.9×10^6 e.v. energy, and, in particular, that we had been able to verify the prediction of Curie-Joliot and Joliot,[1] that carbon bombarded with deutons should yield the same radioactive end product as they obtained by bombarding boron with α-particles. The particles which we obtained from the bombarded carbon were identified as positrons having energies distributed from about 0.7×10^6 e.v. downward, by Dr. Carl D. Anderson and Seth H. Neddermyer, using a Wilson cloud chamber. We have since investigated this and some other processes more closely, and have determined the decay constants with more precision. We have also found that γ-rays are associated with the radioactivity in at least some of these processes.

The procedure is as follows: A target of the substance to be investigated is first bombarded for a suitable length of time, generally fifteen minutes, with an ion current of 10 microamperes, consisting principally of H^3, at 0.9×10^6 volts. The target is then removed from the tube and placed in the bottom of an ionization chamber, and the rate of production of ionization as a function of time is measured. The ionization observed is attributed to particles ejected from the target, and also to γ-rays, if such are present. In order to separate the effect contributed by γ-rays alone, a second ionization chamber is placed directly below the first. The walls and linings of the chambers are sufficiently thick to prevent charged particles from entering the lower chamber and giving a direct effect. Therefore any ionization recorded in the lower chamber is to be attributed to γ-rays, unless neutrons are present, which does not seem probable.

In Fig. 1 are plotted the log intensities for the two chambers against time after bombardment when a carbon target was placed inside the upper chamber. Curve I refers to the upper chamber and curve II to the lower chamber.

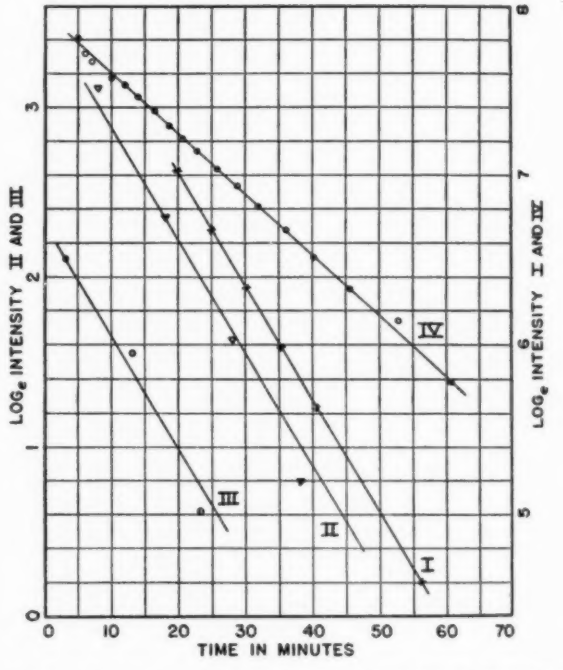

FIG. 1. Intensity of ionization as a function of time after bombardment due to: I, positrons from carbon target; II, γ-rays from carbon; III, γ-rays from carbon after 7.1 cm lead filtration; IV, positrons (?) from B_2O_3 target.

It is seen from these plots that the half period (10.3 minutes) is the same within the experimental error, whether determined from the rate of emission of positrons or from the γ-rays associated with the process. This would

[1] Curie and Joliot, Comptes Rendus **198**, 254 (1934).

seem to indicate that the same radioactive process is responsible for both the positrons and the γ-rays, and the most attractive assumption is that the γ-rays have their origin in the annihilation of the positrons together with electrons.

To determine the absorption coefficient of the γ-rays, we made provision for interposing a sheet of lead 7.1 mm thick between the two chambers. For the first half hour after bombardment, readings were taken every minute on the lower chamber and the lead was put in and removed at intervals of five minutes. We thus obtained alternately four one-minute readings with lead and four one-minute readings without lead. These are plotted on a log scale in Fig. 1, curves II and III, each set of four one-minute readings being averaged. The log difference between the positions of the two curves is 1.23, corresponding to a linear absorption coefficient of 1.58 per cm. Since the source was very close to the lead sheet, a large part of the radiation would necessarily pass through the lead at an angle, tending to compensate the effect of scattering. A calculation from the Gray formula and the Klein Nishina scattering give as the absorption coefficient for 24 x.u. (mc^2) radiation 1.67 per cm, so it seems that the quantum energy of the radiation here observed is, to within our experimental error, equal to mc^2, the rest mass of the electron.

In order to ascertain further that the γ-rays originate in the annihilation of the positrons, we performed the following experiment. A piece of freshly bombarded carbon was placed, active side up, directly above one of the chambers. Supposedly in this case half the positrons are ejected in the downward direction and are annihilated in the carbon, while the other half escape and are annihilated in the air at a considerable distance away from the target and the ionization chamber. However, by covering the target with a sheet of some dense material, the positrons can be prevented from escaping, and they will all be annihilated in, or very near the carbon. Alternate readings were made on the chamber with the carbon covered with aluminum and with it uncovered. The result was that the rate of production of ionization in the chamber was about twice as great with the carbon covered as with it uncovered. In Fig. 2, curve I refers to carbon covered with aluminum, curve II to carbon without aluminum.

As an additional check, we wished to compare the number of γ-ray quanta emitted with the number of electrons. By calibrating the ionization chamber against a standard radium source, we determined that immediately after bombardment about 6×10^4 photons per second are emitted from the carbon target. Making appropriate allowance for solid angle and considering that half of the positrons die in the target and the other half on the walls of the upper chamber, it turns out that there are 500 ion pairs to be associated with each positron passing through the upper chamber. The mean length of path in the chamber is approximately 5 cm, therefore the positrons would be producing, on the average, 100 ions per cm of path, which is a reasonable figure and constitutes evidence that the number of photons is very nearly twice the number of positrons.

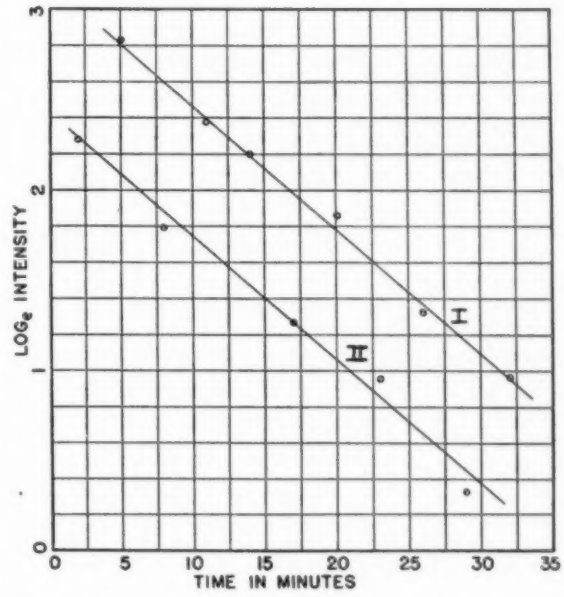

FIG. 2. Intensity of ionization in the chamber: I, with the carbon covered; and II, with the carbon uncovered.

By comparing this with our previous work on carbon,[2] it appears that carbon can be transformed by deutons in the following two ways:

$$(1)\quad {}_6C^{12}+{}_1H^2\rightarrow{}_6C^{13}+{}_1H^1+\gamma,$$

$$(2)\quad {}_6C^{12}+{}_1H^2\rightarrow{}_7N^{13}+{}_0n^1$$
$${}_7N^{13}\rightarrow{}_6C^{13}+(+\epsilon).$$

From our estimate of the number of photons obtained in each case, we are led to believe that the first process takes place about 10 times as frequently as the second. This is on the assumption that the annihilation of one positron produces two photons.

A search for radioactivity produced in a number of other light elements bombarded with deutons was made, namely, LiF, Be, B_2O_3, Mg and Al. The B_2O_3 target gave an effect which was somewhat smaller than that obtained from carbon, and decreased at a rate corresponding to a half life of about 20 minutes. γ-rays were observed in the lower chamber, and the ratio of the effects in the two chambers was the same as in the case of carbon. Although this target has not yet been tested in a cloud chamber, the activity here concerned seems to be of the same nature as that of carbon, and by analogy we suppose that the transmutations are

$${}_5B^{10}+{}_1H^2\rightarrow{}_6C^{11}+{}_0n^1,$$
$${}_6C^{11}\rightarrow{}_5B^{11}+(+\epsilon).$$

A curve showing the rate of decay of the activity of the B_2O_3 target is shown as curve IV in Fig. 1. Appreciable

[2] Lauritsen and Crane, Phys. Rev. **45**, 345 (1934).

activity was observed from all the other substances, but at least a large component of the effect, seemed to have a half life of 10 minutes, which would lead one to suspect that it was due to carbon contamination on the surface of the targets. A closer investigation of their rates of decay will help to decide whether or not carbon is responsible for the whole effect.

We wish again to express our gratitude to the Seeley W. Mudd Fund, through which this work was supported.

H. R. CRANE
C. C. LAURITSEN

Kellogg Radiation Laboratory,
California Institute of Technology,
March 1, 1934.

A Method for Investigating Electrical Breakdown Processes

The ordinary methods of studying spark gap and related types of electrical discharges depend upon the Kerr cell, the rotating mirror, the cathode-ray oscillograph or the use of travelling waves in some type of transmission system. In the Kerr cell and rotating mirror methods luminosity must appear in the gap before any information can be obtained. This luminosity appears after the breakdown process is at least partially completed and it is consequently difficult or impossible to determine the initial conditions of the discharge. The other two methods obviously can yield only information concerning the potential and current-time relations.

The method which we are now using enables us to study the processes occurring before the appearance of luminosity and to obtain the ion distribution before breakdown has been completed. It consists in producing the discharge in a Wilson cloud chamber and was suggested in principle by Professor J. W. Beams. This of course has the disadvantage that the processes must be investigated in an atmosphere saturated with water vapor but for a study of breakdown mechanism this is relatively unimportant.

The circuit which is in use is designed to give voltage impulses of the shortest possible duration. The impulses are applied to the end of a short two-wire transmission line from a condenser spark gap circuit. The sending end of the line is shunted by a second gap arranged so that it is about 30 percent overvolted and also irradiated by ultraviolet light from the first gap. The duration of the voltage impulse applied to the line corresponds consequently to the time taken to build up the voltage across the shunted gap plus the time necessary for the gap to break down. Since this gap is overvolted and at the same time irradiated its time lag is very short. The total duration of the impulse is certainly not over 10^{-7} sec. The cloud chamber is placed at the terminal end of the line which is six meters in length. This end is terminated by the characteristic impedance of the line to prevent reflections. The expansion of the chamber is synchronized with the electrical system by using a third gap energized from a separate transformer to start the discharge in the supply circuit by means of ultraviolet irradiation. The time of the irradiation can be adjusted with respect to the time of expansion. It is perhaps needless to state that great care has been taken to prevent any extraneous voltage impulses from occurring on the transmission system.

For our preliminary work we have used as electrodes a steel needle and a 1/8 inch brass rod rounded to hemispherical shape at the end. With the needle negative the ion cloud is cone shaped, and rather uniform in appearance, with the apex at the needle. Its length is variable sometimes extending the entire distance between the electrodes and sometimes only a part of the distance. It is relatively easy to obtain, appearing on 80 percent of the discharges. With the needle positive the appearance is decidedly different. The discharge is in the form of single streamers usually multiple in number. They have the appearance of single particle tracks but as yet their exact nature has not been determined. They are, however, due to the field as they never appear without the voltage impulse. They are relatively difficult to obtain and are very sensitive to voltage change, a slight increase in voltage producing a diffuse cloud throughout the chamber of no very definite shape.

This study is being continued with electrodes of various geometrical arrangements and with the chamber in a magnetic field, etc. The method is also applicable to the study of breakdown over surfaces and some experiments of this kind are in progress. We believe that it will give information that can be obtained by no other known method.

L. B. SNODDY
C. D. BRADLEY

University of Virginia,
Rouss Physical Laboratory,
March 3, 1934.